“SEISMIC ANALYSIS AND RESERVOIR ASSESSMENT FOR CARBON STORAGE USING MACHINE LEARNING APPROACHES IN QADIRPUR GAS FIELD, CENTRAL INDUS BASIN, PAKISTAN.”

By
MISHAL RAZAQ
M.Phil. Geophysics (2021 - 2023)

Department of Earth Sciences
Quaid-i-Azam University Islamabad, Pakistan

"In the name of Allah, the Most Gracious, the Most Merciful"

“O my Lord, advance me in knowledge” (20:114).

“PAY THANKS TO ALLAH EVERY MOMENT AND GO TO EXPLORE THE HIDDEN TREASURES, ITS ALL FOR YOUR BENEFIT” (AL-QURAN).

WHICH IS IT, OF THE FAVORS OF YOUR LORD, THAT YE DENY? (AR- REHMAN)

CERTIFICATE

It is certified that Mishal Razaq d/o Abdul Razaq Raja carried out the work contained in this dissertation under my supervision and accepted in its present form by Department of Earth Sciences, Quaid-i-Azam University Islamabad, Pakistan as satisfying the requirements for M.Phil. degree in Geophysics.

RECOMMENDED BY:

Prof. Dr. Aamir Ali _____

Supervisor

Department of Earth Sciences

QAU, Islamabad.

Prof. Dr. Mumtaz Muhammad Shah _____

Chairman

Department of Earth Sciences

QAU, Islamabad.

External Examiner _____

Dedication

To the journey of providing the best education for their daughters, I dedicate this thesis to my father (late) and my mother, who both played a significant role in inspiring me to pursue their dream. My father passed away during the first semester of my MPhil degree, and my mother was diagnosed with colon cancer during my last semester. Despite facing challenging circumstances that could have made giving up an easy choice, I found the strength and determination to carry on this journey with the hope instilled in me by ***my faith in Allah****.*

And to the people who stood by my side, provided guidance, assistance, nurtured me, cherished me, comprehended my thoughts, showed concern, expressed affection, and showed me respect throughout this journey.

Acknowledgement

Praise be to Allah Almighty and may peace and blessings be upon the Holy Prophet Muhammad and his descendants. Indeed, All the knowledge and the power belong to the one who created the mankind. It is only His favors, the knowledge He gave to his mankind and the ability to do anything. By His will, we can observe His nature in a scientific way as he described in Al-Quran that he had made things with precision. I am grateful to Allah, for His wisdom behind every bit of his plan that continuously helps me to increase me in my knowledge and abilities that not only leads me to complete this thesis but makes me closer to Him in a way I could never imagine.

I am thankful to my supervisor Prof. Dr. Aamir Ali who took me under his supervision and put his trust in me. He made me realize my shortcomings and invigorated me every time I felt down and propelled me to strive for excellence.

Assisting someone when you're free is simple, but extending help when you're swamped with pending tasks, demonstrating empathy, and aiding them selflessly is a significant challenge. Not everyone possesses the bravery to do this. I am genuinely thankful to you Yawar Amin.

I express my gratitude to Noor ul Huda for assisting me in learning about machine learning, and I appreciate LMKR for assigning tasks that have allowed me to expand my expertise and abilities.

I am thankful to my parents, sisters, friends, khalas and my mamo for their prayers for me.

Abstract

The research addresses critical global issues such as climate change, energy transition, and environmental protection. By evaluating the Qadirpur Gas Field for carbon storage potential and employing cutting-edge machine learning techniques, this study offers practical solutions and insights that can shape both policy decisions and industry practices while promoting a more sustainable and responsible approach to energy and resource management. The key goals involve evaluating the Qadirpur gas field's potential for carbon dioxide (CO_2) storage through well log and seismic data.

The evaluation involved petrophysical analysis, forecasting lithofacies, estimating shear logs, petro-elastic analysis, delineating horizons, and identifying faults using seismic data. The reservoir assessment included analyzing the spatial distribution of impedance and porosity, conducting thermodynamic analysis, and estimating the capacity for secure containment of CO_2. Petrophysical analysis reveals that CO_2 can be securely stored within a 30-meter reservoir zone (depth range of 1336 to 1366 meters) in the Sui Main Limestone (SML) Formation. Porosity values within this zone are favorable, with average values for total porosity of 21.09% and effective porosity of 18.86%.

Lithofacies predictions through Self Organize Maps (SOM) successfully distinguished various lithologies and confirmed that the identified zone is hydrocarbon-bearing limestone. Moreover, a machine learning algorithm namely, Multi-linear Regression was used to predict the shear log, enabling the calculation of petro-elastic properties which are in turn used in the stress state within the reservoir and caprock. Caprock integrity was validated through assessments of permeability and effective porosity variations with lithology, as obtained through the SOM. Seismic analysis revealed that the study area lying in the Middle Indus Basin is relatively stable in terms of tectonic activity.

Spatial distribution analysis of reservoir properties, including impedance and porosity, highlights a promising reservoir with low impedance values and high porosity values, demonstrating its suitability for CO_2 storage. Furthermore, initial temperature and pressure conditions within the SML Formation indicate the feasibility of storing CO_2 in a supercritical state. The developmental history of the field is marked by sequential capacity enhancements,

resulting in continuously diminishing production. This makes the field suitable for Enhanced Oil Recovery, subsequent CO_2 storage and its significance in promoting sustainable energy practices.

Table of Contents

List of Figures

List of Tables

CHAPTER#1

INTRODUCTION

1.1 Introduction

The global challenge of climate change has driven the urgent need for innovative strategies to mitigate greenhouse gas emissions (Meadowcroft and Langhelle, 2009). Carbon capture and storage (CCS) has emerged as a promising solution to reduce anthropogenic carbon dioxide (CO_2) emissions and combat climate change effectively (Anwar et al., 2018). Carbon storage involves capturing CO_2 emissions from industrial processes and power generation and injecting them deep underground into geological formations (Gibbins and Chalmers, 2008). To ensure effective and long-term storage, it is crucial to identify formations that possess the necessary characteristics for secure containment and minimize the risk of CO_2 leakage (Tomic et al., 2018). Several CCS demonstration projects have been finished over the past two decades in countries including US, Canada, Norway, Australia, and Japan. Some of these projects were successful in demonstrating the practicability of CO_2 storage in depleted oil and gas reservoirs, unmined coal beds, and saline aquifers (Furre et al., 2017; Gupta et al., 2020; Hovorka et al., 2013).

Pakistan, like many other countries, is facing the impacts of climate change, including extreme weather events, changing precipitation patterns, and rising temperatures. Pakistan is a signatory to international agreements such as the Paris Agreement, which aims to limit global warming to 2 degrees Celsius well below the pre-industrial levels. To meet such commitments, Pakistan needs to take proactive measures to reduce its carbon emissions for which carbon storage can be an effective strategy (Hussain et al., 2019). Carbon storage can play a crucial role in reducing greenhouse gas emissions, which are the primary drivers of climate change, therefore mitigating the climate change. Pakistan has a history of oil and gas extraction, resulting in depleted reservoirs and possesses substantial potential for storing CO_2 within its oil, gas, and coal fields, as well as in saline aquifers. Additionally, the country holds notable reserves of magnesium and calcium silicates that are well-suited for use as raw materials in the process of carbon mineralization. These reservoirs can potentially serve as suitable sites for CO_2 storage due to their geological characteristics (Rashid et al., 2020). A further advantage of repurposing these sites for carbon storage is the capitalization on the existing infrastructure, making the process more economical. Another advantage of executing CSS projects is that they can stimulate the growth of a knowledge-based economy, create jobs, and foster collaboration between academia, industry, and government institutions.

By 1997, Pakistan had conducted approximately 431 exploratory drilling activities, leading to the identification of 115 discoveries, consisting of 51 oil and 64 gas/condensate findings. Notably, the oil fields' production levels are relatively modest, varying from under 50 to around 18,000 barrels per day. Among the notable discoveries are four significant gas fields, namely Sui, Mari, Uch, and Qadipur, alongside two substantial sites namely, Pir Koh and Khairpur (IEAGHG, 2008). In the Central Indus Basin, the Qadirpur gas field has the potential to act as a favorable option for CCS projects. The geological features of this location suggest the possibility of effectively storing CO_2 emissions underground in a secure manner. The depleted hydrocarbon reservoirs found within the Qadirpur gas field possess the essential geological attributes required for containment purposes.

Seismic analysis and reservoir assessment are crucial factors in determining the viability and achievement of CCS endeavors. These methodologies offer vital insight into the geological and geophysical attributes of potential storage locations, assistance in the selection of sites, evaluation of potential risks, and ongoing storage monitoring over extended periods (Gilmore et al., 2016). Seismic data interpretation involves the process of analyzing the Earth's subsurface through seismic and well log data. This technique serves various purposes: assessing the feasibility of hydrocarbon drilling, acquiring a comprehensive understanding of a specific research area, and potentially expanding an already identified field (Coffeen, 1986). Upon the completion of seismic data interpretation, all available information within seismic data is transformed into structural and stratigraphic models of the Earth, resulting in a seismic section that provides a holistic representation of the geological features. The seismic reflectors depicted on these sections uncover the geological characteristics in the region of interest, subsequently marked for interpretative use (Sheriff, 1999). Reservoir assessment provides insights into the volume of CO_2 that a reservoir can accommodate based on its porosity and permeability. The accurate characterization and assessment of reservoir properties are essential for ensuring the safe and efficient storage of CO_2 in subsurface formations (Kou, 2022). Petrophysical analysis forms the foundation of reservoir assessment by providing insights into the physical and fluid properties of subsurface formations. It involves the study of rock properties, such as porosity, permeability, saturation, and fluid flow behavior (Fischetti and Andrade, 2002). These properties determine the storage capacity, integrity, and containment capability of the reservoir. Reservoir

assessment goes beyond petrophysical analysis and encompasses a comprehensive evaluation of various factors that impact the suitability of a geological formation for carbon storage (Jaiswal, 2022). Important aspects of reservoir assessment include the presence of suitable sealing layers or cap rocks that can prevent the upward migration of CO_2. Identification and characterization of potential leakage pathways or faults are essential for cap rock integrity (Menhali et al., 2014).

Machine Learning aids researchers and geoscientists to extract valuable insights from seismic data, facilitating a deeper understanding of the geological complexities in the region. Through machine learning, patterns and anomalies in seismic data can be detected with precision, enhancing reservoir characterization and predictive modeling for carbon storage feasibility. Additionally, machine learning aids in risk assessment, optimizing injection processes, and expediting data integration, ultimately contributing to more informed decisions, cost-effective operations, and the responsible management of carbon emissions in this critical geological environment. Machine learning is an innovative tool that contributes significantly to analyze vast volumes of complex data, identify geological formations, predicting reservoir properties, storage capacity estimation, real-time anomaly detection, and optimization of injection strategies (Karpatne et al., 2019).

By integrating and interpreting multidisciplinary data, machine learning assists in informed decision-making, ensuring the safety, efficiency, and effectiveness of CCS projects.

1.2 Objectives

The primary objectives include assessing the suitability of the Qadirpur gas field for storing carbon dioxide (CO_2). The assessment encompasses:

1. Petrophysical analysis, lithofacies prediction, shear log prediction, and petro-elastic estimation using well log data of Well Qadirpur-16 to identify the reservoir and analyze the suitability, feasibility, and safety of geological formations for CCS initiatives.
2. Seismic data analysis to characterize the subsurface geological structures and identification of potential pathways and risks for secure CO_2 storage.
3. Demarcation of the potential reservoir zone on the seismic data initially identified using the well log data.

4. Reservoir assessment based on spatial distribution of impedance and porosity, thermodynamic analysis, and storage capacity of the reservoir for secure CO_2 containment.

1.3 Study Area

The chosen site of this dissertation is the Qadirpur region, situated within specific geological coordinates ranging from 27° 55' to 28° 09' N latitude and 69° 11' to 69° 31' E longitude, covering an approximate area of 820 square kilometers (Ali et al., 2005). Qadirpur is positioned in the southern segment of the Central Indus Basin, within the Sindh Province, approximately 8 kilometers from Ghotki. The geological context of this area is shaped by an extensional regime attributed to tectonic activity that commenced during the Cretaceous era (Figure 1.1). This tectonic influence played a pivotal role in shaping the structural elements conducive to petroleum-related activities (Ali et al., 2018; Milan and Rogers, 1993).

Qadirpur stands as Pakistan's third-largest gas field following Sui, boasting an original recoverable reserve of approximately 6 trillion cubic feet. Development of the field unfolded through three distinct phases, progressively elevating its capacity from the initial 235 million standard cubic feet per day (MMscfd) to 500 MMscfd. Subsequently, in 2008, a further augmentation brought its capacity to 600 MMscfd. To ensure the sustained provision of gas over the long term, a compression project was successfully commissioned in 2010.The field's purified gas is channeled to Sui Northern Gas Pipelines Limited, while the raw gas and condensate find buyers in Liberty Power and Pakistan Refinery Limited, respectively. Additionally, permeate gas has been supplied to Engro Power Limited since March 2010.

Figure 1.1: *Tectonic maps of Pakistan depicting the basins and major faults (Rashid et al., 2022). The Qadirpur Gas Field is in the Middle Indus Basin marked by a blue circle.*

1.4 Available Data Set

Seismic data, digital well logs, navigation files, and formation tops files, among other types of data, are employed for the purpose of conducting research. The Directorate General of Petroleum Concessions in Islamabad, Pakistan, has provided a comprehensive set of data files, including SEGY, LAS, and navigation files, among others. The 3D seismic cube was used for seismic analysis and reservoir assessment. Detailed information of well data for this study is presented in the provided Table 1.1. It comprises details of wells, including their precise geographical coordinates, depths, and kb values.

Table 1.1: *Information about all wells used for this dissertation.*

WELL NAME	LATITUDE	LONGITUDE	UWI (M)	TOTAL DEPTH (M)	KB (HEIGHT FROM SEA LEVEL IN METERS)
QADIRPUR- 16	28 O 10' 45.16''N	69 O 37'68.39'' E	1002	1380.00	75.63
QADIRPUR-21	28 O 11 51.78”N	69 O 35' 59.00'' E	1314	1688.00	83.19
QADIRPUR-22	28 O 11 80.08''N	69 O 38' 18.33'' E	1333	1760.00	83.57
QADIRPUR DEEP-01	28° 4' 17.26" N	69° 21' 0.16"E	78	4694.0	0

Qadirpur production data is of paramount importance as it offers historical insights, facilitates benchmarking, and supports informed decision-making in the context of the Qadirpur gas field's production and its role in the energy industry. The graph illustrating in Figure 1.2 depicts Qadirpur complete production data was sourced from the Global Data Oil & Gas Intelligence Center's website. It portrays an assessment of the production pattern for Qadirpur, presented in terms of Barrel of Oil Equivalent per Day (BOE/D), covering the time frame from 1995 to 2050. It provides a historical perspective on the production trends of Qadirpur, allowing stakeholders to understand how production has evolved over the years. This data is crucial for making informed decisions related to energy resource management and allocation. Secondly, by projecting production data up to 2050, it offers insights into the future trajectory of Qadirpur's energy output, aiding in long-term planning and strategic decision-making.

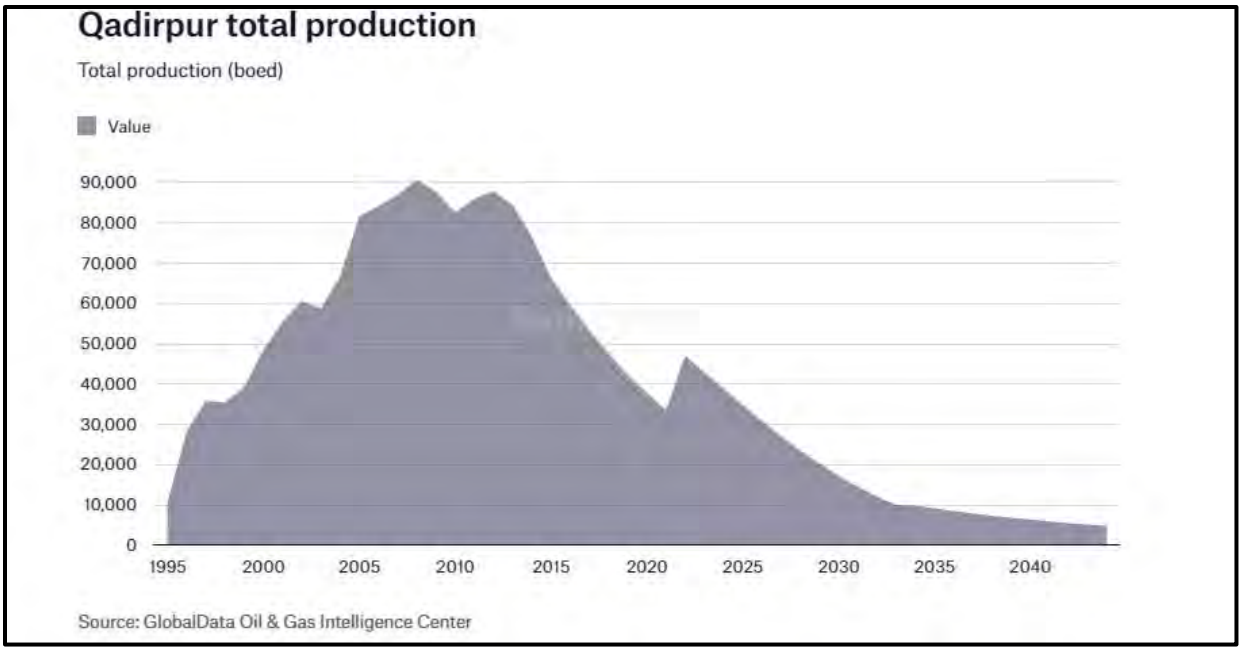

Figure 1.2: *Analysis of the production trend for Qadirpur, depicted in BOE/D, spanning the years 1995 to 2050 (Global Data Oil & Gas Intelligence Center).*

1.5 Methodology

The main objective of the research was to evaluate Sui Main Limestone formation of Qadirpur, as a potential site for CO_2 storage through well log and seismic data. The attributes examined in the assessment of formations for potential CO_2 storage sites encompass basin type, petrophysical analysis, lithological composition, reservoir depth, thickness, structure analysis, fault presence, porosity, permeability, cap rock permeability and the stress conditions within the rock through elastic parameters (Figure 1.3).

The research was initiated by extensively analyzing the geological and tectonic aspects of the region. A suitable zone for CO_2 storage was located through well log analysis. Based on optimum reservoir parameters for CO_2 storage such as depth, thickness, porosity, permeability, hydrocarbon saturation, a zone was demarcated. Lithofacies were predicted based on input log curves through unsupervised neural networking, Self-Organize Mapping. Petrophysical analysis and cluster analysis serve the basis for seismic analysis and reservoir characterization. Sonic log

was predicted through multi linear regression that was utilized for Petro-elastic properties calculation to validated caprock integrity.

Synthetic seismogram, a technique involving one-dimensional forward modeling, was employed. This method utilizes seismic and well data to achieve maximum alignment between synthetic and seismic data at well sites, accurately pinpointing horizon positions. Additionally, two-dimensional time and depth structure maps were generated to delineate and illustrate the subsurface geometry.

For deciphering the spatial distribution of subsurface properties from seismic data, model-based inversion was performed. Model-based inversion offers the advantage of capturing intricate geological details, such as lithological variations, faulting, and fluid content, which impact seismic responses. Spatial distribution of porosity was calculated through Probabilistic Neural Networking (PNN) using well data, seismic data and impedance data obtained from model-based inversion. Through the integration of all the gathered information and production graph, storage capacity of CO_2 was estimated.

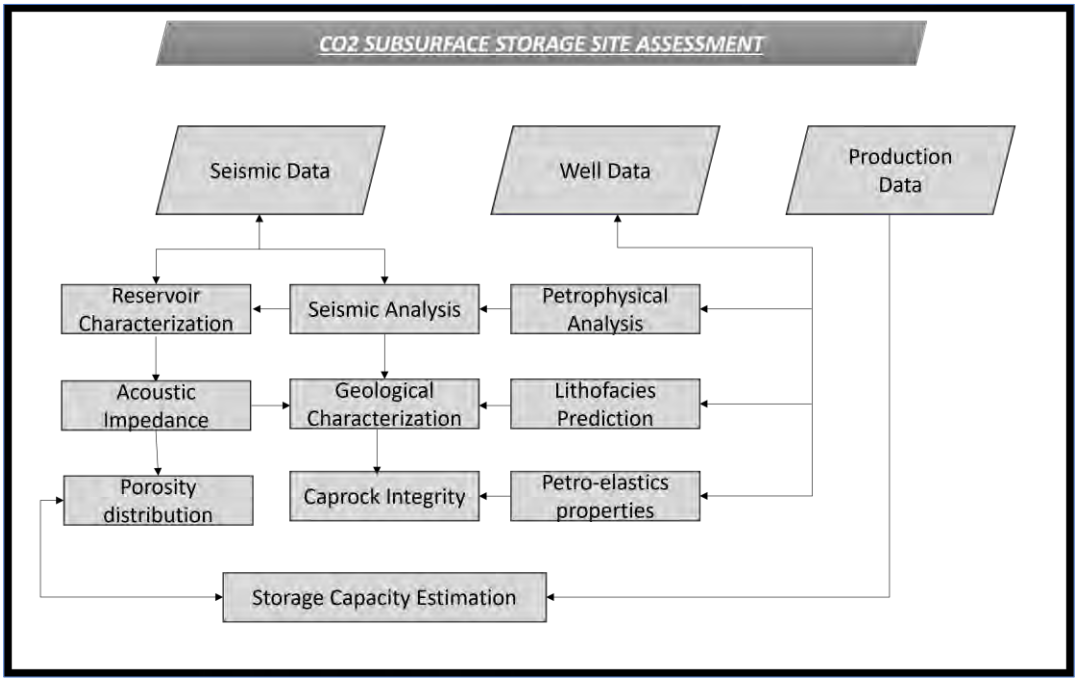

Figure 1.3: *Workflow followed for Characterization of geological formation as a potential storage site for CO_2.*

CHAPTER#2

GEOLOGY AND STRATIGRAPHY

2.1 General Introduction

Geology and stratigraphy play a paramount role in the context of CCS initiatives due to their pivotal influence on the feasibility, safety, and long-term success of CO_2 storage projects. A robust understanding of geology and stratigraphy of the area enables precise site characterization and sustainable CO_2 storage. The study area, Qadirpur Block spans approximately 820 square kilometers and is positioned between 27° 55′ and 28° 09′ N latitude and 69° 11′ to 69° 31′ E longitude on a global map. Qadirpur field lies in the Central Indus Basin, Pakistan. Promising zones within the field consist of Eocene Limestones with fragmented carbonate reservoirs at shallow depths and clastic reservoirs at greater depths.

2.2 Geodynamic setting of Pakistan

Pakistan's tectonic configuration comprises two expansive land masses referred to as Tethyan and Gondwanian, which extend to the Indo-Pakistan crustal plate. The geological structure in Pakistan, particularly in its western region, is intricate due to its location within the Tethyan domain. The Gondwanian realm encompasses the Indus basin, as outlined by Kazmi and Jan in 1997. During the Cretaceous period, a period of dynamic tectonism prevailed, characterized by a relatively high rate of landmass separation ranging from 20 to 30 cm annually over 80 to 50 million years (Gnos et al., 1997). Subsequently, a convergence occurred through the collision of the Indian and Eurasian plates during the Tertiary era. This collision initiated a fracture between the Indian plate and the Afghan Craton, particularly in the northern region, as explained by Banks and Warburton in 1986. The convergent interactions between the Arabian Plate, Afghan Craton, and Indo-Pakistan plates brought about an oblique collision with the Eurasian plate. This collision resulted in the formation of left lateral strike-slip faulting oriented in a northwest to southeast direction within the basement rocks. Consequently, this geological phenomenon facilitated the separation of the Indo-Pakistan Plate (Asim et al., 2014).

2.3 Sedimentary Basins of Pakistan

Pakistan exhibits a remarkable geological diversity, spanning from glaciers to deserts, placing it among the select nations with a vast range of landscapes. This ecological variety corresponds to

a wide array of natural resources. Among these resources, Pakistan possesses an array of natural riches, including reservoirs of hydrocarbons. These hydrocarbon reservoirs have amassed within formations featuring favorable pressure-temperature conditions and are supported by an underlying petroleum source.

Around the world, petroleum plays are situated within different basins. Pakistan encompasses two primary sedimentary basins: the Indus basin situated in the eastern region, and the Baluchistan basin situated in the western part. Alongside the onshore basins, Pakistan also boasts offshore basins known as the Indus offshore and Makran offshore basins, as outlined by Tufail in 2016. The Indus basin is subdivided into three distinct subbasins, as documented by Kadri in 1997:

1. The Upper Indus Basin comprises the Potwar and Kohat basins.
2. The Central Indus Basin encompasses gas fields situated in the Sulaiman fold and thrust belt.
3. The Southern Indus Basin comprises the Kandhkot and Badin regions, along with the Karachi Embayment.

2.4 Tectonics Settings and Structural Style of Central Indus Basin

The Indus Basin is situated in a seismically active region, influenced by the collision of the Indian and Eurasian tectonic plates. During the Cretaceous period, various tectonic events played a crucial role in shaping the Central Indus basin, resulting in a wide range of structural formations. Initially, rifting processes occurred, which eventually led to the development of peripheral fracture architecture. The basin's evolution can be attributed to the Indo-Pakistan and Madagascar movement relative to the African plate. Consequently, the middle Indus basin underwent fragmentation, while the Indian plate began shifting northward in the Mid Cretaceous period. In the late Cretaceous, the Indian plate separated from Madagascar, transforming the Indus basin into a peripheral sag basin (Kazmi and Jan, 1997). Throughout the Cretaceous period, significant NW-SE-oriented strike-slip faults have developed due to the northward movement of the Indian plate toward the Eurasian plate. Tectonic processes have played a crucial role in shaping the structural configuration of the Middle Indus basin. The creation of basement

roots and right-lateral oriented wrench faults occurred during the second phase of uplifting. The rise of Jacobabad High from the late Tertiary period to the present has had a substantial impact on the studied region (Kazmi and Jan, 1997).

2.5 Stratigraphy of Study Area

Stratigraphy offers critical insights into the geological architecture and layering of potential storage sites. By delineating distinct formations, it enables the identification of suitable reservoir rocks and impermeable caprocks crucial for secure CO_2 containment. The stratigraphy of the Qadirpur area, situated within the Central Indus Basin, encompasses a range of sedimentary formations that offer crucial insights into the region's geological history (Figure 2.1). One of the significant formations in this stratigraphic sequence is the Sui Main Limestone Formation, which holds importance in understanding the geological evolution of the area (Siddiqui, 2004).

The Sui Main Limestone Formation is a distinctive unit within the Qadirpur area's stratigraphy, composed primarily of limestone that points to its deposition in a marine setting. This formation is characterized by alternating layers of limestone and shale, with the limestone beds often containing abundant fossil content, indicative of past marine life. As a marker unit, the Sui Main Limestone Formation aids in correlating and interpreting the broader stratigraphic context. As a reservoir, the Sui Main Limestone Formation possesses the potential to host injected CO_2 within its porous structure (Ali et al., 2005).

In contrast, the Ghazij Shale Formation, acting as a cap rock, consists of shale beds with low permeability. This impermeable nature renders the Ghazij Shale Formation well-suited to act as a barrier, preventing the upward migration of stored CO_2 and ensuring its containment within the underlying reservoir.

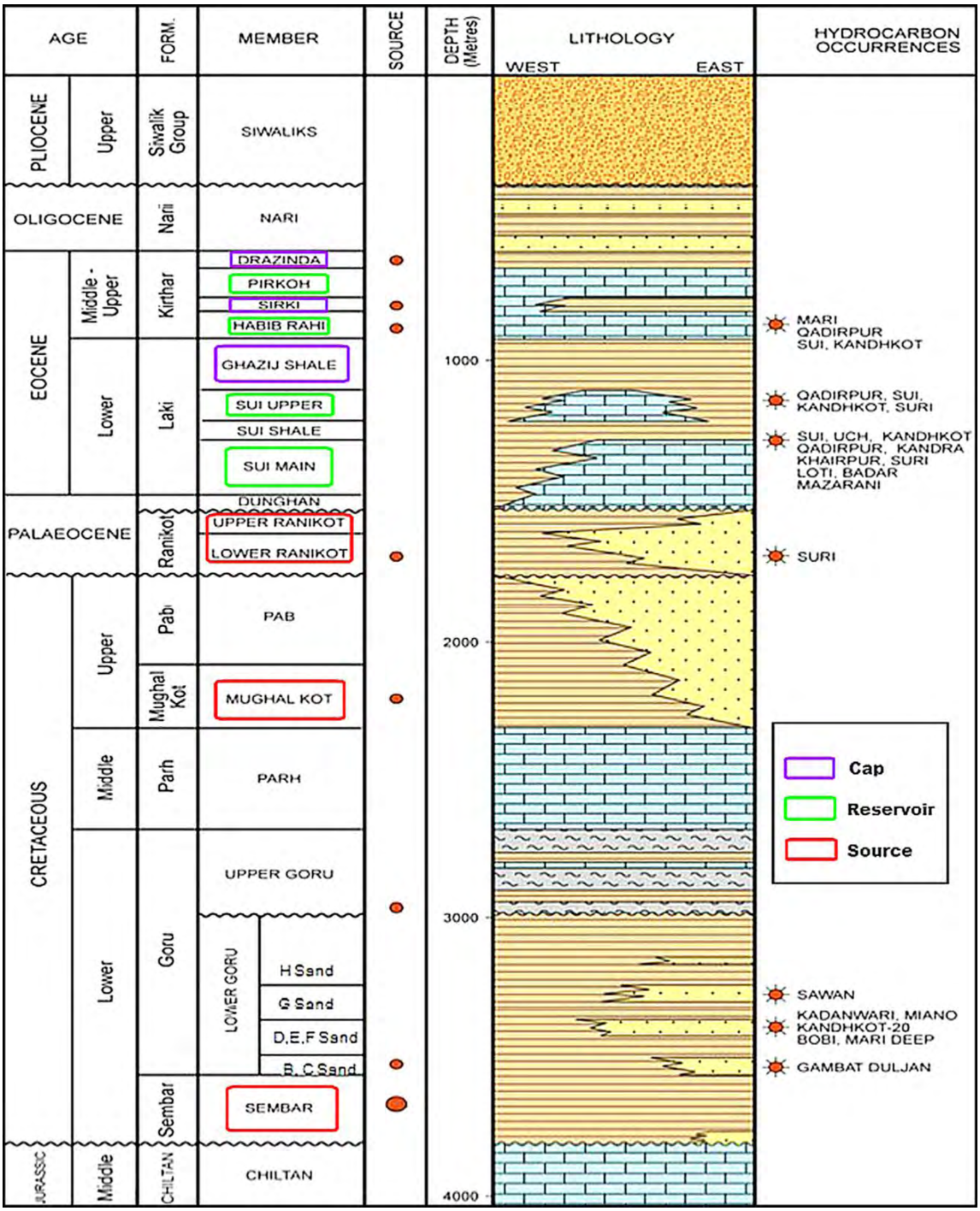

Figure 2.1: *General stratigraphy of the rocks within the Central Indus Basin (Qadirpur locality) (Alam et al., 2002).*

CHAPTER#3

CARBON CAPTURE AND STORAGE (CCS) CONSIDERATIONS

3.1 Introduction

Carbon storage involves capturing CO_2 emissions from industrial processes and power generation and injecting them deep underground into geological formations, particularly depleted oil and gas reservoirs, unmined coal seams or deep saline aquifers. (Gibbins and Chalmers., 2008). Figure 3.1 shows the source of CO_2 capturing, means of transportation, and geological storage sites for CO_2.

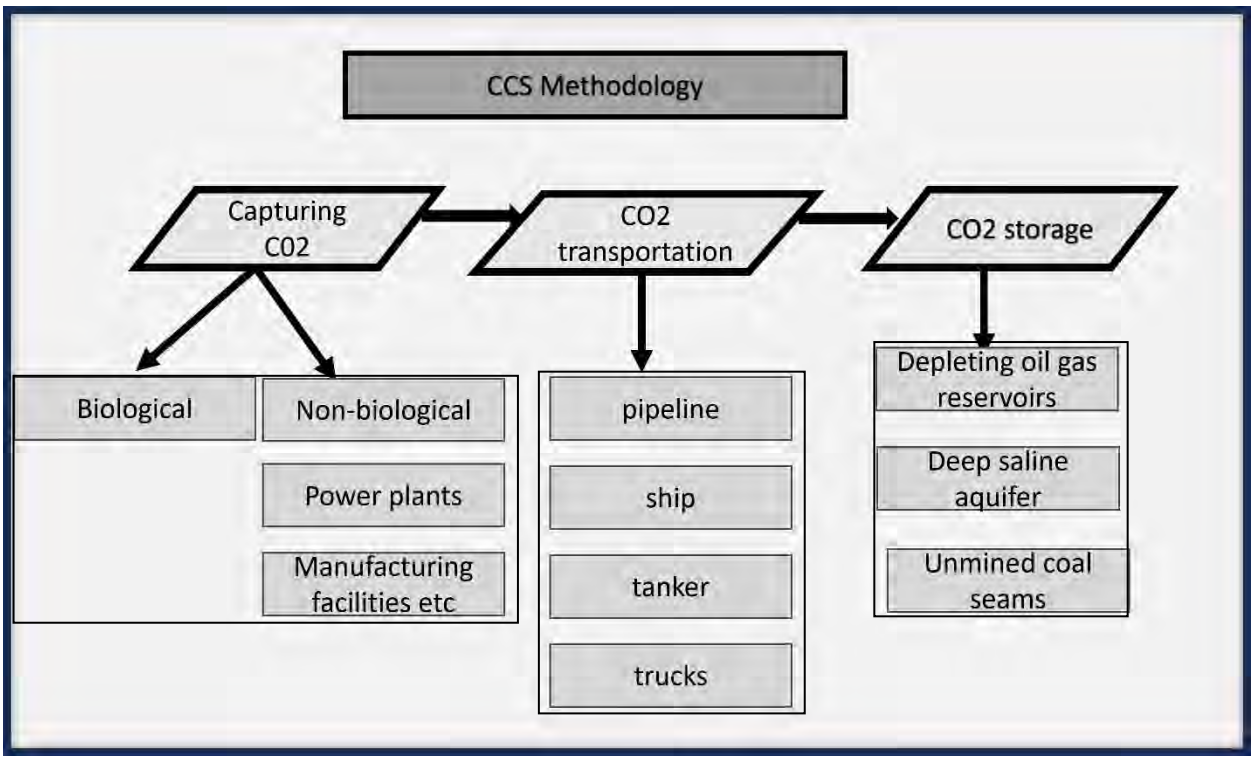

Figure 3.1: *Workflow for CCS methodology from the source of CO_2 capture, means of CO_2 transportation, and locations designated for geological CO_2 storage.*

Considering the varieties of criteria from technical, safety, ecological, and economic perspectives, is essential when contemplating the most suitable CO_2 geological storage option. This comprehensive analysis includes geological, physical, thermodynamic, and hydrodynamic, Techno-economic considerations, plays a crucial role in determining the success of the implementation process (Tomić et al., 2018). After the CO_2 is deposited into the designated

storage location, proper sealing of the wells will be essential to maintain the CO_2 securely in place (Czernichowski et al., 2009).

3.2 Geological formations for CO_2 storage

Globally, CO_2 is stored into the geological formations that provides the optimal solution for safe CO_2 preservation. Geological formations that ensure the long-term storage of CO_2 includes depleting oil and gas reservoirs, saline formations, and unmined coal beds. Other potential sites include oil and gas shales, salt caverns and basalt formations. For EOR (Enhanced Oil Recovery), certain amounts of CO_2 can also be stored during injecting them into well (Tomić et al., 2018).

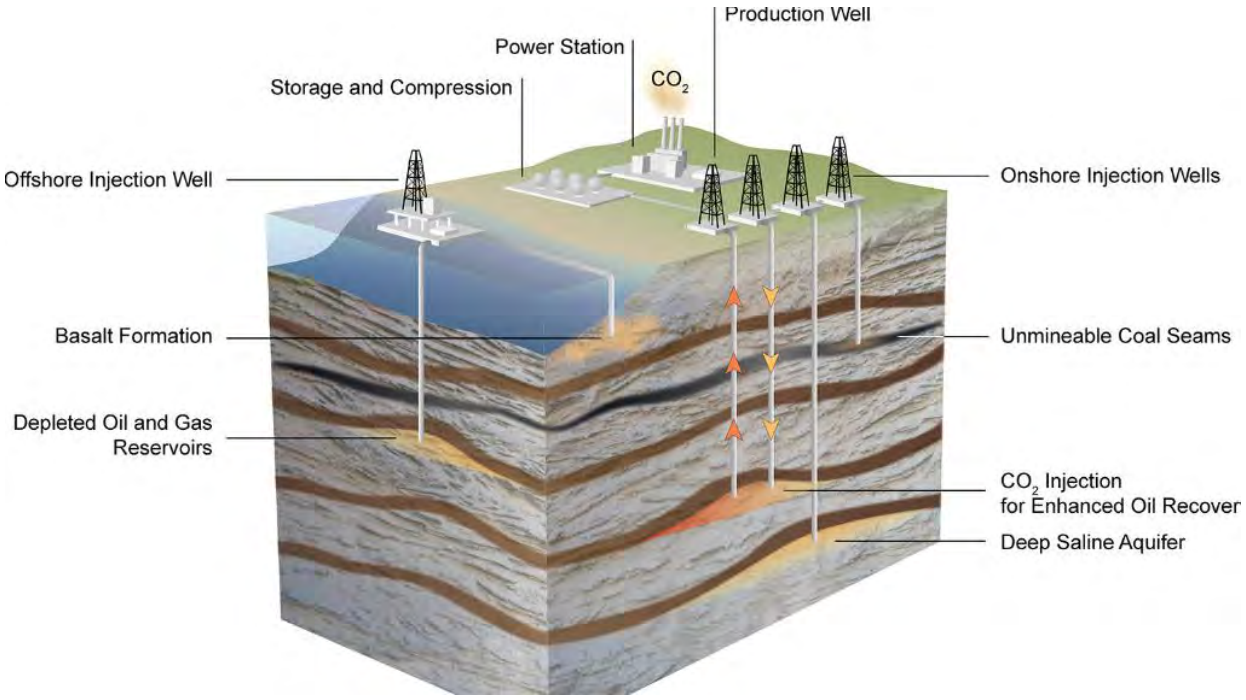

Figure 3.2: *A sketch of geological formations suitable for CO_2 storage depicting the depleted oil and gas reservoirs, deep saline aquifer and unmineable coal seams which can be potential CO_2 storage sites(Ali et al., 2022).*

3.2.1 Depleting oil and gas reservoirs

Most suitable option for safe storage of CO_2 is depleting oil and gas reservoirs. The main cause of low risk for potential CO_2 leakage is due to reservoir exploration, long term production, which leads to the collection of a significant amount of reservoir data, and the accessibility of production history that enables precise storage capacity estimation. The existence of essential infrastructure, such as injection wells and surface facilities, plays a crucial role in substantially cutting down storage expenses. Various pre-existing wells could potentially serve as potential pathways for CO_2 migration to the surface in this type of storage setup (Tomić et al., 2018).

According to the Global CCS Institute (2014), the projected storage capacity ranges between 675 and 900 Gt CO_2.

3.2.2 Saline Aquifers

Saline aquifers are of paramount importance due to their immense storage potential, surpassing other geological formations. However, their significance remains untapped as they lack thorough exploration and essential infrastructure like injection wells and pipelines. Properly utilizing these formations for storage necessitates substantial investments to mitigate the potential risks of CO_2 leakage. Various trapping mechanisms, such as structural trapping, residual trapping, solubility, and mineral trapping, operate over different time frames, thereby enhancing the safety of storage (Aminu et al., 2017). According to Cook (2012), the estimated storage capacity of these aquifers ranges from 1,000 to 10,000 Gt CO_2.

3.2.3 Unmined Coal beds

The concept of storing CO_2 in unmined coal relies on CO_2 adhering to the coal surface and within fractures. In this process, methane is extracted because CO_2 exhibits a higher adsorption capacity than methane (IEAGHG, 2007). This approach serves a dual purpose, functioning as both CO_2 storage and enhanced coalbed methane recovery (ECBM). According to Cook (2012), the estimated storage capacity for this method ranges from 3 to 200 Gt CO_2.

3.3 Geological considerations for CO_2 storage

Geological characteristics of formation evaluated for CO_2 storage site are type of basin, lithology, reservoir depth, thickness, porosity, hydrocarbon saturation, permeability, permeability of cap rock, presence of faults and stress state of rock (Aminu et al., 2017).

When considering CO_2 storage in depleted oil or gas reservoirs, or during the EOR-CO_2 process, various factors are considered. These include the values of original oil in place or gas in place (OOIP or OGIP), the amount of recoverable oil or gas reserves, reservoir pressure and temperature, reservoir rock volume, porosity, water saturation, potential water inflow, phase behavior of CO_2, CO_2 solubility in water, and the possibility of a spill point (Tomic et al., 2018). Tables 3.1 and 3.2 provide the ideal reservoir and fluid parameter values for conducting initial assessments of potential CO_2 storage during the EOR-CO_2 process and in aquifers.

Table 3.1: *Optimal reservoir and fluid parameters for EOR -CO_2 (Terry, 2001).*

	VALUES
DENSITY, API	>25
VISCOSITY, MPAS	<12
OIL SATURATION, %	>30
FORMATION TYPE	sandstone or carbonate
NET THICKNESS, M	5-7,5
PERMEABILITY,	non-critical
DEPTH,M	>600

Table 3.2: *Optimum reservoir and water parameters (Chadwick et al., 2008).*

RESERVOIR AND FLUID PARAMETERS	
DEPTH, M	1000-2500
THICKNESS, M	>50
POROSITY, %	>20
PERMEABILITY, MD	>300
SALINITY, MG/L	>100 000

Considering the criterion given in the Tables 3.1 and3.2, it becomes evident that the most favorable option is to store CO_2 in mature basins with well-established resource potential (estimated hydrocarbon potential - OOIP, OGIP, and recoverable reserves). This choice indicates the availability of abundant data for conducting feasibility studies and guarantees enhanced storage safety (Tomić et al., 2018). Complementary quantitative parameters based on numerical simulation findings (Pratama et al., 2017) are presented in Table 3.3.

Table 3.3: *Optimum reservoir parameters (Pratama et al., 2017).*

RESERVOIR PARAMETERS	
DEPTH, M	>500
RESERVOIR TEMPERATURE, °C	<100
FRACTURE PERMEABILITY, MD	>2
MATRIX POROSITY %	>0,5

3.4 Thermodynamic and hydrodynamic criteria for CO_2 Storage

Thermodynamic considerations involve two main factors: temperature gradient and pressure gradient. CO_2 is introduced into the reservoir in a supercritical state, achieved by compressing and heating it above its critical point, where the pressure of the reservoir exceeds 7.38 MPa and the temperature surpasses 31.1 °C. Under these conditions, CO_2 exhibits properties of both gas and liquid, displaying characteristics such as liquid-like density and gas-like viscosity.

The minimum depth required for CO_2 injection in a supercritical state is approximately 800 meters, considering the hydrostatic gradient in the formation and the Earth's geothermal gradient (25-30 °C per kilometer). As the depth increases beyond this point, the volume of injected CO_2 decreases significantly (Aminu et al., 2017).

A phase diagram of CO_2 for CCS shown in Figure 3.3 illustrates how carbon dioxide (CO_2) transitions between its different physical states (phases) under varying combinations of pressure and temperature conditions. In the diagram low pressure and high temperature conditions represent CO_2 in its gaseous state. The middle region of the diagram, at elevated pressures and

temperatures, CO_2 exists in a state known as "supercritical." In this phase, CO_2 exhibits properties of both a gas and a liquid.

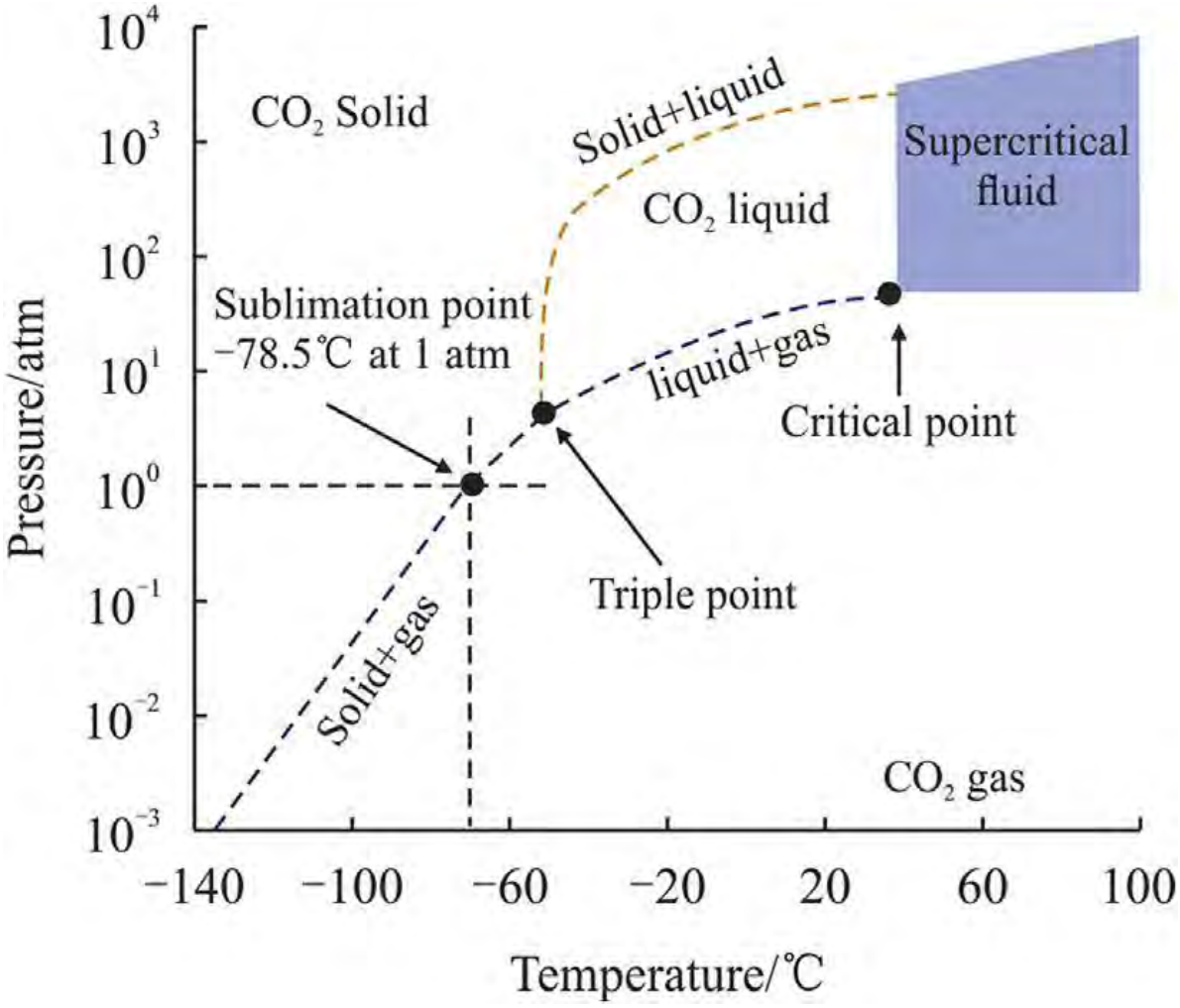

Figure 3.3: *Phase diagram of CO_2 depicting CO_2 transitions between its different physical states (phases) under varying combinations of pressure and temperature conditions (Raza et al., 2019).*

3.5 Seismic analysis and reservoir assessment in CCS projects

Seismic analysis and reservoir assessment are critical components of CCS projects, offering indispensable insights into the geological and geophysical aspects of potential storage sites.

These techniques are pivotal for ensuring the feasibility, safety, and long-term success of CCS initiatives.

3.5.1 Seismic Analysis

Seismic analysis involves the interpretation of seismic data, acquired through techniques like reflection seismology and seismic surveys. Seismic data assist in identifying geological formations, subsurface structures, and potential storage reservoirs. They contribute to site selection and validation, ensuring geologically suitable locations for CO_2 storage. Seismic data allow for the identification and characterization of faults and fractures, which can influence the migration of CO_2 and its containment within the storage formation (Barlass and Head, 2022).

3.5.2 Reservoir Assessment

Reservoir assessment entails comprehensive evaluation of subsurface formations intended for CO_2 storage. Assessing properties like lithology, porosity, and permeability is crucial for estimating storage capacity. Reservoir assessment involves evaluating the integrity of cap rocks, such as shale formations, to ensure their sealing properties and prevent CO_2 leakage (Chadwick et al., 2005). Combining seismic data and reservoir assessment helps identify potential risks, such as fault activation or cap rock failure, contributing to risk management strategies.

3.5.3 Machine Learning Approaches

Machine learning (ML), a rapidly advancing domain in modern times, stands as a significant avenue for predicting future demand through the amalgamation of computer science and data statistics. This endeavor offers an all-encompassing examination of ML's role within CCS, encompassing both classical ML methodologies and prevailing research trajectories in the CCS realm. The investigation reveals the prominent deployment of ML algorithms like artificial neural networks (ANN), PNN, Multi-linear Regression (MLR) and convolutional neural networks (CNN), predominantly in forecasting physical attributes, assessing mechanical robustness, and surveilling the movement and potential escape of CO_2 plumes during storage (Yao, et al., 2023).

CHAPTER#4

WELL LOG ANALYSIS

4.1 Introduction

A continuous depth related record of geophysical parameters along the well bore, depicting the chemical and physical properties of subsurface geological formations is known as well log analysis. In this research, the analysis of well logs assesses the petrophysical characteristics of typical geological formations, identifies rock types, and examines the Petro elastic properties (Figure 4.1). This evaluation is conducted within the framework of CO_2 storage and caprock integrity, aiming to ensure the efficient utilization and secure long-term storage of CO_2.

Petrophysical analysis is the quantitative assessment of well log data to characterize the rock through its physical and chemical properties. In situ reservoir properties such as volume of shale, porosity, permeability, water saturation, hydrocarbon saturation, fluid phase identification and distribution, elastic rock properties are determined through log data. Petrophysics of the most important and useful tools for reservoir characterization (Macini and Mesini, 2006).

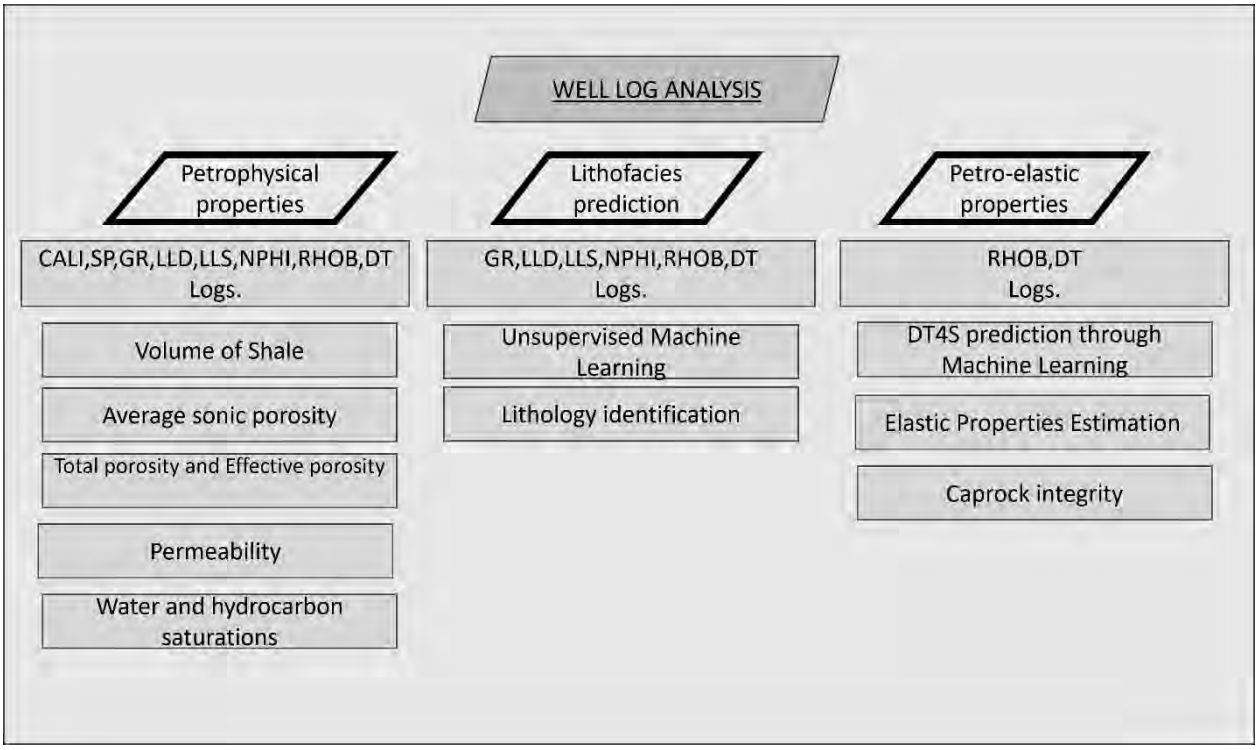

Figure 4.1: *Well log analysis workflow to identify the suitable zone of interest in the subsurface for CO_2 storage.*

4.2 Petrophysical Analysis

Fostering the reservoir model suitable for CO_2 storage requires a detailed log analysis. Comprehensive knowledge about the lithologies found in the subsurface of a prospective storage site is essential. This understanding forms the foundation for creating a dependable reservoir model. Evaluating the rock parameters, crucial for understanding the geological criteria for potential CO_2 storage as discussed in chapter 3, petrophysical investigation was carried out on Qadirpur-16 well, in this study.

Petrophysical analysis evaluates attributes of the reservoir like shale volume, porosity, effective porosity, water saturation, and hydrocarbon saturation. This is accomplished using standard log data and a variety of established empirical relationships (Akhter et al., 2015; Ali et al., 2015). For example, Archie (1942) formulated a mathematical equation for determining water saturation in sedimentary reservoir rocks. Wyllie (1958) introduced a relationship (known as the Time-average equation) for calculating porosity based on P-wave velocity. Additionally, Castagna (1985) provided empirical correlations for computing elastic properties in sedimentary rocks. In our study of the Qadirpur area, we followed the methodology outlined by (Akhter et al., 2015; Ali et al., 2015) to calculate reservoir properties at secondary potential reservoir levels.

4.2.1 Qadirpur-16 petrophysical analysis

Log curves in figure 4.2 were loaded into the software and displayed on separate tracks. The first track presents the caliper (CALI), self-potential (SP), and gamma ray (GR) curves. The second track displays the resistivity curves (laterolog deep (LLD) and laterolog shallow (LLS)), while the third track shows the sonic (DT), bulk density (RHOB), and neutron (NPHI) curves. The fourth track contains the estimated shale volume, with a cutoff value of 40% utilized to distinguish between limestone and shale. This cutoff value determines the presence of limestone if the shale volume is below 40%, as illustrated in Figures 4.2 Proceeding on to the subsequent tracks, the fifth track shows total porosity, and effective porosity. In the last track, water saturation calculations were performed and reported, which were then used to determine the average hydrocarbon saturation value.

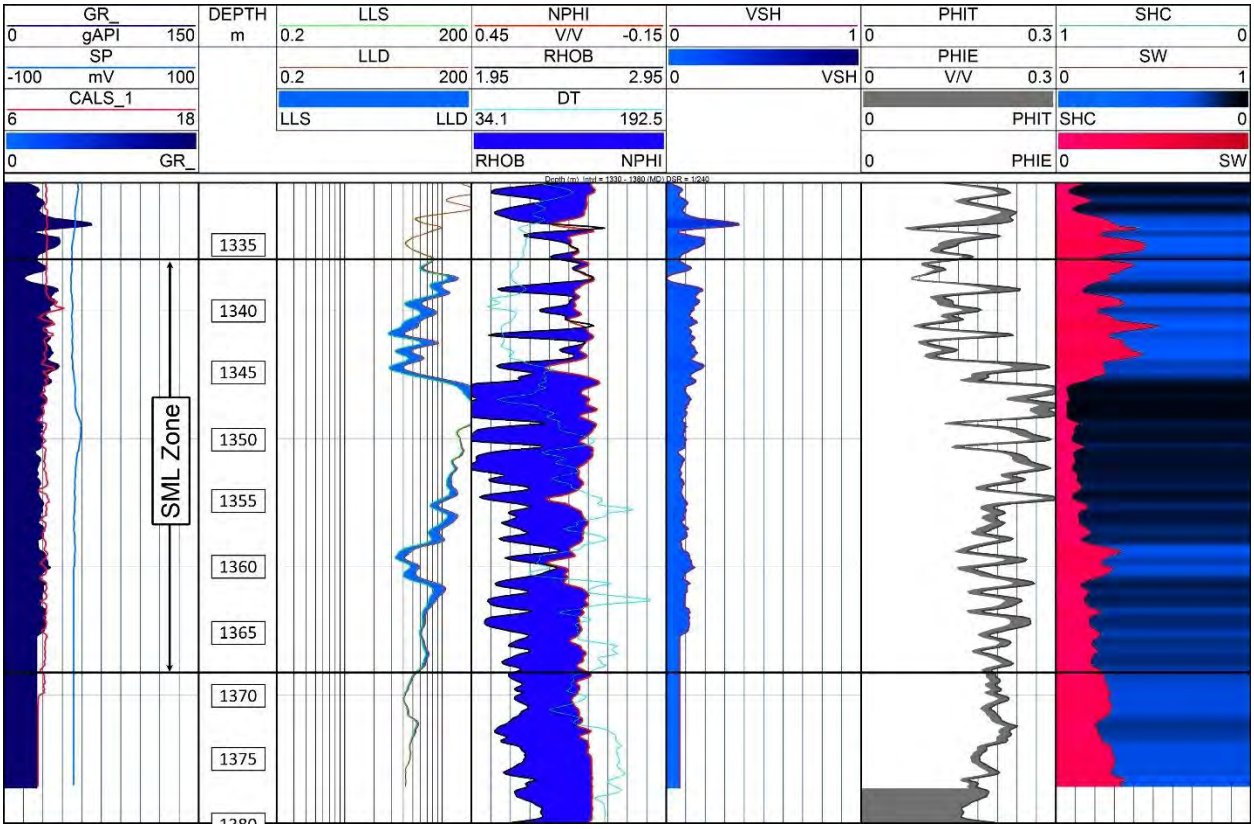

Figure 4.2: *Petrophysical Evaluation of SML of Qadirpur-16 well, Indicating Potential Reservoir Area for CO_2 Sequestration. Tracks 1, 2, and 3 depict lithology, resistivity, and porosity logs. The remaining tracks display inferred properties derived from these logs, facilitating the identification of suitable CO_2 storage sites.*

The main potential zone within the Sui Main Limestone (SML) spans a total width of 30 meters and is situated between depths of 1336 and 1366 meters as depicted in Table 4.1. In this interval, the volume of shale curve displays a significantly distinct behavior with a negative trend. The upper layers of the SML consist of inter-bedded clays and muds, indicating a reservoir of low quality.

Various log curves, including density, sonic, total, and effective porosities, exhibit a positive trend, suggesting the possibility of a hydrocarbon-rich zone. Notably, the effective porosity reaches its highest value within the 1336 to 1366 meters range, with an average of 18.62 percent. Additionally, the hydrocarbon saturation is relatively high at 80.72 percent, while the water saturation measures 19.27 percent in this section.

Table 4.1: *provides the petrophysical characteristics for the SML Formation.*

Calculated Petrophysical Parameters	Zone-01 (1350-1386 meter) PERCENTAGE (%) Sui Main Limestone Thickness = 30m
Average Shale Volume (V_{shale})	10.60
Average Sonic Porosity (PROS)	30.61
Average Porosity (PHIT)	21.09
Average Effective Porosity (PHIE)	18.86
Average Saturation of Water (Sw)	19.27
Average Saturation of Hydrocarbon (Sh)	80.72

4.3 Lithofacies Analysis

Identifying lithofacies is a crucial aspect of reservoir characterization. However, traditional methods that rely on core data can be expensive and challenging to apply to wells without core samples. To address this, we introduce an affordable and automated approach that utilizes Kohonen self-organizing maps (SOM), to identify lithofacies systematically and objectively from well log data. SOMs are unsupervised artificial neural networks that organize the input data into clusters based on well log patterns, revealing trends within the data (Chang et al., 2002).

The process of effectively classifying lithologic units through the application of advanced machine learning techniques, our objective is to leverage data-driven approaches to enhance the accuracy and reliability of lithologic classification, contributing to a deeper understanding of subsurface geology.

4.3.1 Artificial Neural Networks (ANN)

Neural networks, a class of machine learning algorithms, draw inspiration from the intricate interconnectedness of neurons in the human brain. They consist of interconnected nodes, or "neurons," organized in layers. Each neuron processes input data and passes the result to other

neurons. Neural networks are used in machine learning to learn patterns, make predictions, and perform tasks such as image recognition and natural language processing. Central to neural networks are interconnected nodes referred to as "neurons," systematically arranged into layers. These neurons engage in processing and altering input data, progressively extracting more complex features and representations. Leveraging advances in hardware capabilities and inventive algorithms, neural networks have yielded groundbreaking achievements across diverse fields (Krogh, 2008).

The origins of neural networks trace back to the 1940s, marked by the foundational contributions of McCulloch and Pitts regarding artificial neurons. However, their full potential emerged in the 1980s with the introduction of the backpropagation algorithm, enabling efficient training of multi-layer neural networks. Subsequently, an array of variations and architectures has surfaced, encompassing CNNs tailored for image analysis and recurrent neural networks (RNNs) designed for sequence data. Computational techniques for acquiring and structuring novel knowledge leading to the acquisition of fresh skills. Before the network can demonstrate usefulness, it must assimilate information currently available. Following training, it can then serve practical purposes. Broadly, there exist two categories of learning approaches (Mahesh, 2020):

4.3.1.1 Supervised Learning

In this approach, the network is provided with known correct answers that aid in training for a specific problem. Both input and output vectors are utilized. Input vectors furnish initial data, and output vectors enable comparison with inputs to ascertain discrepancies. Reinforcement learning, a specialized form of supervised learning, informs the network only of output correctness. Back-propagation algorithms align with this style.

4.3.1.2 Unsupervised Learning

The network autonomously endeavors to uncover patterns in the input data. Solely input vectors are employed, and generated output vectors aren't employed for learning. Notably, human interaction becomes pivotal for unsupervised learning. This facet proves particularly significant, especially when dealing with expansive or intricate datasets that could be arduous or time-consuming for human computation. SOMs operate within this learning paradigm.

4.3.2 Self-Organizing Maps (SOM)

Kohonen SOMs, introduced by Kohonen in 1982, are unsupervised artificial neural networks designed to create organized feature maps of input data through clustering. These maps preserve the topological relationships among the clusters, resulting in similar high-dimensional input data being mapped close to each other. SOMs function as two-layer, fully connected networks with a weight matrix and are often referred to as "topology-preserving maps" due to their ability to maintain the topological structure among the cluster units (Guthikonda, 2005).

4.3.2.1 Structure of SOM

Structure of SOM's describes its training mechanisms which enable it to capture connections within input data and underlying patterns, creating a compressed illustration in the form of clusters. Figure represents the basic structure of SOM's structure.

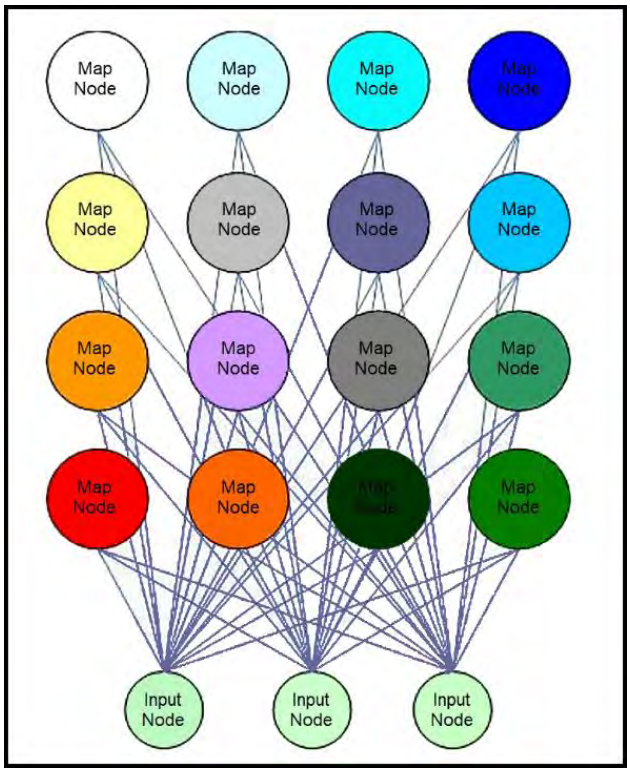

Figure 4.3: *4x4 SOM network is depicted, featuring 4 nodes arranged vertically and 4 nodes horizontally (Guthikonda, 2005).*

While this configuration might seem uncomplicated, it holds noteworthy aspects. Initially, each map node establishes connections with every input node. For this compact 4x4 node network, this amounts to a total of 48 connections (4x4x3). Additionally, it's important to observe that map nodes remain unlinked to each other. This organization, resembling a 2D grid, simplifies result visualization and aligns effectively with the utilization of the SOM algorithm. Such a layout assigns a unique (i,j) coordinate to each map node, simplifying node referencing and distance computation. Despite exclusively being linked to input nodes, map nodes remain unaware of their neighboring nodes' values. The update of a map node's weights is solely influenced by the input vector's information.

4.3.3 Algorithm of SOM

Following steps explains the SOM algorithm (Guthikonda, 2005):

1. Initializing each weigh node.
2. Random vector is chosen from training data set and presented to the network.
3. Best Matching Unit (BMU) is determined, which is weights of node that are most like the input vector. Euclidean distance is the one of the methods to find BMU through formula:

   $$B^2 = \sum_{i=0}^{i=n}(I_i - W_i)^2, \quad (4.1)$$

   where, B represents BMU, I denote current input vector, W is node's weight vector and N is the number of weights.

4. The size of the neighborhood around the BMU is determined by calculating its radius. Initially, this radius is relatively large, often set to match the radius of the network, and it decreases with each time-step. The radius of the neighborhood is calculated through the formula:

   $$\sigma(t) = \sigma_{\circ} e^{-t/\lambda}, \quad (4.2)$$

   $$\lambda = numIterations/mapRadius,$$

where, t represents the current iteration, λ is the time constant and $\sigma_\circ$ is the radius of the map.

5. Any nodes located within the radius of the BMU undergo adjustments aimed at aligning them more closely with the input vector. The extent of weight alteration is influenced by proximity to the BMU, with nodes in closer vicinity experiencing greater changes in their weights. They are computed as follow:

   New weight of the node:

   $$W(t+1) = W(t) + \Theta(t)L(t)(I(t) - W(t)) \quad (4.3)$$

   Learning rate:

   $$L(t) = L_\circ e^{(-t/\lambda)} \quad (4.4)$$

   Distance From BMU:

   $$\Theta(t) = e^{(D^2/2\sigma^2(t))} \quad (4.5)$$

6. For N number of iterations repeat from step 2.

Considerable variation is observed in the equations employed within the SOM algorithm (Figure 4.4). Likewise, ongoing research aims to determine the optimal parameters. Notably contentious aspects encompass the count of iterations, the learning rate, and the neighborhood radius. Kohonen himself has proposed a two-phase training approach. Phase 1 involves reducing the learning coefficient from 0.9 to 0.1 and the neighborhood radius from half the lattice's diameter to immediately adjacent nodes. In Phase 2, the learning rate decreases from 0.1 to 0.0, while the number of iterations in Phase 1 is at least doubled. During Phase 2, the neighborhood radius remains fixed at 1, solely encompassing the BMU. Analyzing these parameters, Phase 1 expedites the network's coverage of space, while Phase 2 fine-tunes the network to achieve a more precise representation.

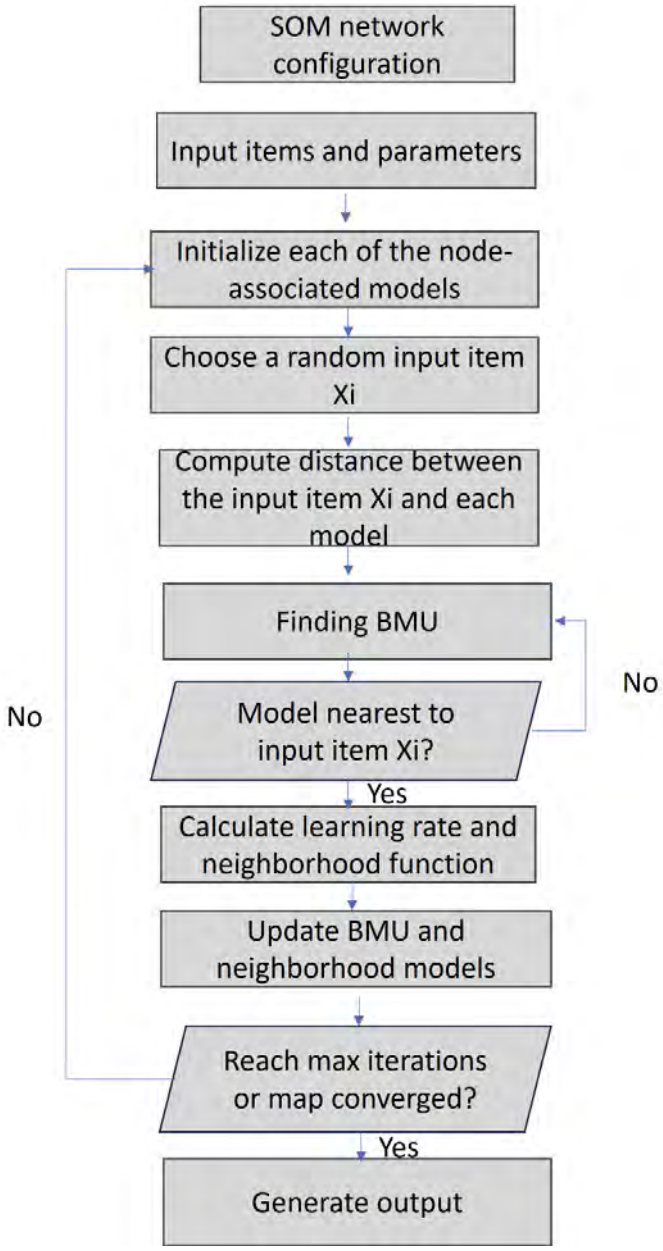

Figure 4.4: *Flowchart depicting sequential steps followed in the application of SOM algorithm.*

Figure 4.5 represents the methodology adopted for implementation of unsupervised machine learning SOM techniques on Qadirpur-16 well through python and R programming language for lithofacies prediction:

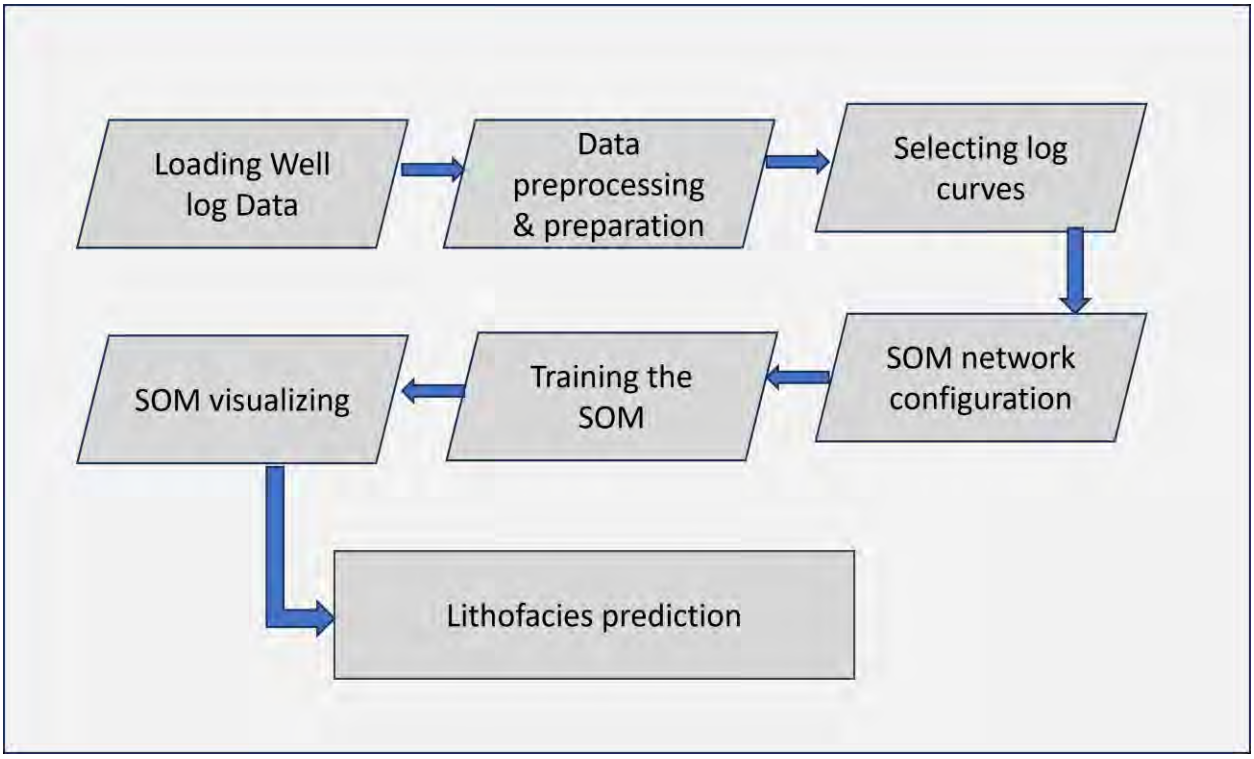

Figure 4.5: *Methodology for unsupervised machine learning SOM approach to predict lithofacies.*

4.3.4 Data loading into python

Importing data involves using specific Python libraries to read and process it. These libraries include pandas, NumPy, SciPy, lasio, segyio, matplotlib, seaborn etc. Choose the curve to use (correlation, discard curve with low correlation). Identify missing values in the training and testing data and remove the NaN values. Merge data into a single data-frame for further processing.

4.3.5 Data Preparation and Processing

4.2.5.1 Selection of logs through Heatmap analysis:

Heatmap depicts the 2D visualization of correlation matrix between variables on each axis. The correlation value ranges from-1 to 1, indicating strongly negative correlation as -1 and strongly positive as 1. Zero value indicates no correlation between the variables.

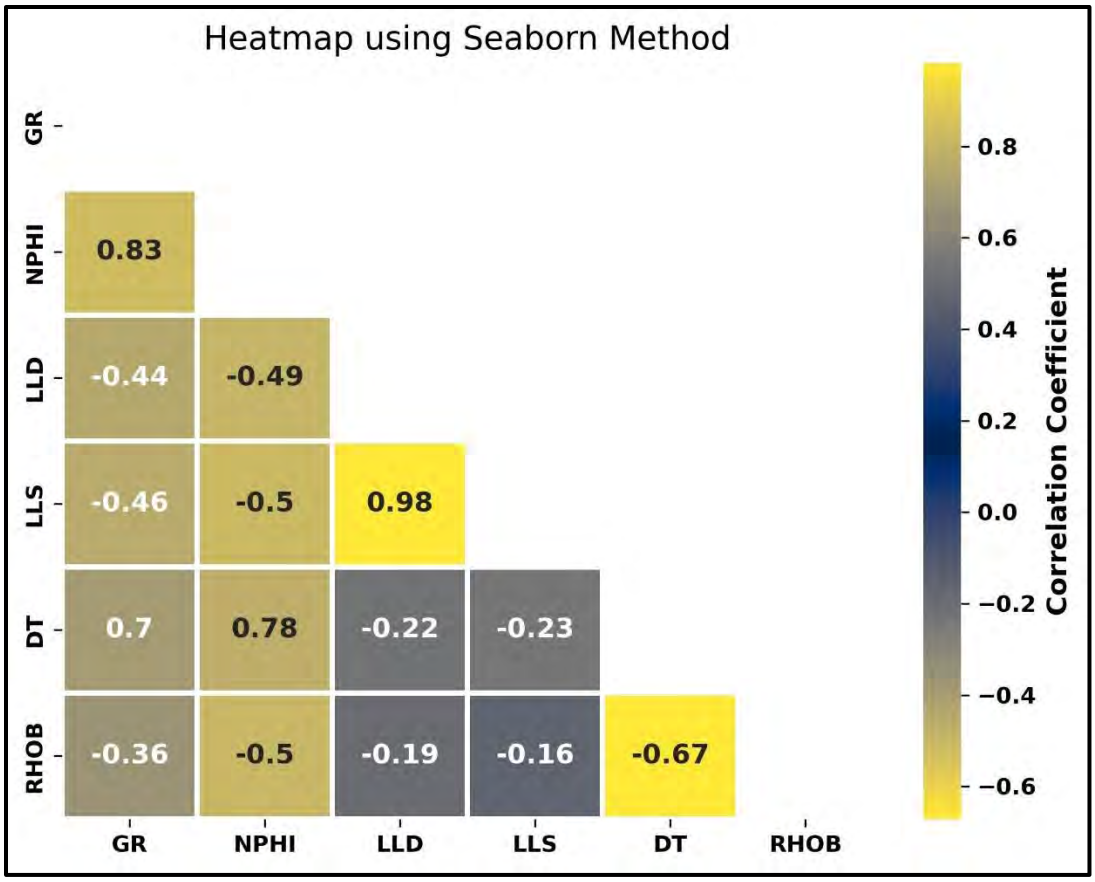

Figure 4.6: *Heatmap Analysis of log curves used as an input for lithofacies classification, depicting the correlation values between logs.*

Through Figure 4.6 heatmap analysis, we examine the correlations and relationships among GR, NPHI, LLD, LLS, DT and RHOB curves. This technique provides visual insights into the interdependencies between variables, depicting correlation value range between -0.67 to 0.98 aiding in identifying significant patterns and potential features for classification.

4.2.5.2 Boxplot and Histplot analysis for identifying outliers:

Boxplot and Histplot analysis are powerful techniques used to identify outliers in a dataset. Outliers are data points that significantly deviate from the overall pattern of the data and can potentially impact the accuracy of classification models.

Boxplots provide a visual representation of the distribution and spread of data. Outliers can be identified as points that lie outside the "whiskers" of the boxplot. The histogram plots assist in

visually identifying the presence and magnitude of outliers in the well data. Outliers often stand out as data points that fall far from the bulk of the distribution, and they can be detected through their placement in sparsely populated bins. Figure 4.7 shows the data distribution of each log curve as normal with only a few outliers, depicting the reliability of dataset used for prediction.

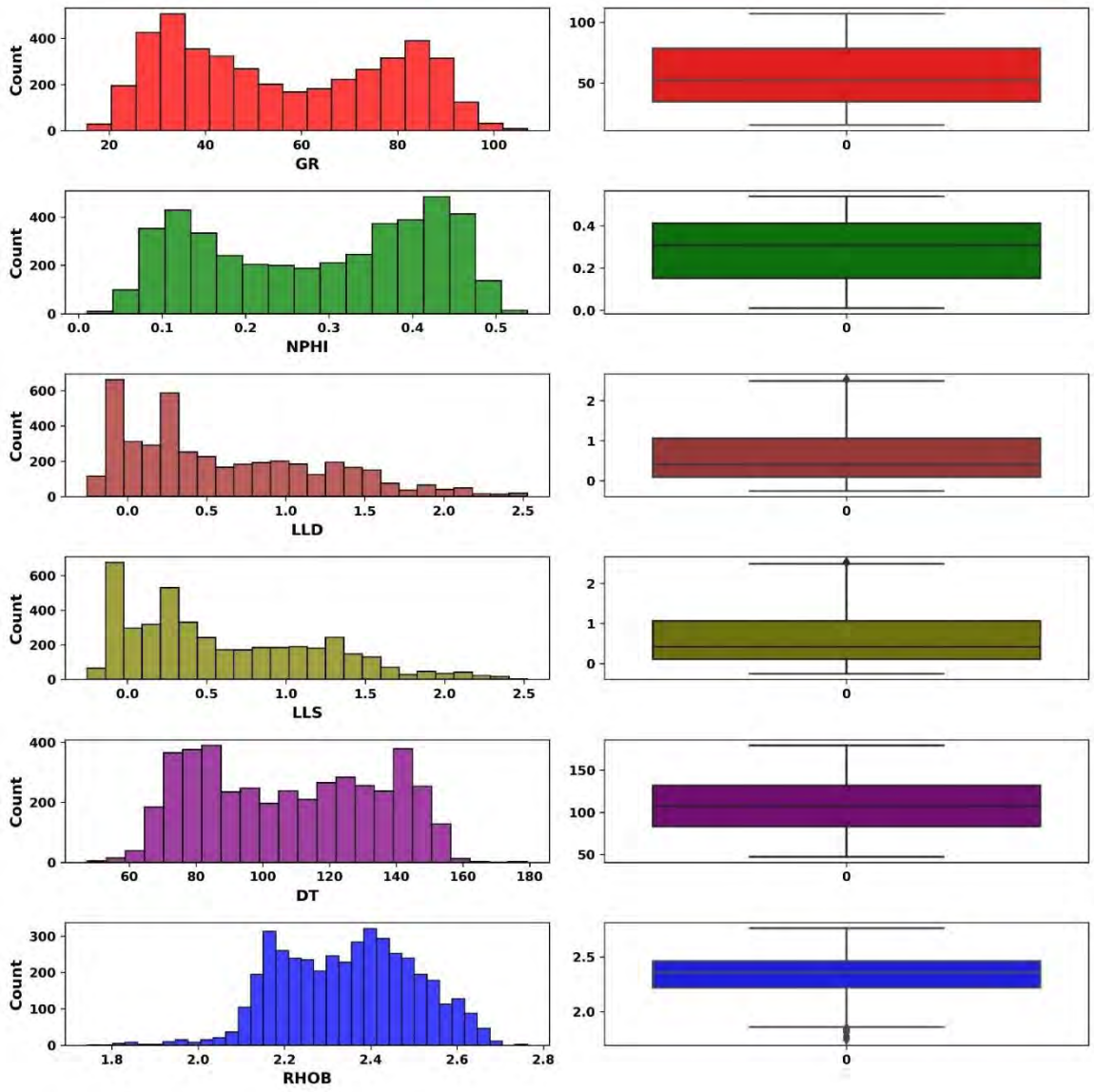

Figure 4.7: *Histogram and boxplot analysis of logs indicating the outliers present in each input log. These outliers are depicted as extreme values with low count in the histograms and as black circles lying outside the respective box of each log in the boxplots.*

4.3.5.1 Outlier Removal:

Outliers in a dataset can negatively impact the accuracy and performance of machine learning models. To mitigate this, we can use advanced techniques like One-Class Support Vector Machine (SVM) and Isolation Forest to identify and remove outliers (Figure 4.8).

Data normalization is a crucial preprocessing step to ensure that features are on a similar scale, preventing certain features from dominating others in machine learning algorithms. MinMaxScaler was used for normalization that scales features to a specified range, usually between 0 and 1 (Figure 4.9).

One-Class SVM is a machine learning algorithm that identifies anomalies or outliers based on the concept of margin maximization. It learns the distribution of the majority class and identifies instances that deviate significantly from it. It identifies 43 outliers from the total number of data set. Isolation Forest is an ensemble-based algorithm that creates a random forest of isolation trees. It isolates outliers by partitioning data points using random splitting rules and identifying instances that require fewer splits to be isolated. It identifies 44 outliers from the total number of data set.

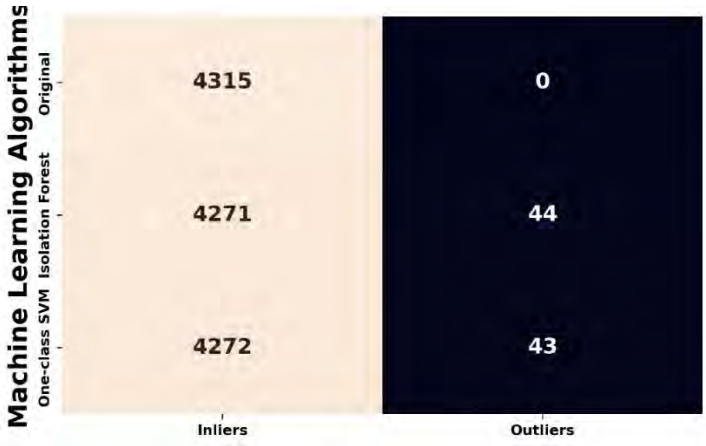

Figure 4.8: *Identification of outliers and inliers through isolation forest and one class SVM algorithms.*

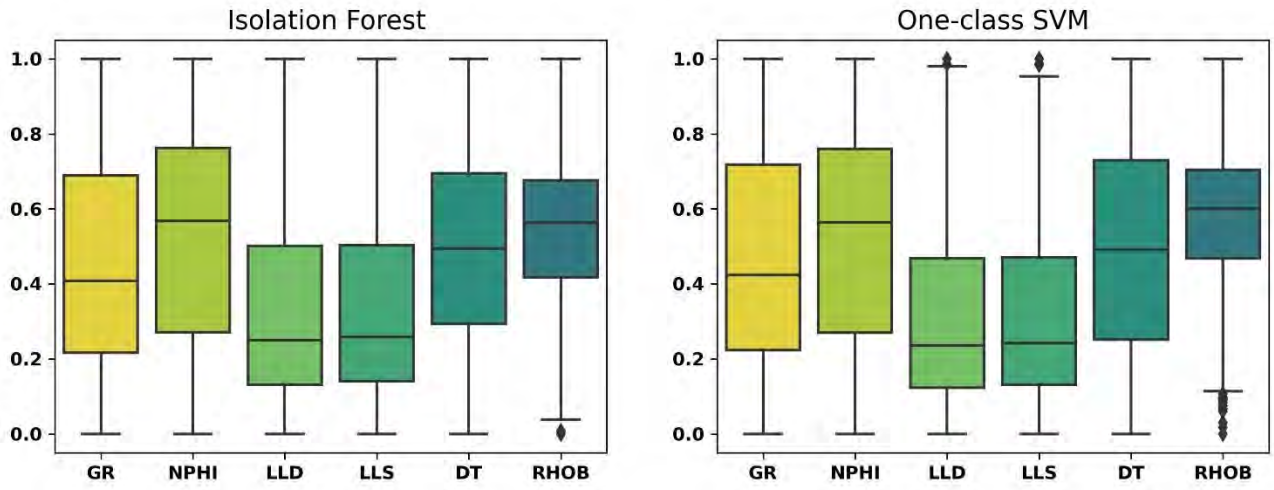

Figure 4.9: *Boxplot after normalization and removal of outliers from data.*

4.3.6 Model Training

The training data after processing is first transformed into a matrix and then scaled. Afterward, the SOM grid is defined with specific dimensions and topology. Using this grid, a SOM model is constructed by incorporating the training data, the predefined grid structure, learning rate, and iteration count. Visualizations are generated to illustrate the model's progression, including plots showcasing changes during training, the count of units within each cluster, distances between neighboring units on the SOM grid, and codebook vectors of the trained SOM. Furthermore, the codebook matrix is extracted from the trained model, enabling the calculation of within-cluster sum of squares (WCSS) for varying cluster numbers. To facilitate interpretation, plot margins are adjusted, and a plot depicting WCSS values for different cluster counts is generated.

4.3.6.1 Training process

The training process of a SOM involves the gradual adjustment of neuron weights within the map based on input data. Neurons are nodes within the SOM grid, and their weights define the map's representation of data patterns. During training, the weights are iteratively updated to align with input data, leading to the map's ability to capture and organize complex relationships. Figure 4.10 represents 100 iterations with the mean distance to the closed unit.

Figure 4.10: *Graphical representation of number of Iterations during training data and the mean distance to closest unit.*

4.3.6.2 WGSS Analysis

The Within-Group Sum of Squares (WGSS) analysis is a method to determine the optimal number of clusters in a SOM or any clustering algorithm. WGSS measures the compactness of clusters by calculating the sum of squared distances between data points and their assigned cluster centroids. By plotting the WGSS values against different numbers of clusters, an "elbow point" can be identified. This point signifies a balance between cluster compactness and preventing overfitting. The optimal cluster count is often chosen at the elbow point, as it provides a suitable trade-off between data separation and cluster complexity. WGSS analysis (Figure 4.11) of the input dataset reveals four clusters based on the calculated sum of squared distances between data points.

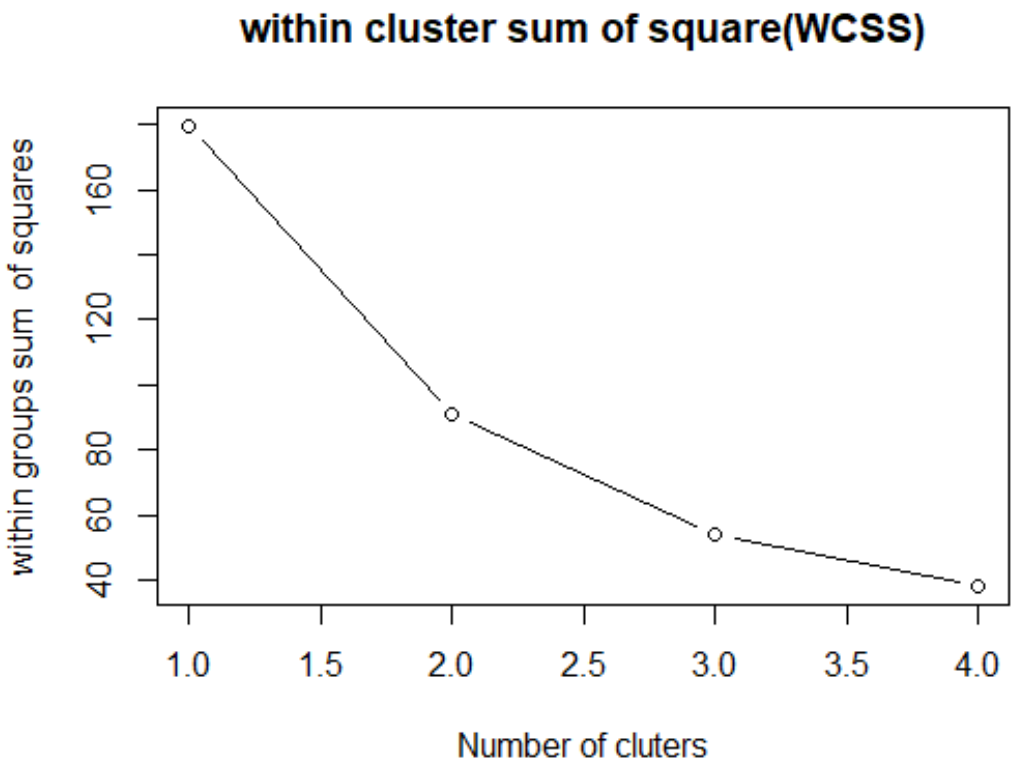

Figure 4.11: *WCSS representing Four clusters based on calculated sum of squared distance between input data points.*

4.3.6.3 Codes plot

A codes plot is a visual representation of the codebook vectors associated with neurons in SOM. Codebook vectors are weight vectors that evolve during training to represent specific data patterns. In a codes plot, these vectors are visualized in a scatterplot-like format. The spatial arrangement of codebook vectors reflects the SOM's organization of data. By analyzing the codes plot, insights can be gained into how the SOM clusters similar data points, revealing the map's ability to capture data distribution, uncover clusters, and identify regions of interest. Figure 4.12 provides insight into how the SOM has organized and clustered your well log data based on the patterns present in RHOB, LLD, LLS, GR, DT, and NPHI logs.

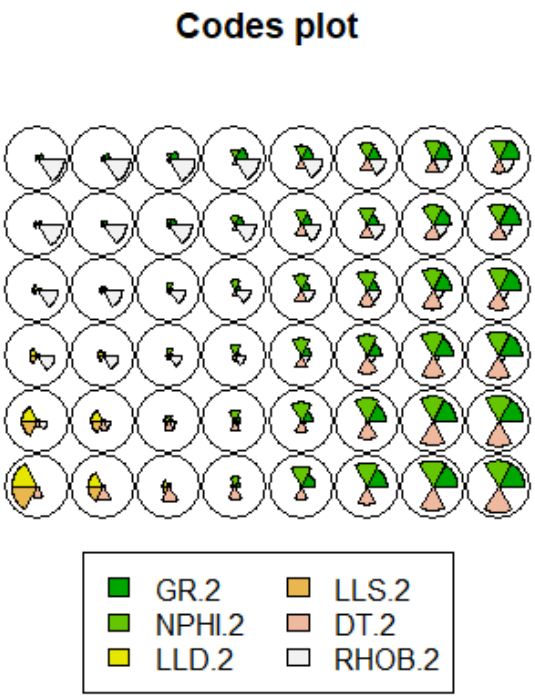

Figure 4.12: *Code plot of SOM cluster analysis based on the patterns present in RHOB, LLD, LLS, GR, DT, and NPHI logs.*

4.3.6.4 Cluster plots

A cluster plot is a graphical display that showcases the results of clustering achieved by a trained SOM. Through its organization of data points based on similarity, the SOM assigns them to specific clusters. In a cluster plot, data points are differentiated using colors, each denoting membership in a distinct cluster. The cluster plot offers a visual avenue to comprehend how well the SOM groups alike data points and how effectively it captures intricate patterns or outliers within the dataset. By examining the cluster plot, patterns and trends in data become more discernible, aiding in insightful data analysis.

Figure 4.13 describes a visual representation of data clustering, where data points are grouped into four clusters (pink, red, blue, and green) and the plot illustrates how the data points are arranged within each of these clusters.

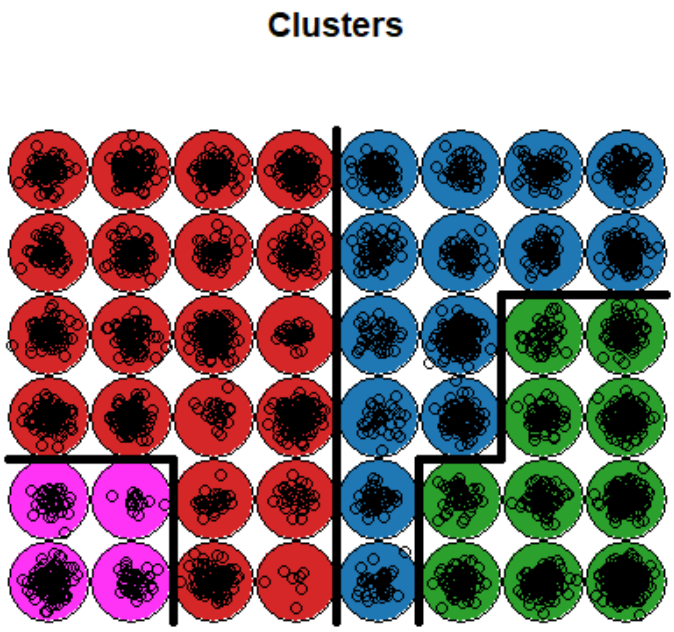

Figure 4.13: *Cluster plot representing four clusters of pink, red, blue, and green colors, and distribution of data points along them.*

4.3.7 Lithofacies prediction

The outcomes of the SOM cluster analysis reveal compelling insights into lithofacies patterns within the well log data. Through the utilization of the SOM, distinct four clusters with green, red, blue and pink colors emerge, each representing a distinct lithofacies grouping based on shared characteristics Figure 4.14. These clusters delineate geological formations and lithological variations that might otherwise be challenging to discern. The visualization of the SOM cluster results provides a comprehensive spatial representation of lithofacies associations, enabling geoscientists to identify geological trends and transitions in depth. By mapping each cluster to specific lithofacies classes, the SOM facilitates the classification of subsurface geological units. This analytical approach not only enhances our understanding of lithofacies distributions but also assists in geological interpretation and subsurface modeling, ultimately contributing to informed decision-making in various geoscience applications.

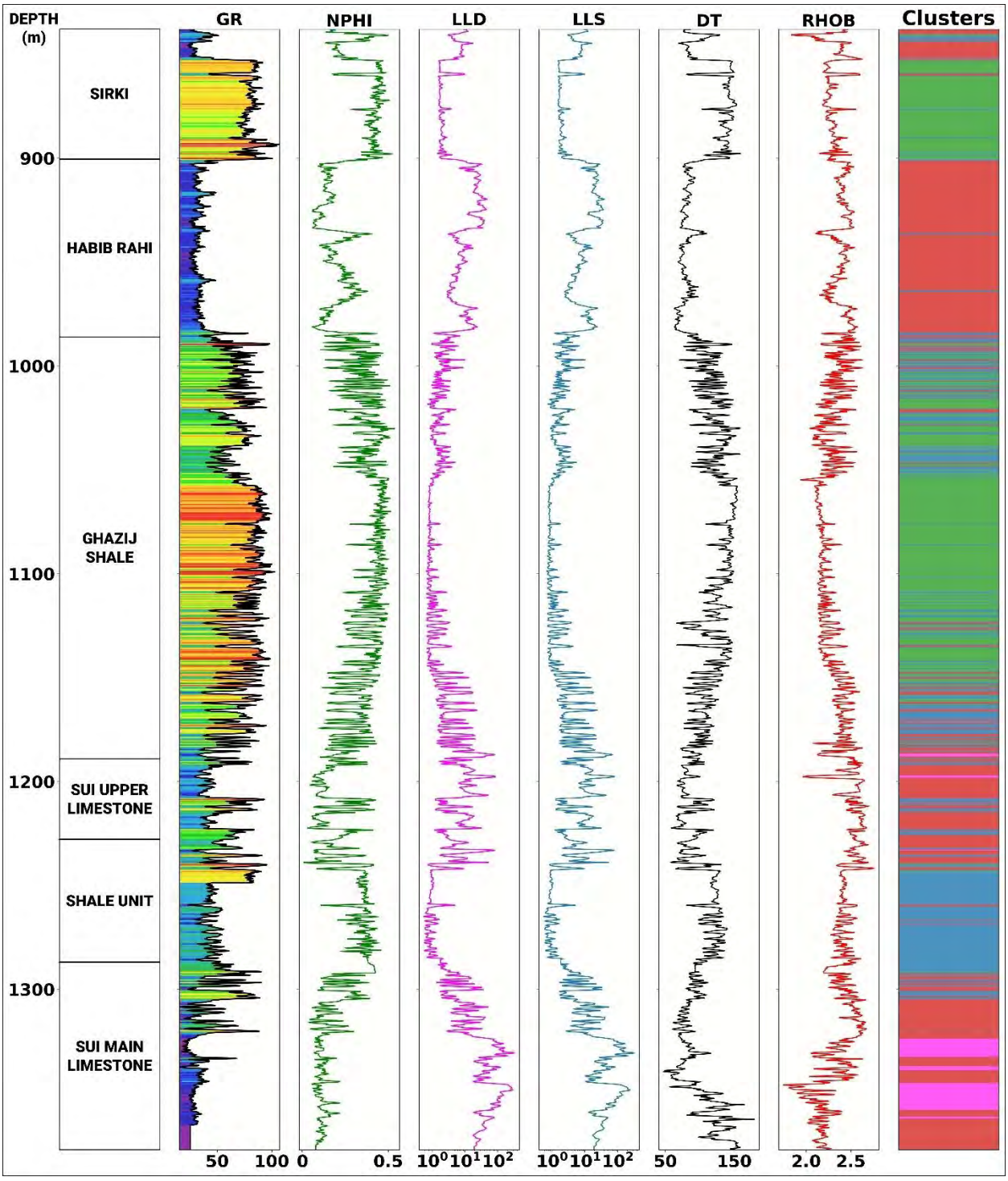

Figure 4.14: *Lithofacies prediction of Well Qadirpur-16 based on SOM. The predicted facies are in accordance with the known lithology of the respective formations with limestone depicted by red color, shale by green, limy-shale by blue, and the hydrocarbon-filled limestone by pink.*

4.4 Sonic Log Prediction Through Multi-Linear Regression (MLR)

The process of predicting sonic logs using Multi-Linear Regression MLR involves utilizing a statistical technique to establish a predictive relationship between sonic log measurements and other relevant attributes. Sonic logs, which provide information about subsurface rock properties, are valuable in various industries, including geophysics and oil exploration.

4.4.1 Input data

The process of predicting the DT4S values for Qadirpur well 16 involves using MLR based on various input logs. These logs include LLD, LLS, RHOB, GR, NPHI, and DT from the Qadirpur-deep well 01 as shown in Figure 4.15.

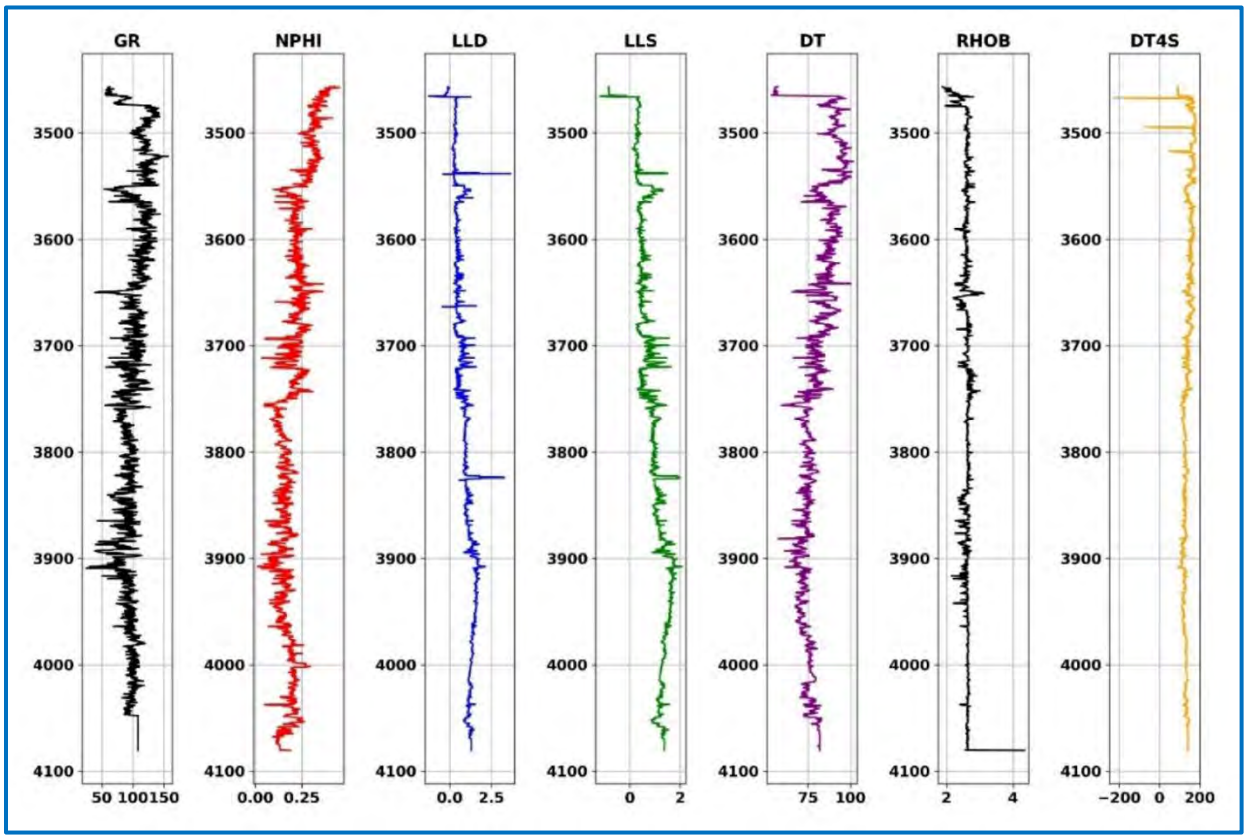

Figure 4.15: *Logs of well Qadirpur deep-01 used as input for sonic log prediction through MLR algorithm.*

4.4.2 Training through Multi linear regression

The approach involves using MLR to predict DT4S values for Qadirpur well 16 based on a combination of attributes from Qadirpur-deep well 01 Figure 4.16. The equation offers a formula to estimate DT4S by considering the coefficients associated with each attribute. This predictive model can provide insights into subsurface properties and aid in various geophysics and reservoir analysis applications.

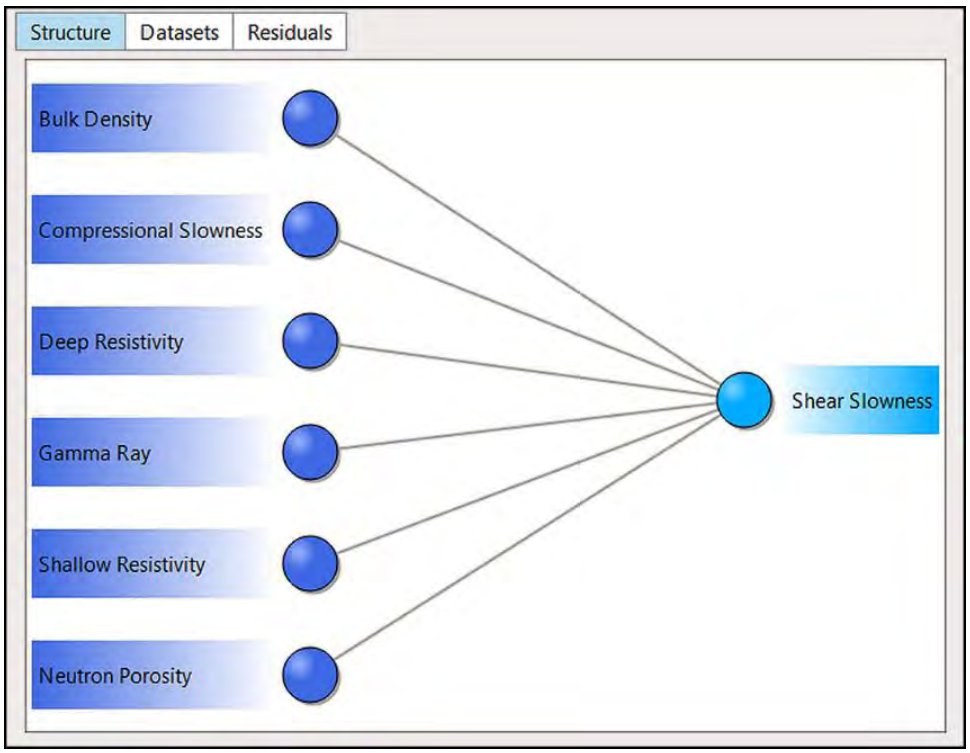

Figure 4.16: *Structure representing a relationship between the attributes (logs) of Well Qadirpur Deep-01 used to predict the shear log through MLR.*

The relationship between sonic log measurements and other relevant logs is described in equation:

$$\boldsymbol{Shear\ Slowness} = +\mathbf{0.8727102} * \boldsymbol{Bulk\ Density}(\boldsymbol{RHOB}) + \mathbf{1.681528} * \boldsymbol{Compressional\ Slowness}(\boldsymbol{DT}) - \mathbf{9.696571} * \boldsymbol{log10}(\boldsymbol{Deep\ Resistivity}(\boldsymbol{LLD})) + \mathbf{0.1073887} * \boldsymbol{Gamma\ Ray}\ (\mathrm{GR}) + \mathbf{8.443502} * \boldsymbol{log10}(\boldsymbol{Shallow\ Resistivity}(\boldsymbol{LLS})) + \mathbf{25.56316} * \boldsymbol{Neutron\ Porosity}(\boldsymbol{NPHI}) - \mathbf{13.08389} \quad (4.6)$$

The equation 4.6 represents the outcome of MLR, where the input attributes are combined with specific coefficients to estimate the DT4S values. Each coefficient signifies the strength and direction of the relationship between the corresponding attribute and the predicted DT4S value.

For instance, the coefficient of Bulk Density (RHOB) is 0.8727102, indicating that an increase in Bulk Density leads to a corresponding increase in the predicted DT4S value. Similarly, the coefficient of Compressional Slowness (DT) is 1.681528, suggesting that higher values of Compressional Slowness result in higher predicted DT4S values. The logarithmic terms, such as log10(LLD) and log10(LLS), imply that the relationship between these attributes and DT4S is logarithmic rather than linear. The success of this MLR model rests on the assumption that the chosen attributes exhibit linear or logarithmic relationships with the target DT4S value. The coefficients derived from the regression analysis reflect how each attribute contributes to the prediction of DT4S.

4.4.3 Testing through cross plot of Actual vs Predicted log

The cross plot in Figure 4.17 visually represents the relationship between predicted and actual DT4S values for well Qadirpur Deep-01. To assess the accuracy of the predictions, R-squared (R2) score was used (Figure 4.17). R-squared score provides insight into the goodness of fit of the model by measuring the proportion of variance explained by the attributes. The high R-squared score of 0.9042 indicates that the predictive model is performing well.

Once the model is trained, it can be applied to the attributes of Qadirpur well 16 to predict its sonic log values (Figure 4.18). The coefficients in equation 4.6 represent the contribution of each attribute to the predicted sonic log value.

By applying this approach, we effectively estimate sonic log values for Qadirpur well 16 based on the attributes of Qadirpur-deep well 01. Ultimately, this methodology aids in enhancing the understanding of subsurface properties and contributes to decision-making processes related to reservoir analysis and hydrocarbon exploration.

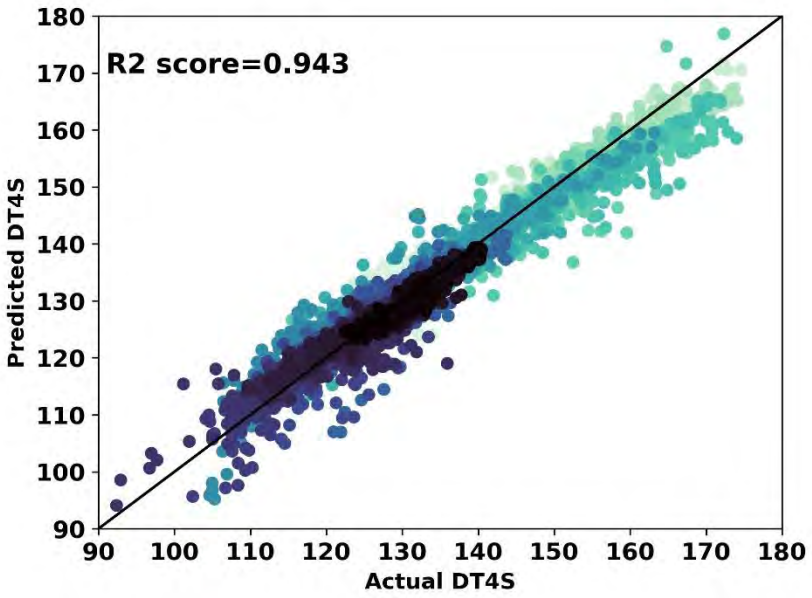

Figure 4.17: *The cross plot of DT4S predicted and Actual DT4S of well Qadirpur Deep-01 with 0.9042 R2 score representing a higher R-squared score, which signifies a larger proportion of the variance is explained by the model.*

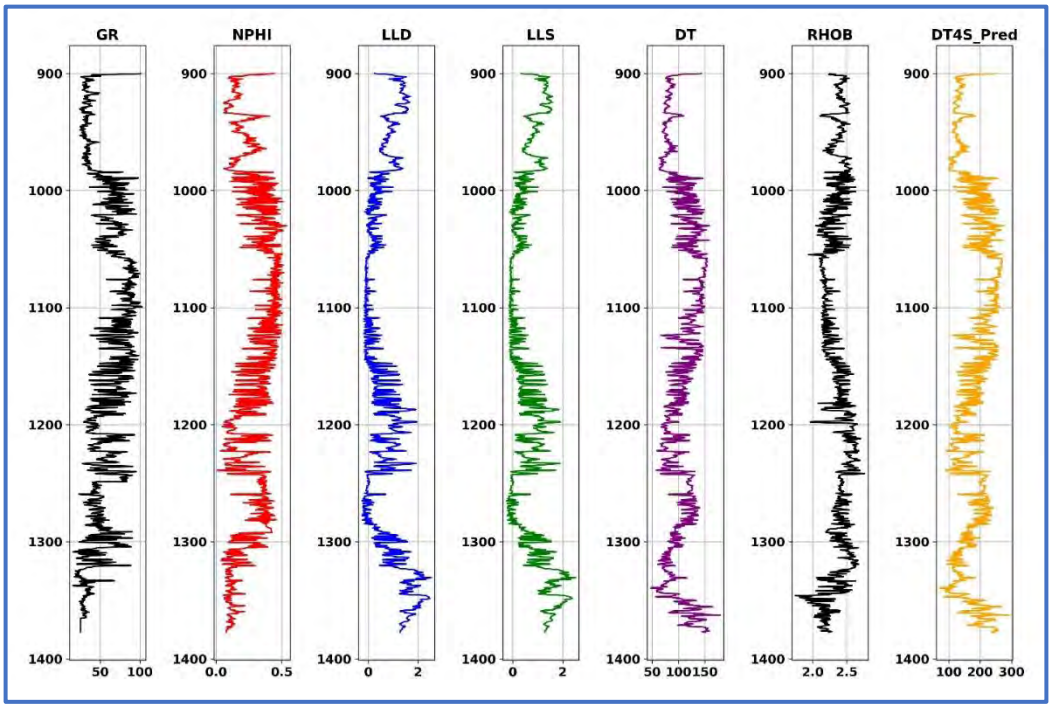

Figure 4.18: *Predicted DT4S Values for Qadirpur Well 16 along with GR, NPHI, LLD, LLS, DT, RHOB logs Using MLR with Qadirpur-deep 01 Attributes.*

4.5 Petro elastic Analysis

Petroelastic properties are derived from the data collected through well log measurements. These properties play a pivotal role in advancing the evaluation of the formations within the well. Specifically, these petroelastic characteristics serve as key indicators for assessing the integrity of the caprock.

In the case of the Qadirpur-16 well, petroelastic parameters are computed utilizing the compressional velocity (Vp) and the predicted shear velocity (Vs) logs. These parameters hold significance in characterizing the petroelastic behavior of the subsurface formations. By utilizing these calculated parameters, the analysis aims to provide insights into the stability of the caprock and the overall geological context within the well. In our study of the Qadirpur area, we followed the methodology outlined by (Mavko et al., 2020) to calculate Petro-elastic properties (Figure 4.19).

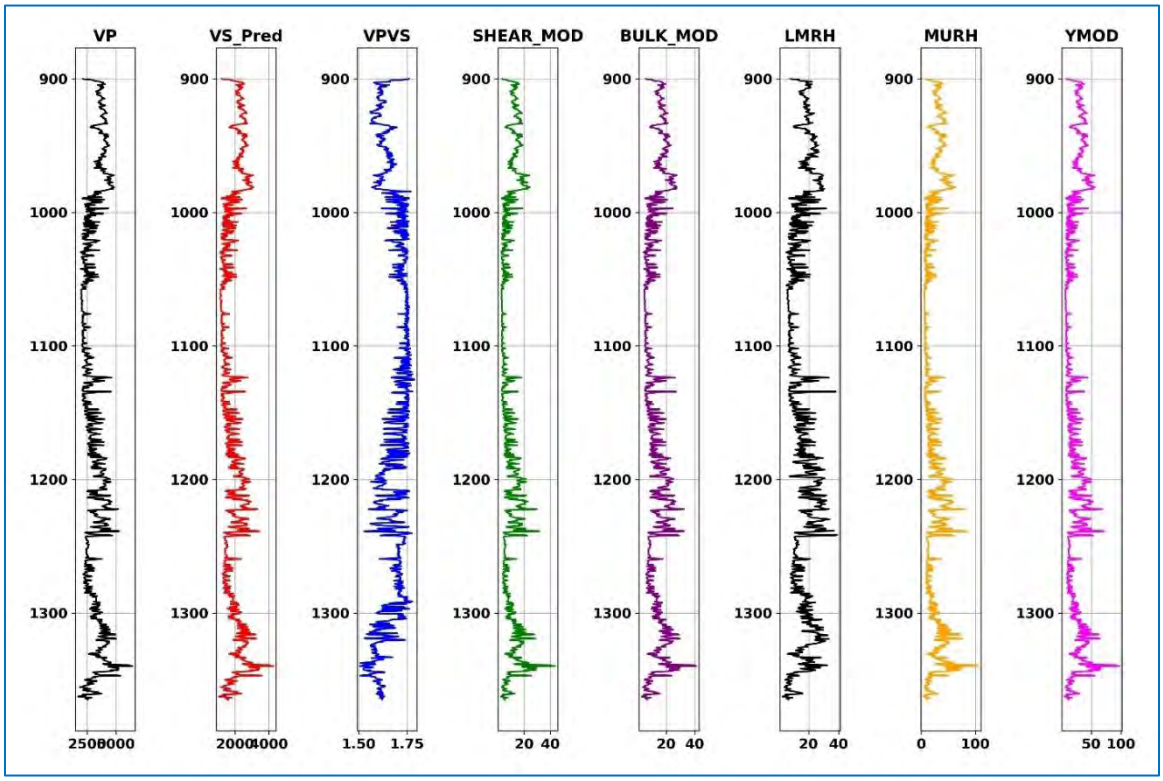

Figure 4.19: *Petro-elastic properties for Qadirpur 16 well estimated using the DT4P, RHOB, and the predicted DT4S logs.*

4.6 Caprock Integrity

The variation of porosity and permeability with lithology as shown in figure 4.20, the analysis helps in identifying regions within the caprock that may pose a risk to caprock integrity. For effective CO_2 storage, it's essential to ensure that the caprock has low permeability and acts as an impermeable seal to prevent CO_2 leakage. Conversely, the reservoir should have sufficient porosity and permeability to accommodate the injected CO_2. This integrated approach allows for a comprehensive assessment of caprock integrity, helping to mitigate risks associated with CO_2 storage and ensuring the long-term containment of CO_2 within the geological formation.

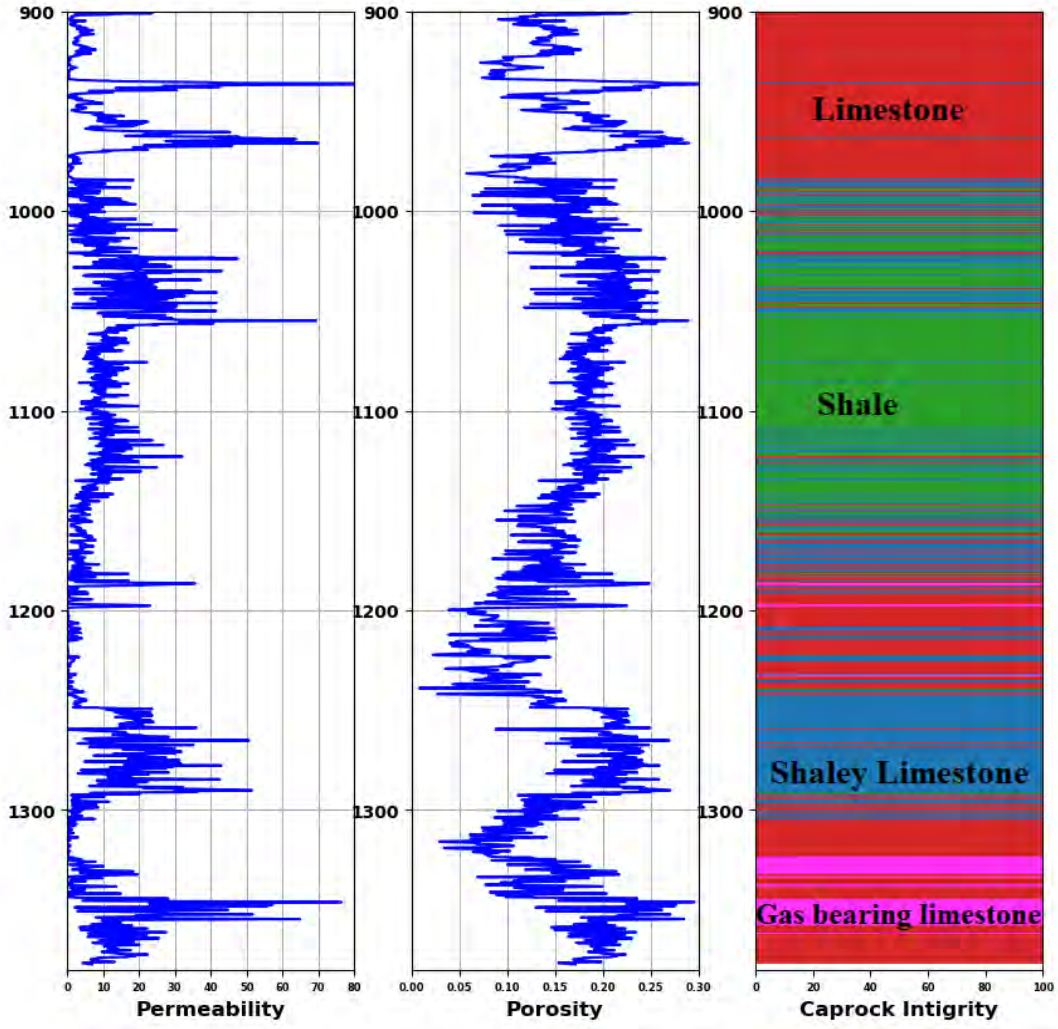

Figure 4.20: *Permeability calculated from Wyllie–Rose approach, PHIE and lithofacies obtained from SOM, depicting the variation of porosity and permeability with lithology.*

CHAPTER#5

SEISMIC ANALYSIS

5.1 Introduction

Seismic analysis is a fundamental component in the assessment and planning of carbon storage strategies, particularly in the context of CCS initiatives. It involves the comprehensive utilization of seismic data to evaluate the geological formations' suitability for secure and long-term CO_2 storage. Seismic interpretation is concerned with delineating horizons, identifying faults, and analyzing the subsurface structures prevalent within the region of interest. It involves creating maps that encompass stratigraphic details and structural insights, which collectively illuminate subsurface features, including hydrocarbon reservoirs (Coffeen, 1978). This seismic interpretation transformation results in a seismic section that serves as a comprehensive representation of the geological characteristics of the Earth. Within these seismic sections, the seismic reflectors play a crucial role by revealing insights into the potential presence of hydrocarbons and the geological composition of the area under investigation (Sheriff, 1999).

5.2 Methodology

Well log analysis forms the foundation for delineating potential seismic data horizons, establishing a connection between well and seismic data. Nevertheless, the well data exists in the depth domain while seismic data operates in the time domain. To bridge this gap, a time-depth chart specific to a particular well is necessary. This chart facilitates the creation of synthetic seismograms, effectively aligning the two datasets (Bacon et al., 2007).

The focus of this dissertation is a zone in SML Formation which was marked by tying the seismic data to Qadirpur-16 well through synthetic seismogram. The upper and lower boundaries of this specific zone were delineated on the seismic profile. The procedural steps for this workflow are outlined in Figure 5.1.

5.3 Base Map

The primary data representation in the Base Map (Figure 5.2), incorporates the arrangement of wells in conjunction with the orientation of 3D lines and cross lines.

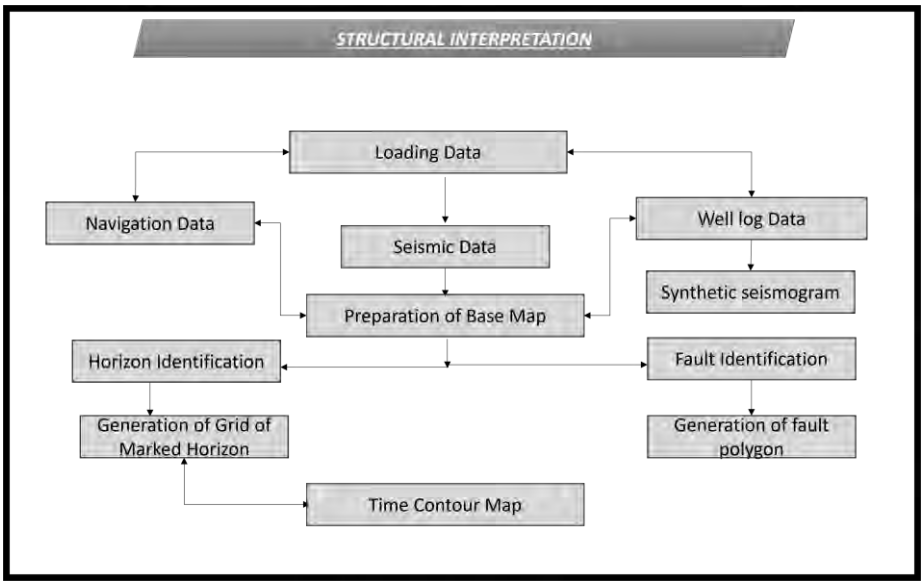

Figure 5.1: *The workflow for seismic Interpretation carried out in this dissertation.*

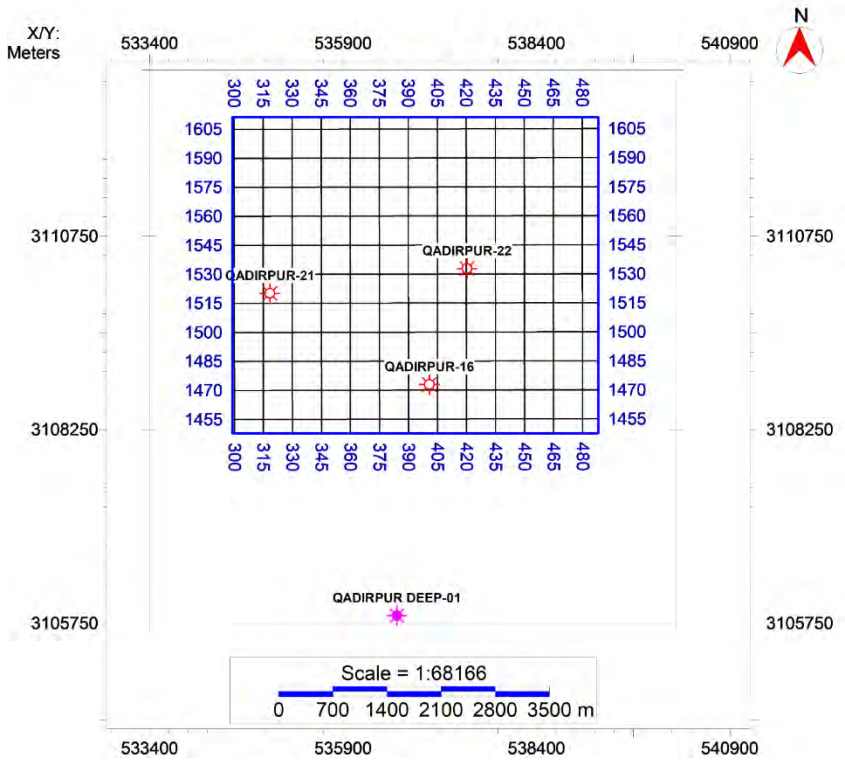

Figure 5.2: *Base Map illustrating the 3D Seismic Survey of the Study Area, depicting the orientation of in-lines, crosslines, and the placement of wells, along with their projected coordinates.*

5.4 Seismic to Well Tie

Synthetic seismogram generated through the DT and RHOB logs is helpful in demarcation of horizons. This process holds significant importance in seismic interpretation. The disparity in impedance between two layers serves as a metric for reflectivity, subsequently subjected to convolution using an extracted wavelet (Figure 5.3). To accurately establish horizons on the zone of interest, a correlation between seismic data (in the time domain) and well data (in the depth domain) is established.

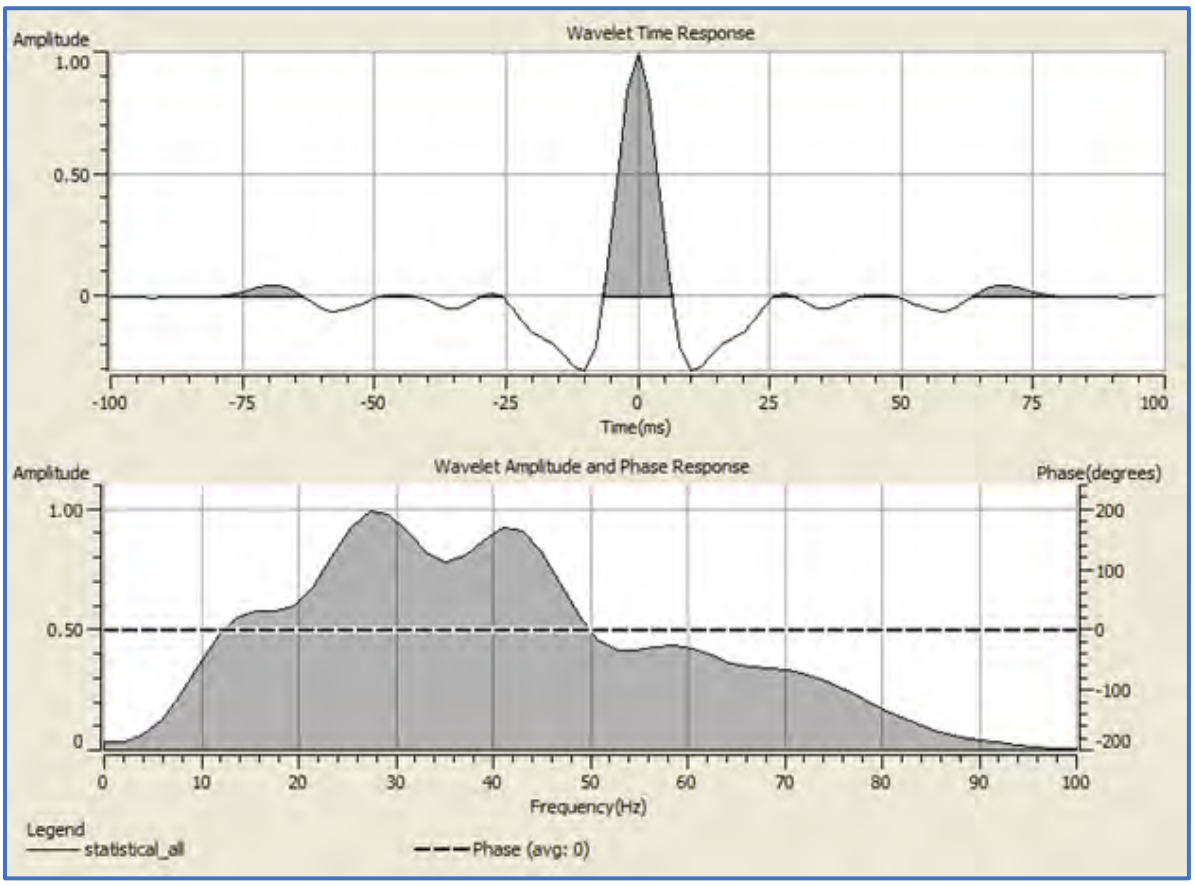

Figure 5.3: *Extracted wavelet from seismic data near well Qadirpur-16, depicting frequency along with amplitude and phase spectrum.*

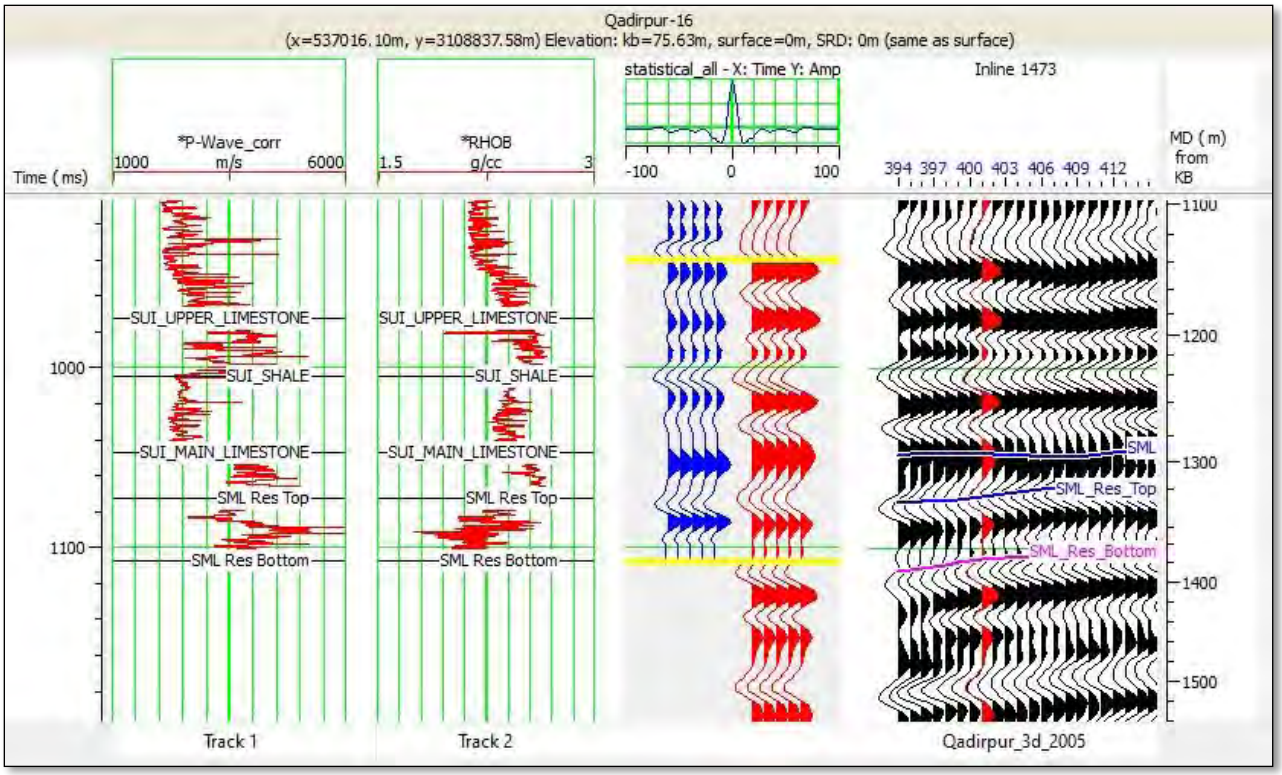

Figure 5.4: *Synthetic Seismogram illustrating the Seismic-to-Well Tie between Seismic traces along line 1471 and Qadirpur-16 Well with 83.38% correlation coefficient.*

5.5 Delineation of Target Horizon

After establishing a seismic-to-well tie, the process of marking horizons on 3D seismic data gains significance. This tie involves correlating the seismic data with the well log data, aligning them in terms of time-depth relationship. Once this alignment is achieved, the positions of defined zone Within SML Formation through the well log analysis, was then be marked onto the seismic sections (Figure 5.5). The marked horizons provide a spatial context and interpret subsurface structures, stratigraphy, and potential reservoirs more effectively.

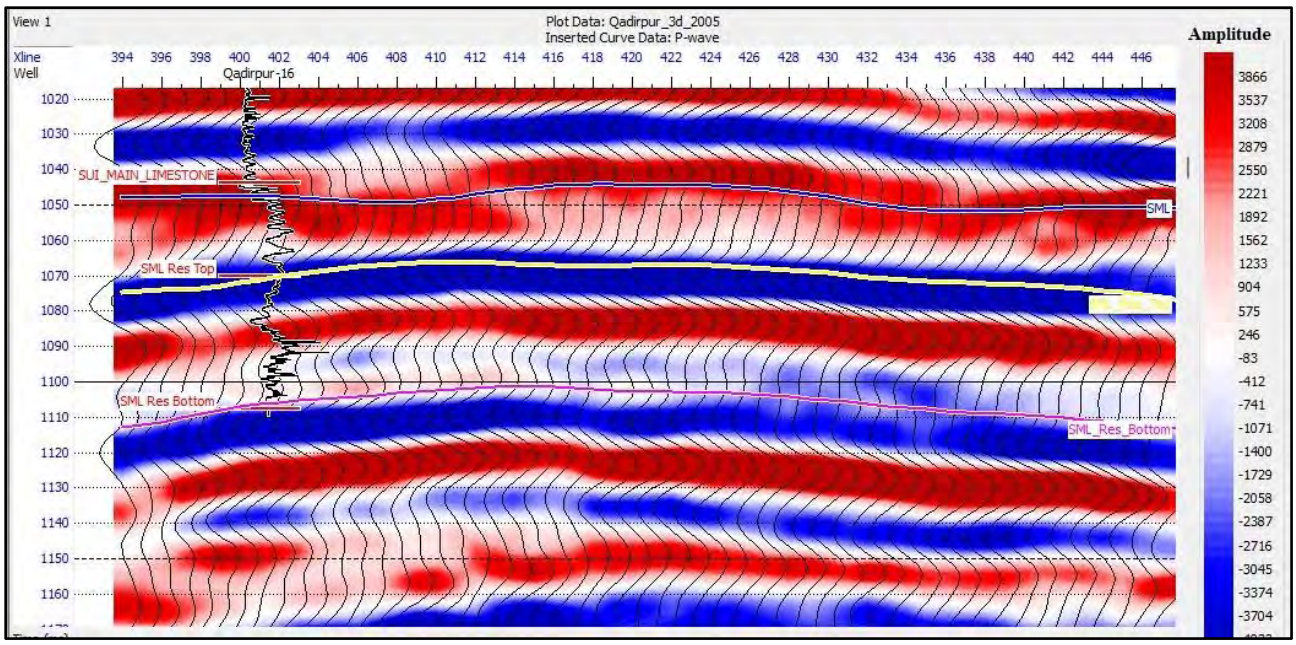

Figure 5.5: *Marked seismic horizons on inline 1473, using synthetic seismogram developed for Well Qadirpur-16 and its surrounding traces.*

5.6 Time Contour Maps

The culmination of interpreted seismic data is visualized through time structure maps. These maps, created through contour representations, convey crucial details about the formation's characteristics such as inclination, faulting, folding, and dip. The outcome of seismic interpretation is encapsulated in contour maps, which illustrate the subsurface variability of the structure. Contours, depicted as lines with consistent or similar values, can pertain to parameters like depth, elevation, time, or other variables. In this context, the contours represent lines of travel time, reflecting the journey around the given subsurface structure. Consequently, these contour maps serve as the primary information source for seismic exploration experts, and the overall success of the endeavor hinges upon this final visualization (Coffeen, 1986). Figure 5.6 indicates that horizon for the top of the reservoir of interest is shallower towards center and deeper towards the north-west and south-east. Similarly, the horizon for the bottom of the reservoir indicates that the formation is deeper towards north-west and south-east (Figure 5.7).

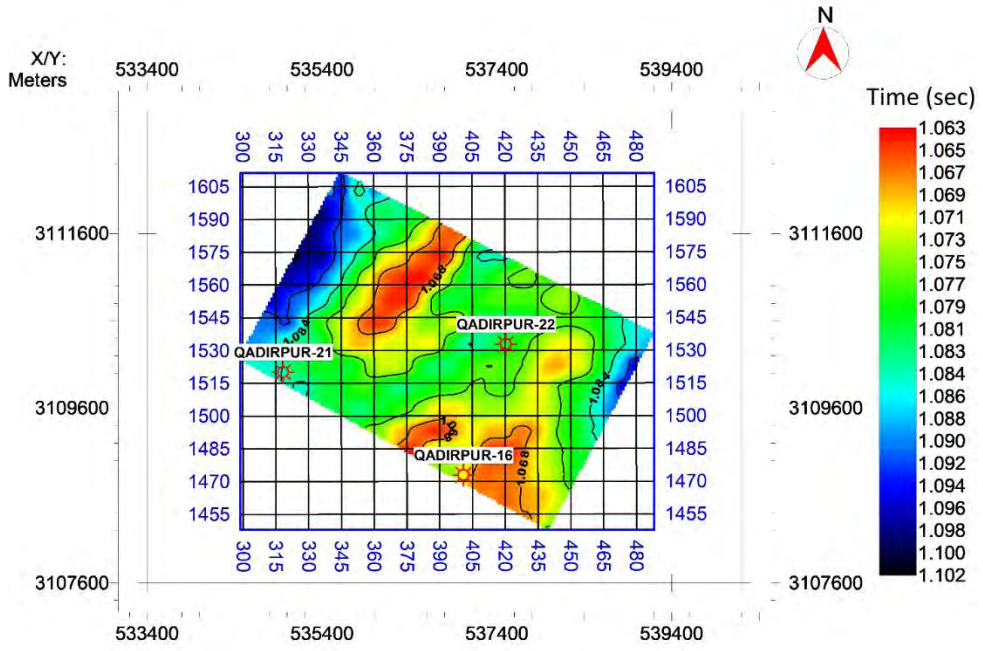

Figure 5.6: *Time contour map representing the top of the zone within SML Formation. The horizon is relatively deeper towards the north-west and shallower towards south-east.*

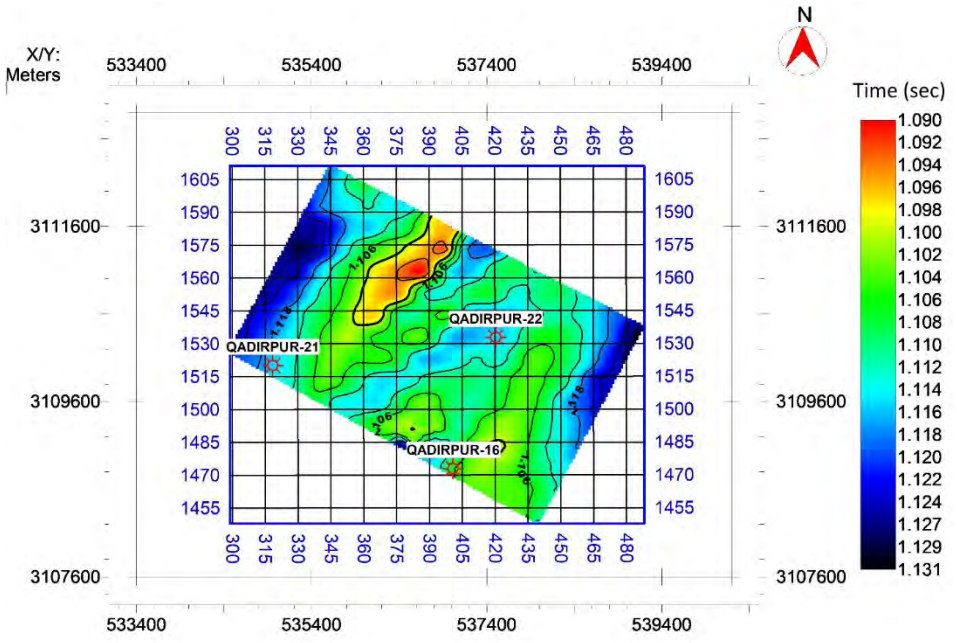

Figure 5.7: *Time contour map representing the bottom of the zone within SML Formation depicting that the formation is deeper towards north-west and south while relatively shallower towards center.*

CHAPTER#6

RESERVIOR ASSESSMENT

6.1 Introduction

Reservoir assessment plays a critical role in evaluating the suitability of geological formations for carbon storage, and model-based inversion coupled with porosity estimation emerges as a powerful methodology in this context. This approach involves leveraging advanced geophysical techniques to derive essential subsurface properties and characteristics, enabling a comprehensive understanding of the reservoir's potential for carbon storage. Porosity estimation, a key component of reservoir assessment, involves quantifying the volume of void space within the rock, which is crucial for understanding fluid storage and migration capabilities. By integrating porosity estimates derived through PNN, and the model-based inversion results, a comprehensive view of the reservoir's storage potential can be observed (Niu et al., 2013).

6.2 Model-Based Inversion (MBI)

MBI is a form of post-stack inversion designed to calculate acoustic impedance (AI) from seismic datasets. It is also referred to as blocky inversion. This technique is rooted in the convolutional theory, asserting that seismic traces can be generated by convolving wavelets with the reflectivity function (Russell and Hampson, 1991). Despite the presence of noise within seismic traces due to various factors, such as instrumentation, multiples, and cultural interference, the equation governing the seismic trace remains:

$$Seismic\ trace = Wavelet * Reflectivity + Noise \qquad (6.1)$$

In instances where the noise is independent of the seismic signal, it becomes feasible to deduce the Earth's Reflectivity function from the trace. To initiate the inversion process, it is crucial to have an initial low-frequency model based on well log data, which represents the AI. This model serves the dual purpose of supplying the missing low- and high-frequency components within the seismic datasets and aiding in mitigating the inherent lack of uniqueness in the solution. The procedural steps encompassed in the model-based inversion, as detailed in this study, are as follows (Maurya and Singh, 2015):

1. AI at well locations is computed utilizing the available well log data.

2. Seismic horizons are chosen across the seismic section, offering control for interpolation and structural insight between well positions.
3. Interpolation is executed along the designated seismic horizons and between well locations, leading to the formulation of an initial AI model.
4. The initial impedance model is segmented into blocks of chosen dimensions.
5. Statistical wavelet is extracted from the seismic section.
6. The Earth Reflectivity is convolved with the wavelet to generate a synthetic seismic trace, distinct from the observed seismic trace.
7. A Least Squares optimization process is conducted, aiming to minimize the disparity between the real and modeled reflectivity sections. The approach involves assessing the discrepancy between synthetic and real traces and adjusting block size and amplitude to curtail errors.
8. Iteration of step 7 is performed until the lowest misfit between the real seismic data and synthetic trace is attained.

An optimum extracted wavelet is important for accurate inversion results. A proper seismic to well tie with a correlation coefficient of 86% was developed and a proper wavelet was extracted (Figure 6.1). This wavelet was then used to invert the seismic data into the impedance model.

6.2.1 Low Frequency Model

In the realm of model-based inversion, a "low-frequency model" is a simplified representation of subsurface properties that primarily focuses on the longer wavelengths and lower-frequency components of seismic data. Its primary purpose is to capture fundamental aspects of the subsurface, making it a practical and effective tool for understanding and characterizing significant subsurface properties. By emphasizing these lower-frequency components, the low-frequency model facilitates a more efficient and insightful interpretation of seismic data. The low frequency model was generated using the impedance log of well Qadirpur-16 and the seismic data (Figure 6.2).

6.2.2 Output Wavelet

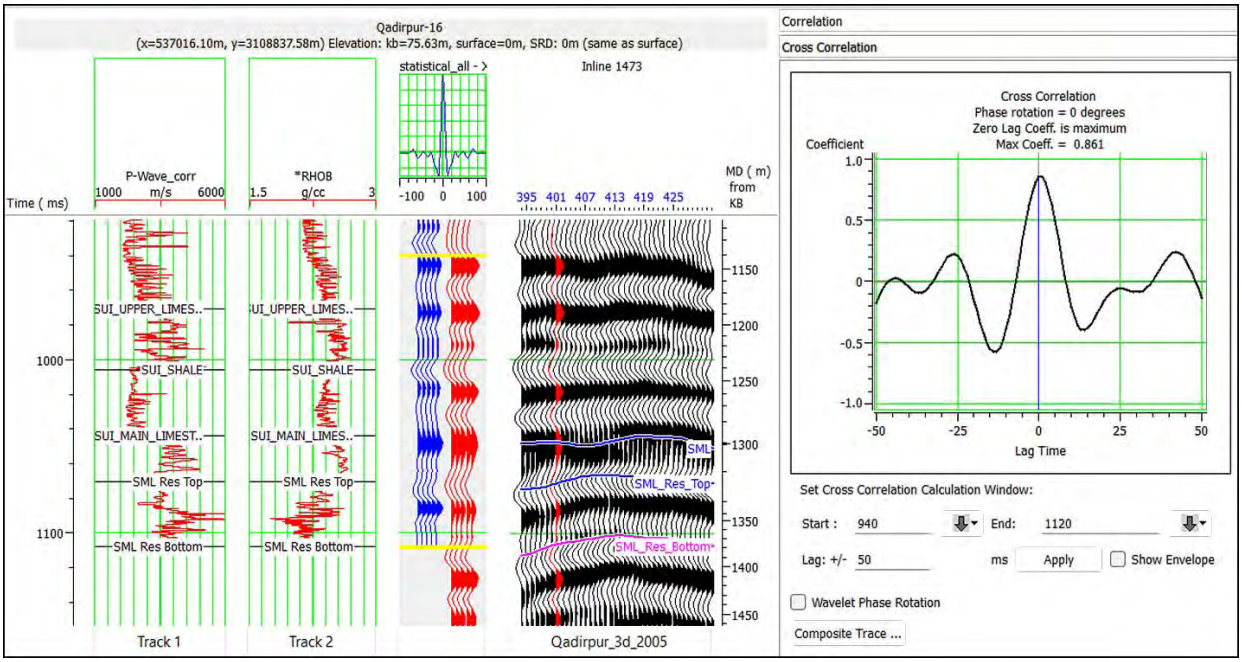

Figure 6.1: *Wavelet extracted from the correlation of synthetic seismogram of Well Qadirpur-16 with seismic traces surrounding the well. The correlation coefficient for the seismic to well tie is 86%.*

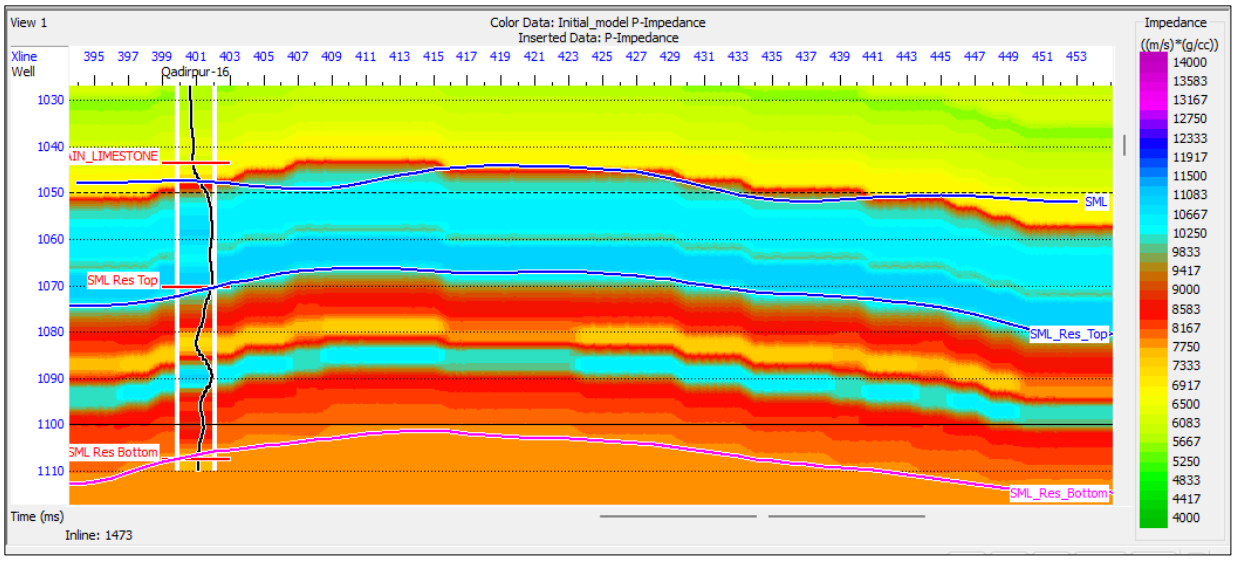

Figure 6.2: *Initial impedance model or a low-frequency model utilized for applying model-based inversion in the conducted research.*

6.2.3 Model Based Inversion Results

The application of Model-Based Inversion yields valuable results related to AI. This technique, which involves the iterative adjustment of subsurface models to match observed seismic data, produces insights into the acoustic properties of the subsurface geological formations. Model-Based Inversion, in conjunction with well and seismic data, serves as a powerful tool for enhancing our knowledge of the subsurface and supporting informed decisions in geological and geophysical applications. Furthermore, it demonstrates the ability to accurately capture lateral variations in lithology, highlighting the diverse geological composition across the formation of interest. The impedance values in the reservoir zone within the SML Formation indicate the presence of hydrocarbon (Figure 6.3, 6.4).

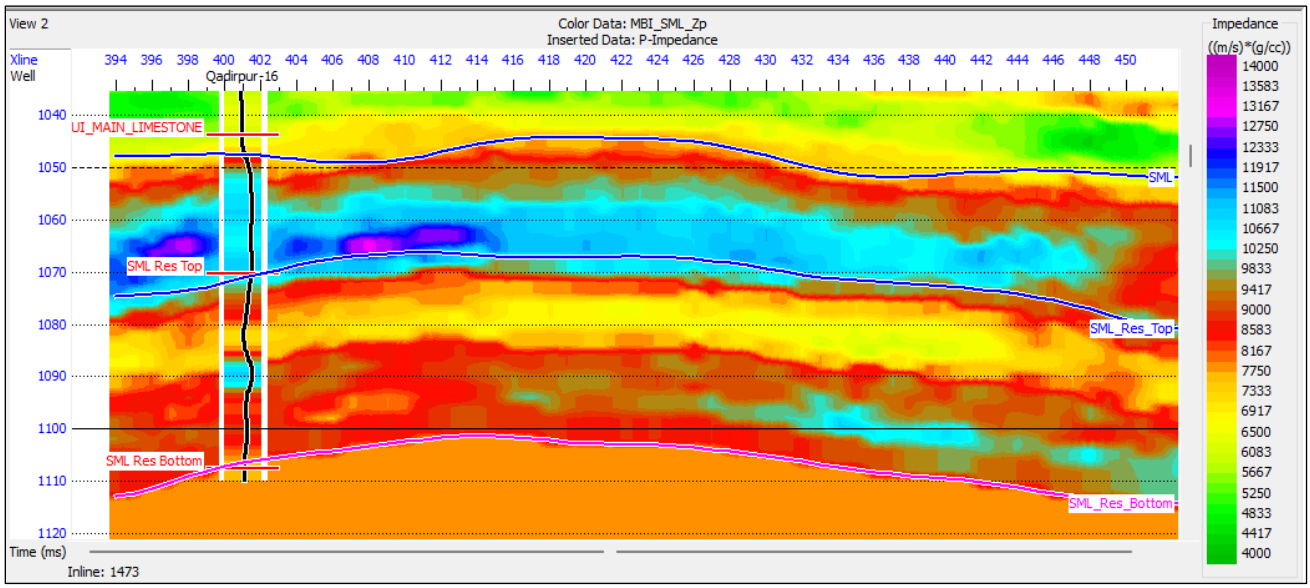

Figure 6.3: *The application of Model Based Inversion on inline 1473 in conjunction with the Qadirpur-16 well produces AI outcomes. Additionally, this inversion technique effectively records lateral changes in lithology.*

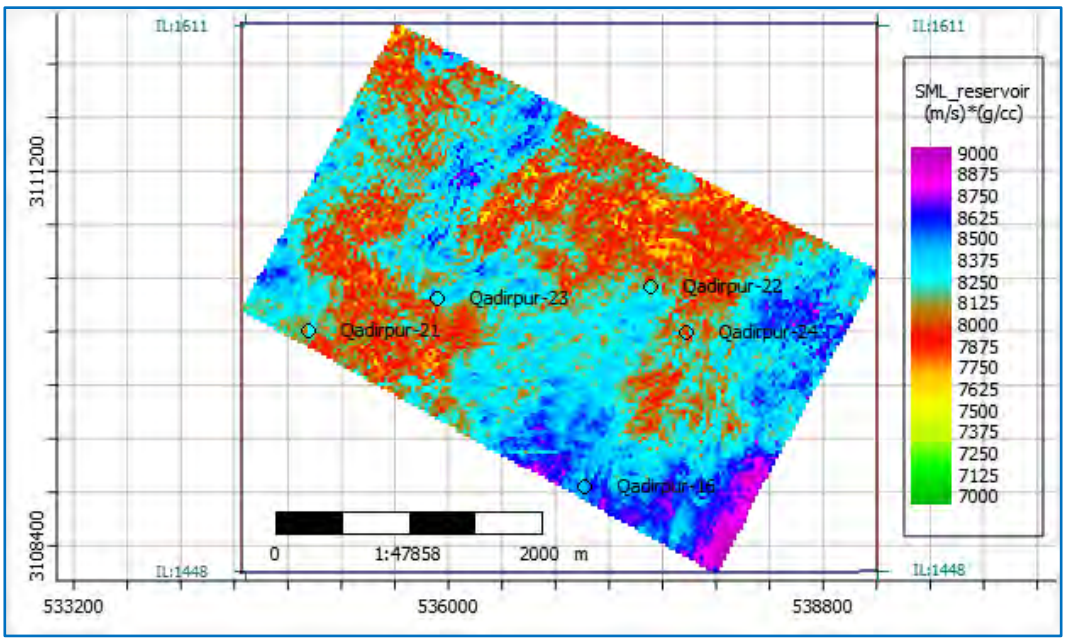

Figure 6.4: *Slice of AI obtained through MBI depicting the zone marked within Sui Main Limestone Formation along its values on color bar.*

6.3 Estimating Porosity from Seismic Attributes Through PNN

The process of Emerge involves the integration of well log and seismic data. Its primary aim is to forecast a specific property like porosity from well logs using seismic data attributes. The seismic attributes might be internally computed or externally provided. The procedure unfolds in several phases:

1. Investigating both well log and seismic data at well sites to identify the suitable attribute set.
2. Developing a correlation using techniques like MLR or Probabilistic Neural Networks (PNN).
3. Employing the established correlation on a 3D SEG-Y volume to generate a volumetric representation of the desired well log property.

6.3.1 Probabilistic Neural Networks (PNN)

PNN is a type of ANN designed for pattern recognition and classification tasks. It is particularly useful for probabilistic modeling and classification problems where the outputs are associated with probability distributions. PNN employs a distance-based interpolation scheme and is trained to recognize patterns by utilizing known training examples. The network calculates probabilities for every class and subsequently assigns the input pattern to the class with the greatest likelihood.

The foundation of the PNN approach is rooted in a mathematical interpolation scheme, which employs a neural network framework for its implementation. This technique is underpinned by the calculation of weights based on the distance in the attribute space between known and unknown points. PNN leverages measure or derived parameters as independent variables to predict a single dependent variable's value. The process of constructing a PNN model begins with partitioning a sample set derived from well logs into training, validation, and test subsets. The training phase continues until specific criteria are met, such as minimizing the mean square error objective or reaching a maximum iteration limit. The test subset is solely utilized to gauge the prediction capabilities of the PNN through a blind test and is not involved in the development of the neural network model (Leiphart and Hart, 2001; Mohamed et al., 2017).

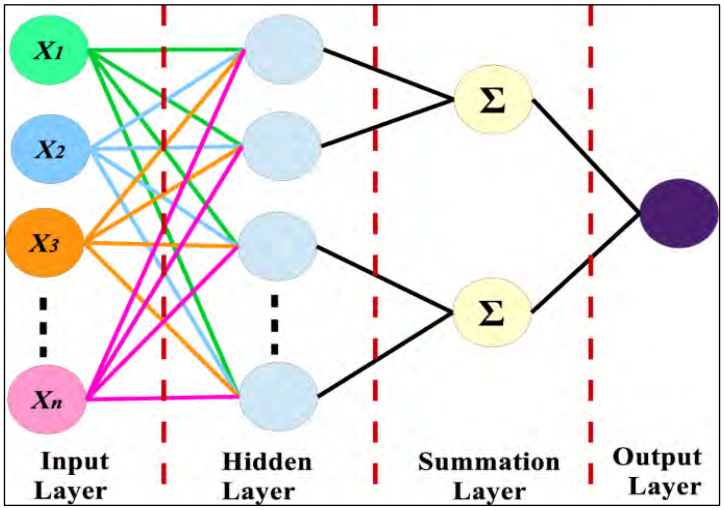

Figure 6.5: *Architecture of PNN, showing the NN between input layer, hidden layer, summation layer and output layer (Ghahramani, 2015).*

6.3.2 Data Preparation

The data set used for estimating spatial distribution of porosity includes PHIE log of Qadirpur-16, which is designated as the target variable, representing the porosity levels within the geological formation of interest, and harnessed as an integral part of the training dataset. Additionally, seismic data obtained from the Qadirpur area is integrated, providing valuable insights into the subsurface structures that may influence porosity. The inversion volume, derived through model-based inversion technique, was used as an external attribute along with the PHIE log (Figure 6.5) to initiate the PNN based training.

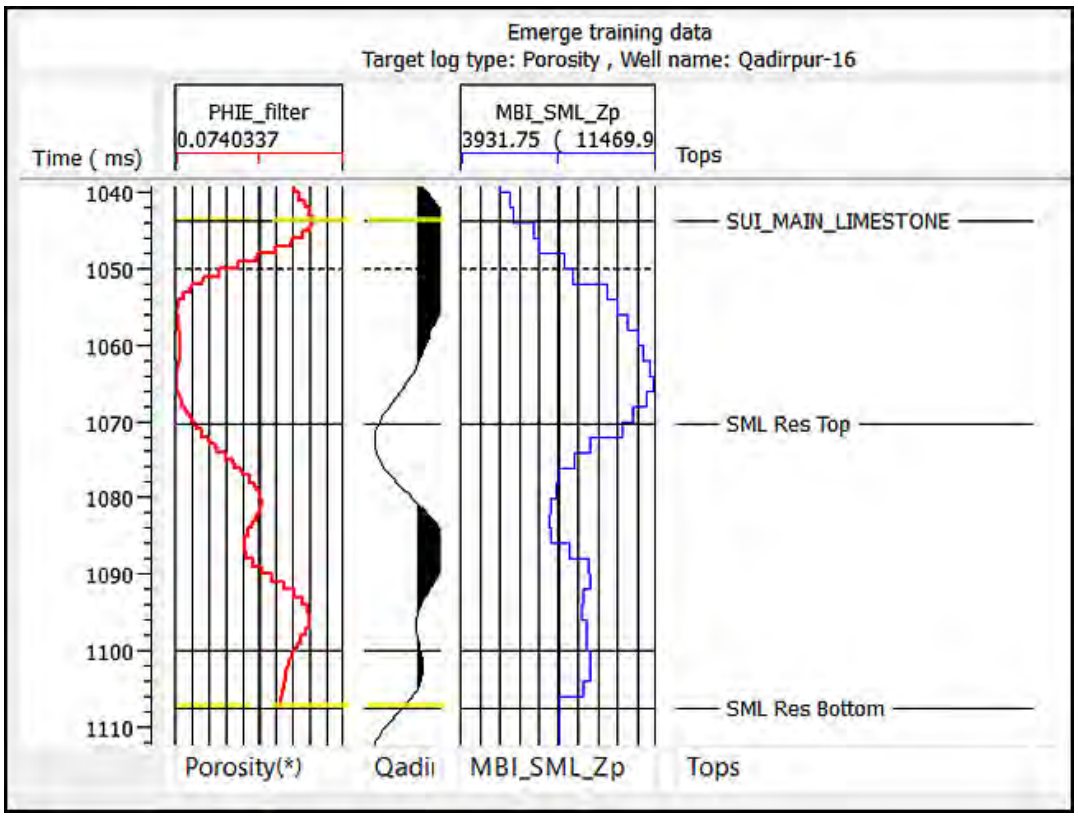

Figure 6.6: *The PHIE log is specified as target log from Qadirpur-16 well, seismic data of Qadirpur and inversion volume obtained through model-based inversion as an external attribute are used as training data sets.*

6.3.3 Single-attribute transforms

Twenty nonlinear transformations were used on both the target parameter (porosity) and the external attribute (Inversion Result) for the purpose of analysis along with the 3D seismic data. Initially, single-attribute transforms were applied to the data and a porosity log was synthesized (Figure 6.7).

Single Attribute Correlation Results

	Target	Attribute	Error	Correlation
1	Porosity	Dominant Frequency	0.018304	0.930897
2	(Porosity)**2	Dominant Frequency	0.018587	0.909230
3	Sqrt(Porosity)	Dominant Frequency	0.019229	0.935132
4	Log(Porosity)	Dominant Frequency	0.020871	0.934827
5	(Porosity)**2	Average Frequency	0.025379	0.825477
6	Porosity	Average Frequency	0.026586	0.847644
7	Sqrt(Porosity)	Average Frequency	0.027695	0.852288
8	1 / (Porosity)	Dominant Frequency	0.028270	-0.922502
9	Log(Porosity)	Average Frequency	0.029201	0.852488
10	(Porosity)**2	(MBI_SML_Zp)**2	0.032882	-0.688343
11	Porosity	(MBI_SML_Zp)**2	0.033046	-0.751726
12	(Porosity)**2	MBI_SML_Zp	0.033276	-0.677462
13	(Porosity)**2	Sqrt(MBI_SML_Zp)	0.033652	-0.670370
14	Porosity	MBI_SML_Zp	0.033831	-0.737688
15	Sqrt(Porosity)	(MBI_SML_Zp)**2	0.033858	-0.779981
16	(Porosity)**2	Log(MBI_SML_Zp)	0.034138	-0.662138
17	Porosity	Sqrt(MBI_SML_Zp)	0.034323	-0.728576
18	1 / (Porosity)	Average Frequency	0.034814	-0.841373
19	Porosity	Log(MBI_SML_Zp)	0.034877	-0.718015
20	Sqrt(Porosity)	MBI_SML_Zp	0.034926	-0.764364

There are 160 attributes (sorted by the Training Error).

Figure 6.7: *A list displaying single attributes, showcasing non-linear transformations of the target and external attribute, accompanied by error and correlation outcomes indicating a strong average correlation of 80.16%.*

6.3.3.1 Application of Single Attribute Regression

The application of Single Attribute Regression reveals a significant correlation of 93.0897% between the dominant frequency attribute and the PHIE log of the Qadirpur-16 well (Figure 6.8). This correlation suggests a strong relationship between the dominant frequency of certain subsurface signals, likely obtained from seismic data, and the porosity levels represented by the PHIE log. The accompanying statistics provide further insight into the accuracy of this relationship, with an average error of only 0.02. The slope of 0.0106603 and the intercept of -0.100157 in the regression equation contribute to a precise estimation of porosity based on dominant frequency attributes.

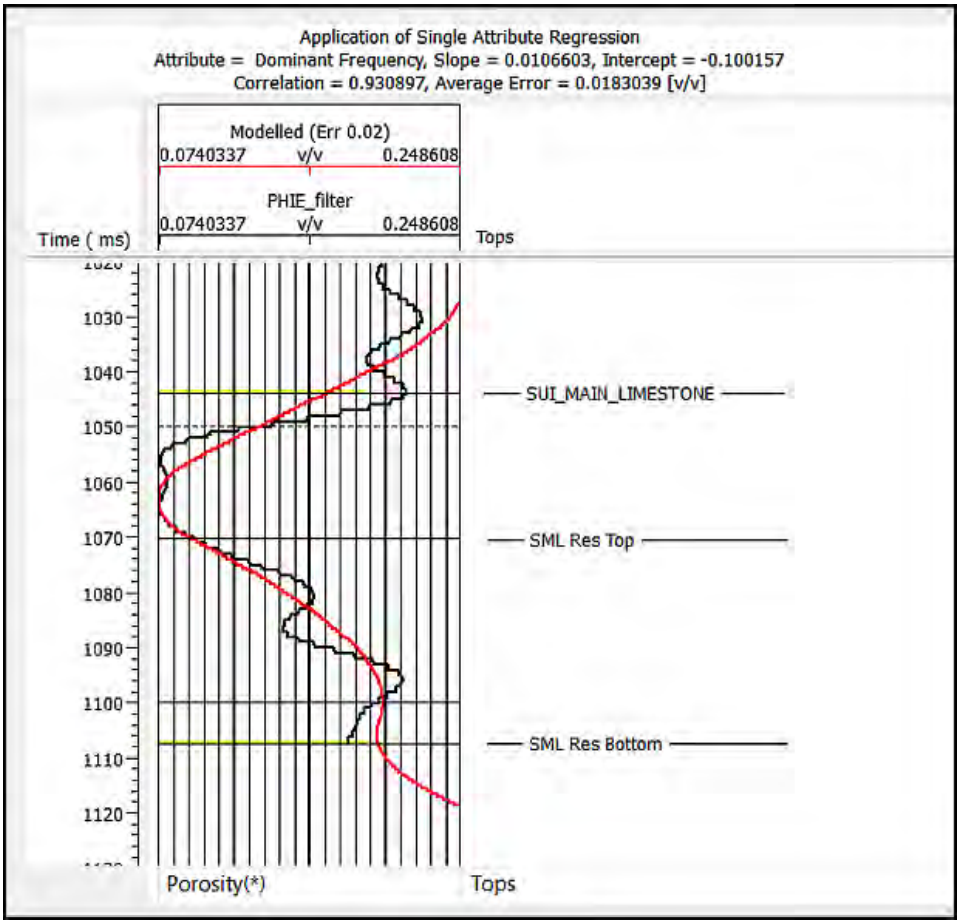

Figure 6.8: *Application of Single Attribute Regression depicting 93.0897% correlation of dominant frequency attribute with PHIE log of Qadirpur-16 with average error 0.02, slop 0.0106603 and intercept -0.100157*

6.3.4 Multi Attribute List

The multi-attribute list, consisting of twenty carefully selected attributes, plays a pivotal role in the endeavor to target and accurately estimate porosity within the geological formation of interest. Through the process of targeted porosity estimation and training, the aim is to minimize error and enhance the precision of porosity predictions (Figure 6.9).

Multiple Attribute Correlation Results

Multi-Attribute List: Multi Attribute List 1

	Target	Final Attribute	Training Error
1	Porosity	Dominant Frequency	0.018304
2	Porosity	Filter 55/60-65/70	0.012758
3	Porosity	Integrated Absolute Amplitude	0.010708
4	Porosity	Amplitude Weighted Frequency	0.009246
5	Porosity	Integrate	0.007853
6	Porosity	Instantaneous Phase	0.007053
7	Porosity	Instantaneous Frequency	0.006237
8	Porosity	Derivative	0.006020
9	Porosity	Filter 35/40-45/50	0.005619
10	Porosity	Amplitude Weighted Phase	0.005485
11	Porosity	Filter 45/50-55/60	0.004851
12	Porosity	Derivative Instantaneous Amplitude	0.004424
13	Porosity	Quadrature Trace	0.004225
14	Porosity	Second Derivative	0.004029
15	Porosity	Time	0.003367
16	Porosity	Cosine Instantaneous Phase	0.002986
17	Porosity	Filter 15/20-25/30	0.002860
18	Porosity	Amplitude Envelope	0.002641
19	Porosity	Y-Coordinate	0.002608
20	Porosity	Second Derivative Instantaneous A...	0.002599

There are 20 attributes (sorted by the Training Error).

Figure 6.9: *Multi attribute list displaying twenty attributes used for targeted porosity and training error depicting the error is minimized.*

6.3.4.1 Application of Multi Attribute regression

The application of Multi Attribute Regression in this context showcases a remarkably strong correlation of 99.086% between a comprehensive set of twenty attributes and the PHIE log of the Qadirpur-16 well (Figure 6.10).

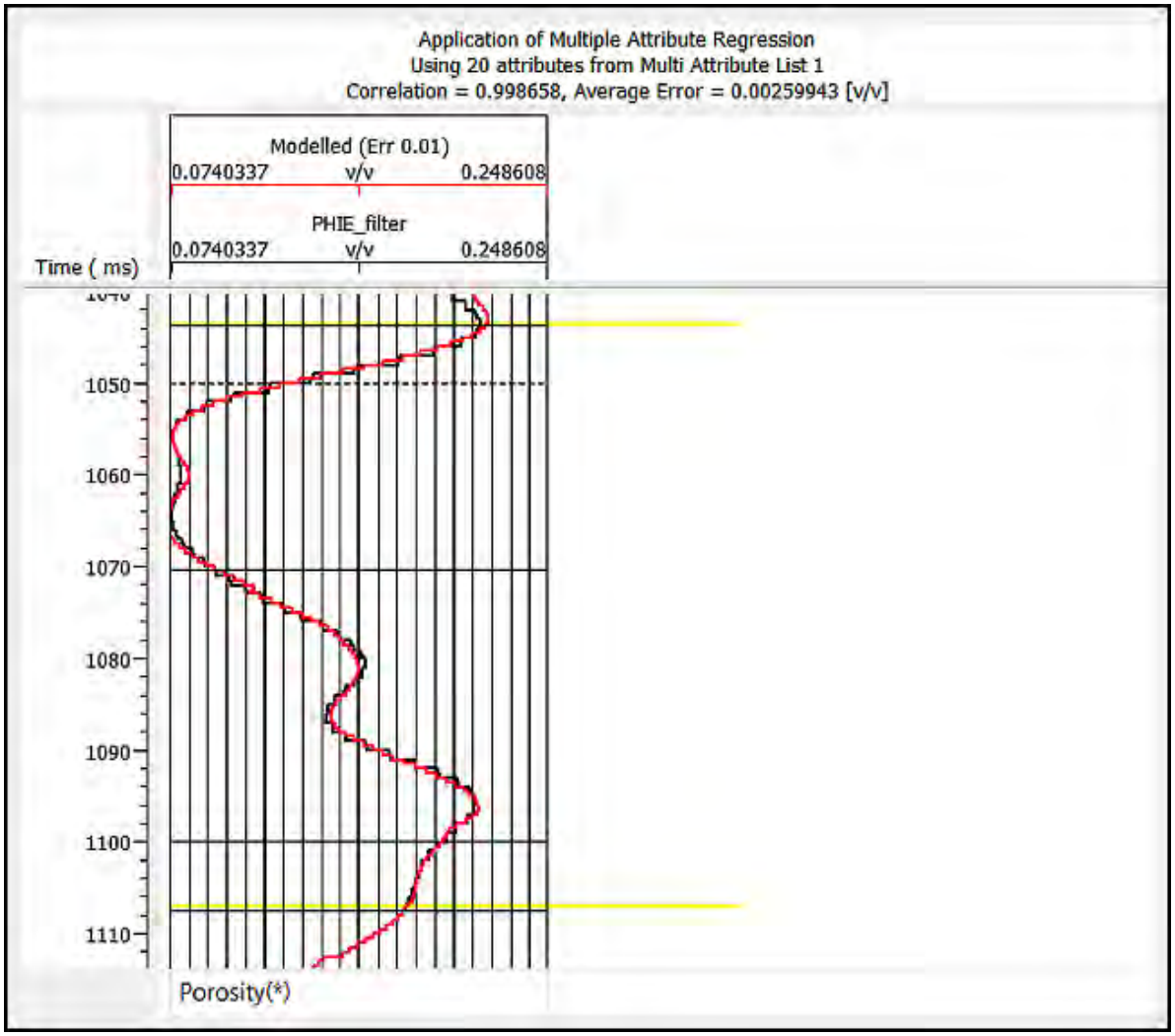

Figure 6.10: *Application of Multi Attribute Regression depicting 99.086% correlation of twenty attributes with PHIE log of Qadirpur-16 with average error 0.002.*

Multi Attribute list yokes the collective power of multiple attributes, resulting in more accurate, comprehensive, and reliable subsurface characterizations.

6.3.5 Training Neural Networks Through PNN

The training conducted using a PNN has yielded remarkable results, showcasing 99.9357% correlation between a comprehensive set of twenty attributes and the PHIE (Porosity) log of the Qadirpur-16 well (Figure 6.11). This high correlation indicates a strong and reliable relationship between the selected attributes and the porosity levels within the subsurface formation. Additionally, the exceptionally low average error of merely 0.001 highlights the precision and accuracy of the PNN model in estimating porosity. This training outcome underscores the effectiveness of employing advanced machine learning techniques, like the PNN, to analyze complex geological and geophysical data.

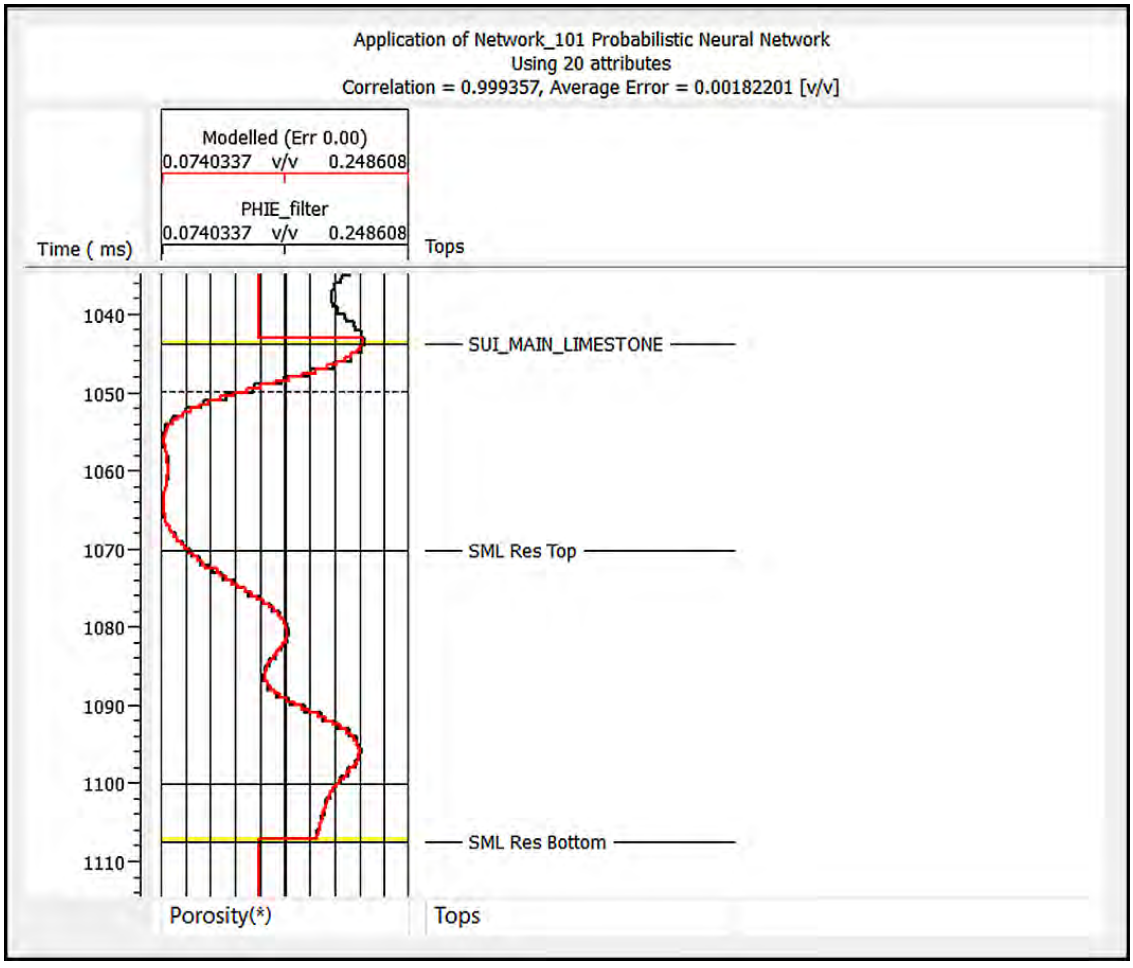

Figure 6.11: *Application of PNN depicting 99.9357% correlation of twenty attributes with PHIE log of Qadirpur-16 with average error 0.001.*

6.3.5.1 Cross plot of Actual Porosity and Predicated Porosity

The PNN model demonstrates a remarkable 99.9357% correlation with an average error of 0.001, the cross-plot analysis is expected to show a tight cluster of points near the diagonal line (Figure 6.12). This visual representation would further validate the model's effectiveness in estimating porosity levels within the Qadirpur-16 well's subsurface formation. It serves as a powerful illustration of the model's precision and its potential for reliable reservoir assessment and management in the Qadirpur area.

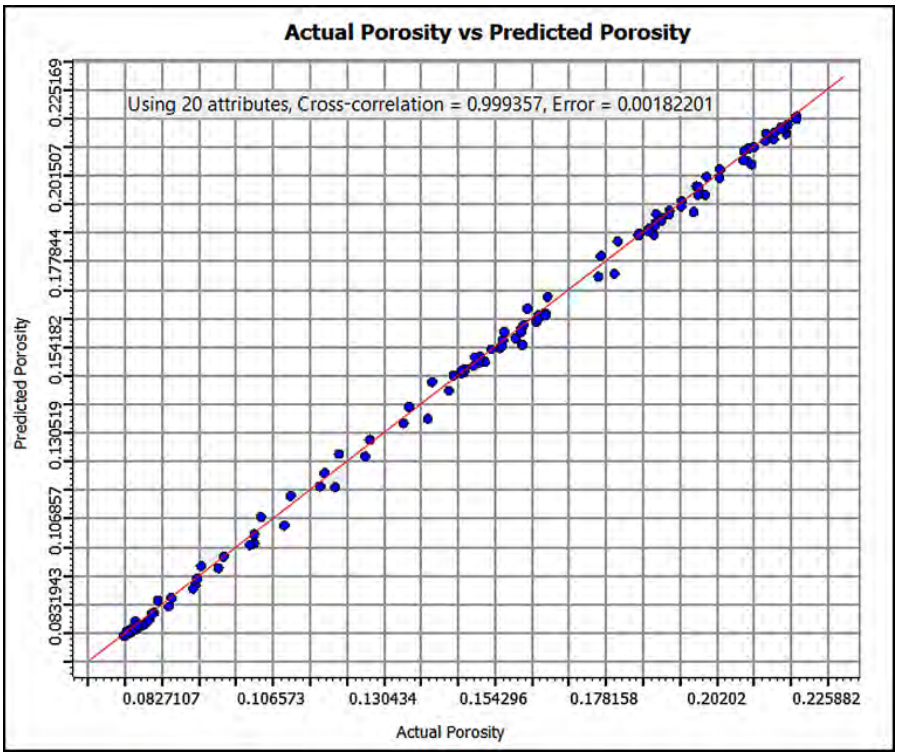

Figure 6.12: *Cross plot analysis representing actual porosity on x-axis and predicited porosity on y axis.*

6.3.6 Application of the Trained Neural Network (PNN) to the 3D volume

The application of PPN generates porosity distribution maps. These maps provide a spatial representation of porosity values within the subsurface geological. The color bar accompanying the map serves as a visual indicator, with different colors corresponding to varying porosity values. This color-coded representation allows for a quick and intuitive interpretation of porosity

distribution patterns, aiding geoscientists, and reservoir engineers in understanding the subsurface characteristics and potential reservoir quality within the Qadirpur area. Such applications of ANN and data visualization tools play a crucial role in reservoir assessment and the efficient management of geological resources. Figure 6.13 indicates the spatial distribution of the PHIE values predicted through the PNN algorithm. High values of PHIE within the zone of interest suggests both the exploitation potential of the zone and the storage capacity (Figure 6.13). The slice for the whole reservoir indicates that the PHIE values are high throughout the reservoir particularly around Well Qadirpur-16 (Figure 6.14). Furthermore, the slice taken for the lower portion of the zone of interest depicts that this zone is particularly favorable in terms of hydrocarbon potential and eventually in the storage of CO_2 (Figure 6.15).

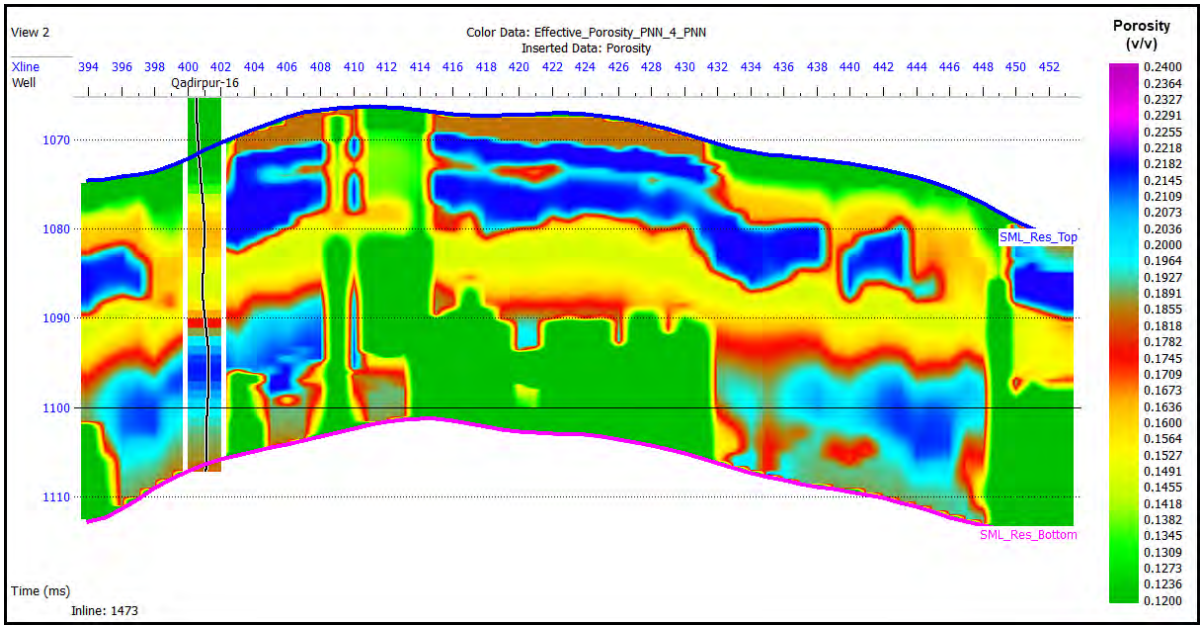

Figure 6.13: *The application of PPN on inline 1473 in conjunction with the Qadirpur-16 well generates porosity distribution with the color bar indicating its values. Porosity values are high throughout the reservoir zone.*

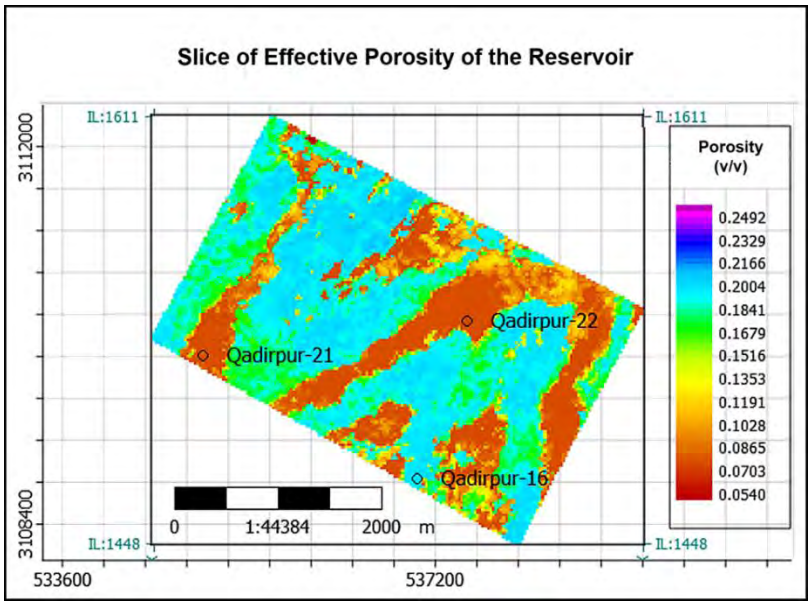

Figure 6.14: *Slice of effective porosity distribution of the zone marked within Sui Main Limestone Formation. The slice indicates high values of PHIE throughout the zone.*

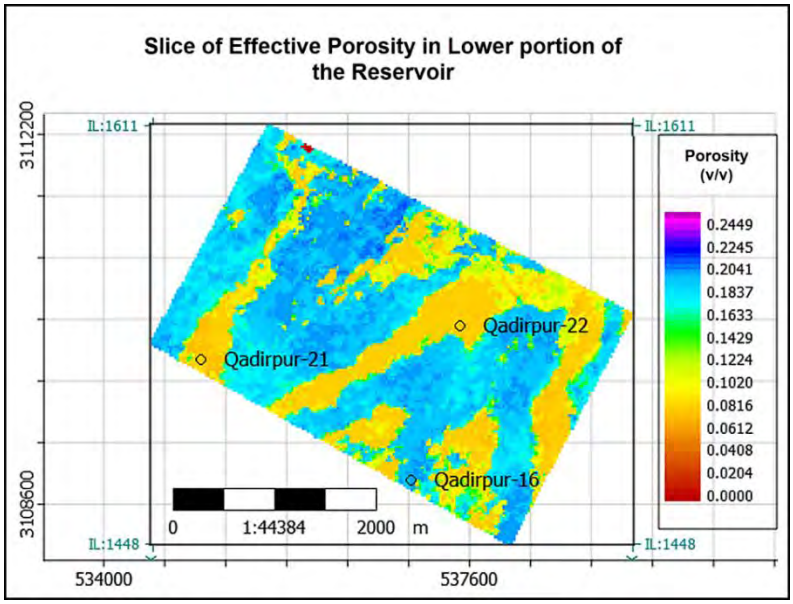

Figure 6.15: *Slice of effective porosity distribution in the lower portion of the zone marked within Sui Main Limestone Formation. The PHIE values are even higher in this portion compared to the upper portion.*

6.4 Thermodynamic analysis for CO_2 storage

Thermodynamics helps describe how CO_2 transitions between different phases (gas, liquid, or solid) under varying temperature and pressure conditions within the storage reservoir (Figure 3.3). Phase diagrams and equations of state (EOS) are commonly used to predict phase behavior. Tables 6.1 and 6.2 represent the initial reservoir pressure and temperature of SML, used for prediction of CO_2 phase behavior within SML (Figure 6.16).

Table 6.1: *The Initial Pressure Levels in Gas Fields Located in Pakistan (Siddiqui, 2004).*

	Fields (Arranged in Structurally Descending Order)	Well Number (Operator)**	Datum of Pressure Measurement (m, subsea) (Reservoir)†	Initial Reservoir Pressure (psig)
1	Zin	well-1 (PPL)	7 (SML)	279
2	Khairpur	well-2 (PPL)	567 (SML)	1000
3	Rodho	well-2 (OGDC)	574 (Dunghan)	1356
4	Loti	well-1 (OGDC)	647 (SML)	1385
5	Mari	well-1 (MGCL)	651 (HRF)	1164
6	Rodho	well-2 (OGDC)	863 (Pab)	1686
7	Qadirpur	well-1 (OGDC)	880 (HRF)	1367
8	Sara	well-1 (Tullow)	882 (SML-Sand Unit)	1401
9	Jandran	well-1 (OGDC)	895 (Takatu)	1716
10	Pirkoh	well-1 (OGDC)	919 (Ranikot)	2148
11	Hasan	well-1 (PPL)	944 (SML)	1560
12	Sui	well-1 (PPL)	945 (Drug)	1892
13	Suri	well-1 (Tullow)	974 (SML-Sand Unit)	1566
14	Sadiq	well-1 (PPL)	994 (SML)	1665
15	Sui	well-1 (PPL)	1067 (SML)	1965
16	Hamza	well-1 (PPL)	1117 (SML)	1788
17	Pirkoh	well-1 (OGDC)	1183 (Pab)	2274
18	Uch	well-1 (PPL)	1186 (SML)	2015
19	Kothar	well-1 (OGDC)	1213 (Ranikot)	1611
20	Qadirpur	well-1 (OGDC)	1250 (SML)	2036
21	Kandhkot	well-9 (PPL)	1250 (SML)	2016
22	Kandhkot	well-14 (PPL)	1293 (SML)	2063
23	Kandhkot	well-7 (PPL)	1350 (SML)	2119
24	Dhodak	well-2 (OGDC)	1471 (Lower Ranikot)	3272
25	Mazarani	well-3 (PPL)	1772 (SML)	2915
26	Mazarani	well-1 (PPL)	1835 (SML)	2925

*Used in Figure 20. Reservoir pressures of the three Kandhkot wells are original as the field production was started after completion of 20 wells. Mazarani field was put

Thermodynamic analysis for CO_2 storage via phase behavior begins with initial temperature and pressure conditions (Figure 6.16) and applies EOS and phase equilibrium principles to predict and understand how CO_2 will behave within the geological reservoir.

Table 6.1: *Temperature of different formation within Qadirpur Area (Ali et al., 2022)*

Depth, thickness and temperature of stratigraphic formations in the Qadirpur Area as encountered by Well Qadirpur Deep-01.

Formation	Age		Depth	Thickness	Temperature
		Ma	m	m	K
ALLUVIUM	Recent	1	0	95	306.15
UNCONFIRMITY		2			
PLIESTOCENE		3			
SIWALIKS	Pleistocene/ Pliocene	18	95	387	309.15
UNCONFIRMITY		23.5			
E. MIOCENE		29			
NARI	Miocene/ Oligocene	41	482	220	321.15
DRAZINDA	Middle Early Eocene	43	702	56	328.15
PIRKOH	Middle Early Eocene	45	758	109	330.15
SIRKI	Middle Early Eocene	47	867	46	333.7
HABIB RAHI	Middle Early Eocene	49	913	85	335.15
GHAZIJ	Middle Early Eocene	56	998	199	337.75
SUL	Middle Early Eocene	57	1197	58	340.95
Sui Shale	Middle Early Eocene	58	1255	51	345.95
SML	Middle Early Eocene	59	1306	143	347.55
DUNGHAN	Paleocene	61	1449	46	352.15

This analysis supports the planning, execution, and monitoring of carbon capture and storage (CCS) projects, contributing to the responsible management of CO_2 emissions and climate change mitigation efforts.

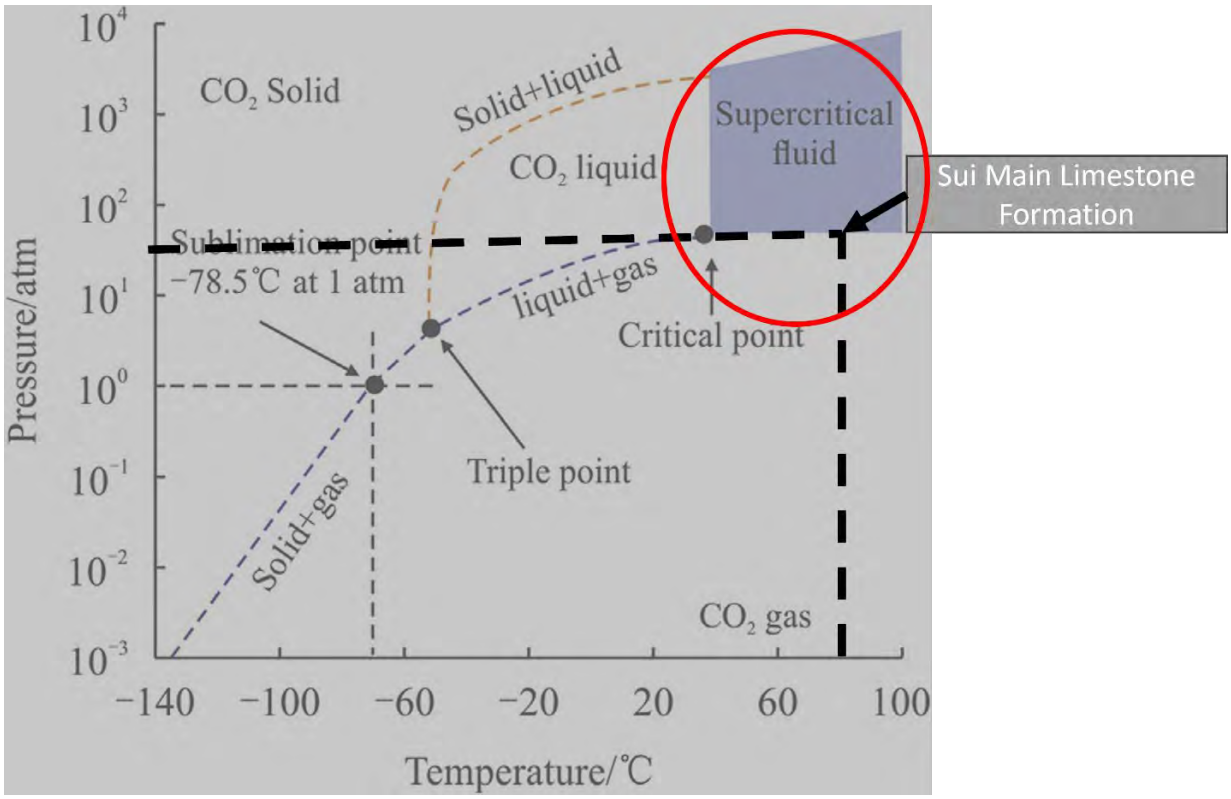

Figure 6.16: *Initial temperature and pressure settings within the SML Formation indicate the potential phase behavior of CO_2. These conditions suggest that, given other relevant parameters, it is feasible to store CO_2 in the formation in a supercritical state.*

6.5 Storage Capacity Estimation

The overall CO_2 storage potential within Pakistan's oil and gas fields is evaluated at around 1.7 Gt (gross tonnage) CO_2. Nevertheless, none of the oil fields exhibit a storage capacity exceeding 10 Mt, thereby lacking significant storage potential. In contrast, thirteen gas fields are projected to possess a storage capacity surpassing 10 Mt, accumulating to an estimated total of 1.6 Gt CO_2. Notably, among these, the Sui, Mari, Qadirpur, and Uch gas fields stand out, holding the potential to store over 200 Mt CO_2 each (IEAGHG, 2008). Table 6.3 represents original recoverable Reserves and approximate CO_2 storage potential of Gas Fields in Pakistan (Naseem, 2014) and Table 6.4 shows the calculated OGIP (Ali at al., 2005). According to these estimates the significant energy resources available in the country, highlighting the potential for both hydrocarbon production and carbon capture and storage (CCS) initiatives. The coexistence of

ample recoverable reserves and substantial OGIP opens opportunities for Pakistan to strategically address its energy needs while actively contributing to global efforts in reducing greenhouse gas emissions through CCS projects.

Table 6.2: *Original recoverable reserves and estimated CO_2 storage capacity of gas field in Pakistan (IEAGHG, 2008)*

Following is a table that show the estimated CO_2 storage capacity of gas fields in Pakistan.(IEAGHG, 2008)

Gas field	Original Recoverable Reserves 10^9 m^3	Estimated CO_2 storage capacity 10^6 tons	Gas field	Original Recoverable Reserves 10^9 m^3	Estimated CO_2 storage capacity 10^6 tons
Sui	244.2	476.3	Bobi	1.2	2.3
Mari	178.4	347.9	Sari	1.1	2.2
Uch	114.7	223.7	Bhatti	1.0	1.9
Qadirpur	112.7	219.7	Panjpir	0.9	1.9
Pirkoh	51.0	99.4	Turk Deep	0.9	1.8
Khairpur	28.3	55.2	Nakurji	0.7	1.4
Kandhkot	22.2	43.2	Mukhdumpur	0.7	1.3
Kadanwari	20.6	40.2	Mazarani	0.5	1.0
Dhodak	16.5	32.1	Sonro	0.5	1.0
Ratana	9.9	19.3	Dabhi	0.5	0.9
Nandpur	8.4	16.3	Koli	0.4	0.8
Loti	7.8	15.3	Mahi	0.4	0.7
Dakhni	7.2	14.1	Daru	0.4	0.7
Adhi	3.3	6.4	Rodho	0.4	0.7
Turk	3.2	6.3	Kothar	0.3	0.7
Zin	2.8	5.5	Buzdar	0.2	0.4
Khorewah	2.8	5.5	Nari	0.2	0.4
Jandran	2.3	4.5	Nur	0.2	0.3
Bukhari	1.9	3.8	Kato	0.1	0.3

Table 6.4: *Estimated Hydrocarbon potential (OGIP) of Qadirpur Area through Qadirpur-01 well and Qadirpur-05 well (Ali et al., 2005).*

ORIGINAL GAS IN PLACE

Original gas in place is calculated by following formula:

Gr = [43560 x Area x Net pay x porosity x (1 - Sw) x (Pf2/Pf1) x RF]
Gr = [43560 * A * h * Φ * (1 - Sw) * (Pf2/Pf1) * RF]
Gr = Volumetric recoverable gas reserves in standard cubic feet (SCF)
RF = recovery factor

Data procured from Qadirpur well #1 and Qadirpur well #5 suggest the following:

Net Pay	h	= 45.934
Average porosity	Φ_{av}	= 0.22
Area of reservoir	A	= 8895.6
Water Saturation	S_w	= 0.22
Recovery Factor	RF	= 0.75
Surface pressure	Pf1	= 15psi
Reservoir pressure	Pf2	= 1980psi

Gr = [43560 * A * h * Φ * (1 - S_w) * (Pf2/Pf1) * RF] Gr
= 6.58287480090TCF

The Qadirpur gas field underwent development in three sequential phases, progressively raising its capacity from an initial 30,00 to 90,000-barrel oil per day (boed) (Figure 6.17). Subsequently, in 2008, the capacity attained the maximum production. To ensure a consistent supply of sales gas over the long term, a compression project was additionally initiated and became operational in 2010. Starting in 2020, there was a decline in production, and it transformed into a gas reservoir with diminishing reserves suitable for EOR Figure 6.17.

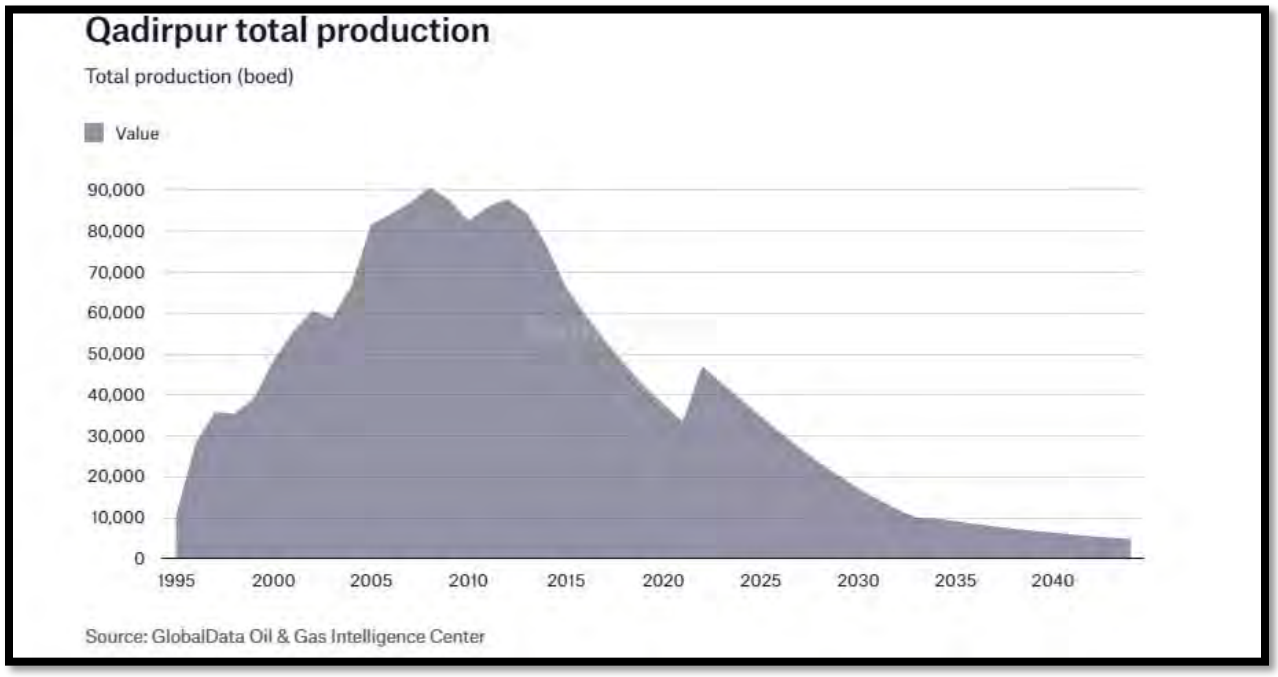

Figure 6.17: *Qadirpur total production data spanning from 1995 to 2040, depicting how the reservoir has behaved over this time frame, encompassing factors like gas production rates, pressure dynamics, and temperature variations.*

Typically, a reservoir with sufficient porosity should have the capacity to trap and retain injected CO_2 over the long term. Porosity allows for the physical storage of the CO_2 within the pore spaces of the rock formation. However, other factors like permeability (the ability of the rock to transmit fluids) and caprock integrity (the sealing properties of the rock above the reservoir) are equally critical in determining the suitability of a reservoir for CO_2 storage. A detailed reservoir characterization and feasibility study as described in chapter 6, to assess specific reservoir meets

the necessary criteria for safe and effective CO_2 storage. Figure 6.19 depicts the spatial distribution of porosity across the area.

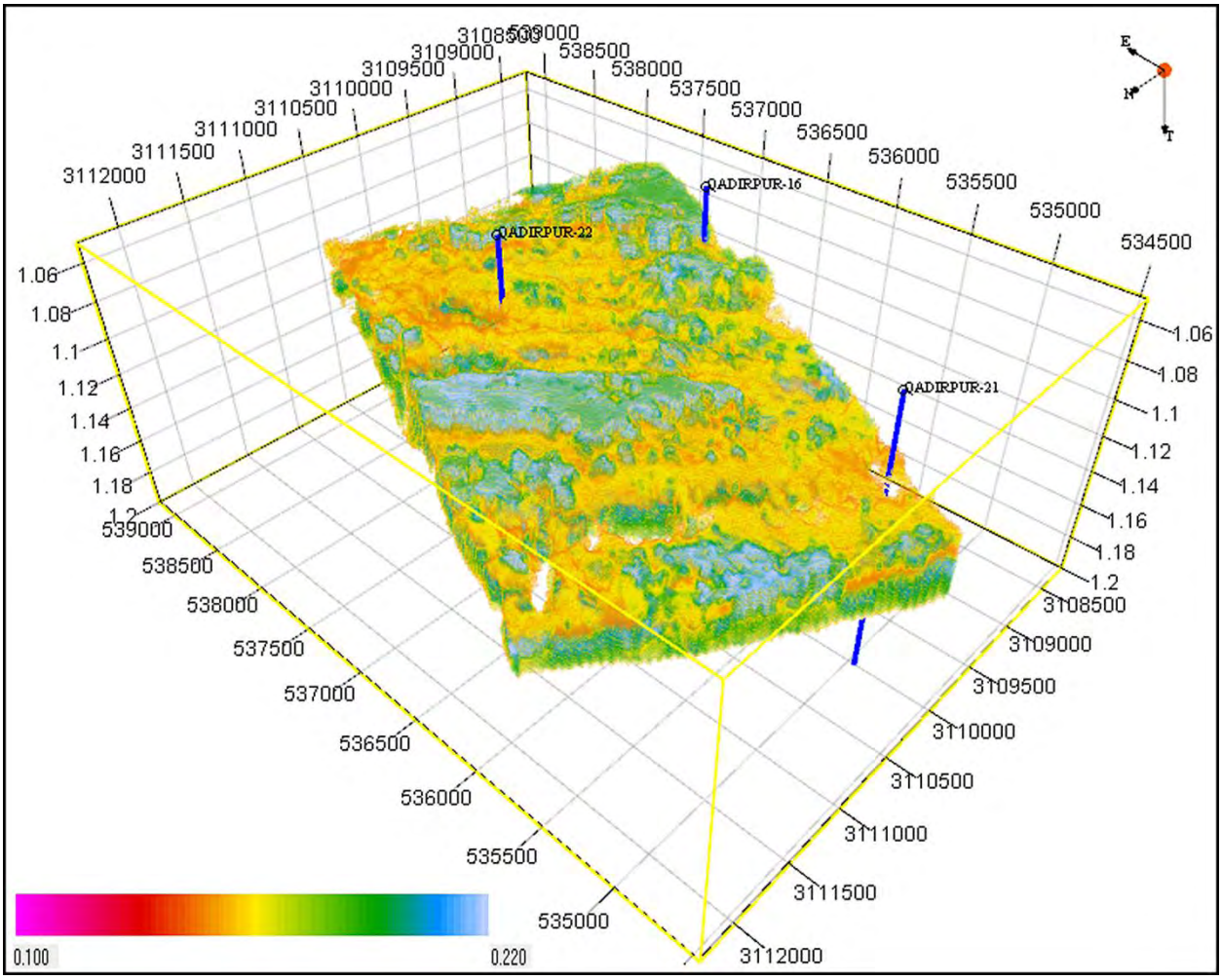

Figure 6.18: *3D visualization depicting the spatial distribution of porosity in the Qadirpur region, obtained using PNN, covering a range from 0.14 to 0.22. The color bar illustrates the corresponding values within the 3D section, including the presence of wells.*

The significance of higher values of spatial porosity distribution within the zone in SML Formation in Qadirpur area cannot be overstated when assessing the feasibility of carbon dioxide (CO_2) storage. These elevated porosity levels (Figure 6.20) are paramount as they directly

correlate with increased storage capacity, enabling the safe containment of larger volumes of CO_2 emissions.

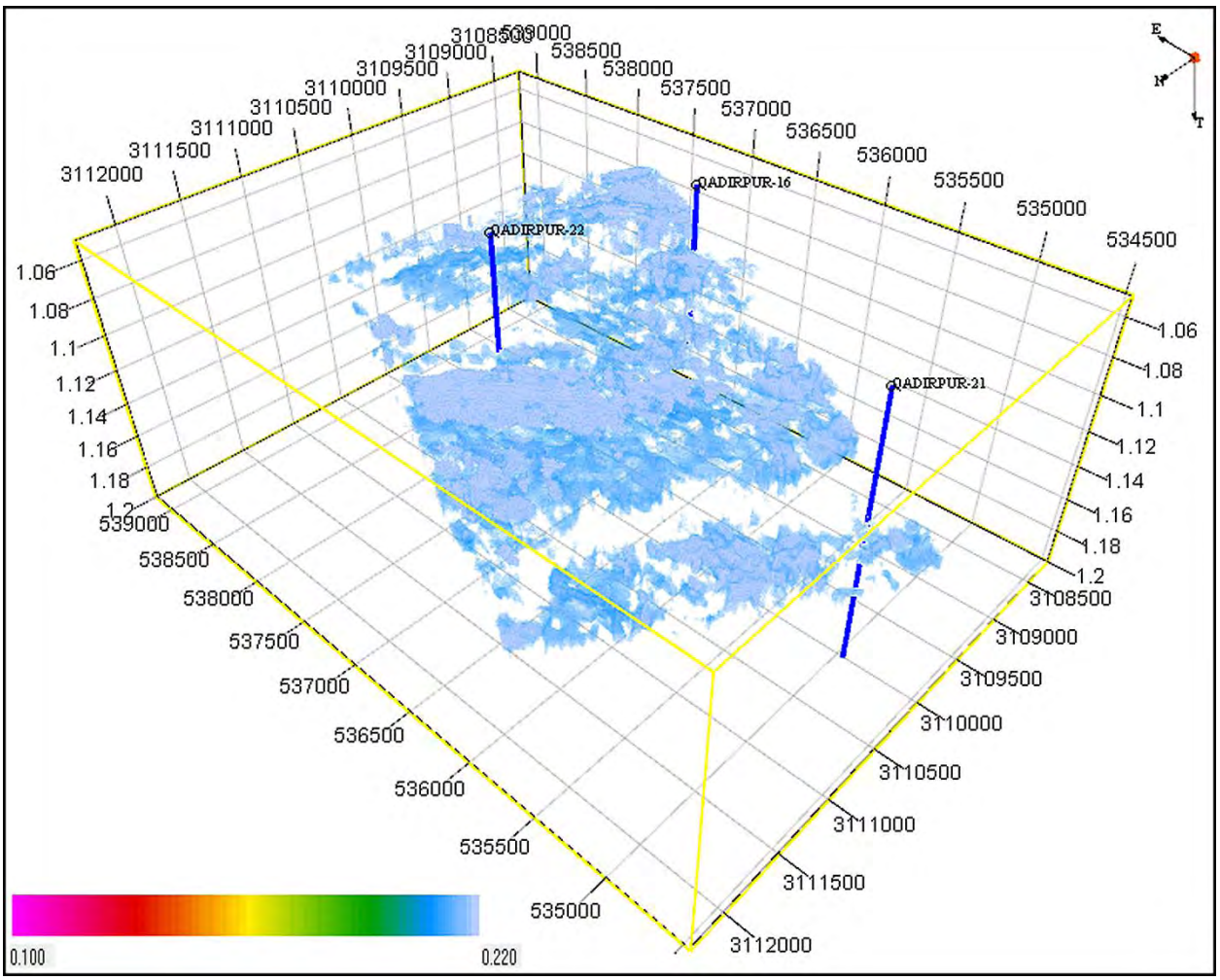

Figure 6.19*: 3D visualization depicting the spatial distribution of higher values of porosity within the zone in SML Formation in the Qadirpur region, obtained using PNN, covering a range from 0.18 to 0.22.*

CHAPTER#7

DISCUSSION AND CONCLUSIONS

7.1 Discussion

The findings of this thesis offer a comprehensive and integrated analysis of the SML Formation within the Qadirpur Area of the Central Indus Basin, Pakistan, with a primary focus on its potential as a site for CO_2 storage. The research objectives encompassed a wide range of geological and geophysical investigations to evaluate the suitability, feasibility, and safety of utilizing this geological formation for CCS initiatives. According to Tomic et al. 2018, sedimentary basins are considered the most suitable geological formations for the storage of CO_2. In terms of safety, the geological storage of CO_2 requires regions that are geologically stable in terms of tectonic activity (Tomic et al., 2018). Considering both these factors, the SML Formation of Qadirpur Area, lying in Central Indus Basin, seemed suitable for CO_2 storage and therefore required an elaborate analysis.

Geological characteristics of formation evaluated for CO_2 storage site are lithology, reservoir depth, thickness, porosity, permeability, permeability of cap rock, presence of faults and stress state of rock (Aminu et al., 2017). For this purpose, petrophysical analysis, lithofacies prediction, shear log prediction, and petro-elastic estimation was carried out using well log data from Well Qadirpur-16. This comprehensive well log analysis played a pivotal role in identifying potential reservoirs and assessing their properties (Figure 4.2). The well log analysis revealed a zone within the SML Formation, located at depths ranging from 1336 to 1366 meters and with a thickness of 30 meters (Figure 4.2). Furthermore, this zone exhibits favorable characteristics for secure CO_2 storage including an average PHIT of 21.09%, PHIE of 18.86%, SW of 19.27%, and 81.73% HS making it conducive to CO_2 containment (Table 4.1). As outlined by Terry in 2001, the recommended depth for suitable reservoirs is deeper than 600 meters, accompanied by a net thickness within the range of 5 to 7 meters, and an oil saturation exceeding 30%. According to the findings of Chadwick and colleagues in 2008, the ideal depth falls within the range of 1000 to 2500 meters, with a thickness exceeding 50 meters, and a porosity level greater than 20% to consider it viable for CO_2 storage. This makes the reservoir zone within SML Formation conducive for CO_2 storage.

Moreover, the lithofacies prediction in Well Qadirpur-16 using SOM clusters provides a valuable insight into the geological composition of the area. It successfully distinguished four distinct

lithologies, including shale, limestone, shaley limestone, and hydrocarbon-bearing limestone (Figure 4.14). This analysis validates the presence of a hydrocarbon-bearing limestone zone within the identified depth range, reinforcing the potential for CO_2 storage. The petro-elastic properties (Figure 4.19) derived through predicted DT4S plays a significant role in terms of CO_2 storage. Furthermore, the caprock integrity was validated through permeability and effective porosity variations with lithology (Figure 4.20). These analyses are pivotal for assessing the mechanical behavior of the reservoir and caprock, providing critical insights into the stress state within the geological formation.

The study also ventured into seismic data analysis, allowing for a characterization of subsurface geological structures and the identification of potential pathways and risks for secure CO_2 storage. The resulting seismic assessments and reservoir characterizations revealed a relatively stable geological setting within the study area (Figure 5.4). This stability positions the region as a favorable candidate for CO_2 storage (Tomic et al., 2018). While dealing with depleted oil and gas reservoirs or during EOR-CO_2 process, analysis of certain parameters is required namely, OGIP, recoverable oil or gas reserves, reservoir pressure and temperature, reservoir rock volume, and porosity distribution (Hsu, 2012). Spatial distribution of reservoir properties, including impedance (Figures 6.3-6.4) and porosity (Figures 6.13, 6.14, 6.15, 6.18, and 6.19), further emphasized the area's potential for CO_2 storage. The reservoir of interest within the SML Formation exhibited relatively low impedance values ranging from 7000 to 9000 (m/s).(g/cm^3) (Figures 6.3-6.4) and high porosity values ranging from 0.12 to 0.24 v/v (Figures 6.13, 6.14, 6.15, 6.18, and 6.19). This spatial variation in reservoir properties, coupled with lithology data, suggests the presence of an excellent reservoir suitable for secure CO_2 containment. Additionally, the assessment of initial temperature and pressure settings within the SML Formation indicated the potential phase behavior of CO_2 (Tables 6.1 and 6.2). These conditions suggested the feasibility of storing CO_2 in a supercritical state, given other relevant parameters.

This research further emphasized the significance of the Qadirpur gas field as a standout candidate for CO_2 storage, with the potential to store over 200 million metric tons of CO_2 (Table 6.3). The field's developmental history, marked by sequential capacity enhancements and the implementation of a compression project in 2010, reflects a proactive approach to ensure a consistent supply of sales gas over the long term. However, it is crucial to note the transition of

the Qadirpur gas field into a gas reservoir suitable for EOR starting in 2020. This transformation indicates a shift in the field's utilization strategy, with a focus on maximizing gas recovery.

7.2 Conclusion

In conclusion, this thesis presents a comprehensive evaluation of the SML Formation within the Qadirpur Area, Central Indus Basin, Pakistan, as a promising site for CO_2 storage. Through a multidisciplinary approach encompassing petrophysical analysis, lithofacies prediction, seismic assessments, and reservoir characterizations, the following key conclusions emerge:

- The petrophysical analysis identifies a specific zone within the SML Formation with a % 18.86 PHIE and 80.72 % HS, characterized by favorable properties for secure CO_2 storage such as depth, tectonic stability, and seal integrity.
- Lithofacies analysis validates the presence of a hydrocarbon-bearing limestone zone within the identified depth range, further reinforcing the reservoir's potential for CO_2 containment.
- Seismic assessments indicate a stable geological setting, making the study area a favorable candidate for CO_2 storage.
- Spatial distribution of reservoir properties showcases the area's excellent reservoir potential, with low impedance values and high porosity values contributing to its suitability for CO_2 containment.
- The assessment of initial temperature and pressure settings suggests the feasibility of storing CO_2 in a supercritical state within the SML Formation.
- The Qadirpur gas field emerges as a significant CO_2 storage asset, with substantial capacity and a history of proactive reservoir management.

However, the transition of the Qadirpur gas field into a gas reservoir suitable for EOR signals a dynamic approach to resource utilization. In this evolving landscape, it is essential to adapt strategies for long-term reservoir management while considering the shifting demands and opportunities in the field. Overall, the research underscores the considerable potential of the Qadirpur Area for CO_2 storage and the importance of informed decision-making in reservoir development and carbon capture initiatives.

References

Akhter, G., Ahmed, Z., Ishaq, A. and Ali, A., 2015. Integrated interpretation with Gassmann fluid substitution for optimum field development of Sanghar area, Pakistan: a case study. *Arabian Journal of Geosciences*, *8*, pp.7467-7479.

Alam, M. S. M., Wasimuddin, M, Ahmad, S. S. M., 2002. Zaur structure, a complex trap in poor seismic data area, BP Pakistan Exploration and Production Inc. PAPG/SPE ATC conference. Islamabad, Pakistan, pp 1–3.

Ali, A., Ahmad, Z. and Akhtar, G., 2005. Structural interpretation of seismic profiles integrated with reservoir characteristics of Qadirpur area. *Pakistan Journal of Hydrocarbon Research*, *15*, pp.25-34.

Ali, A., Alves, T.M. and Amin, Y., 2022. Integrated geophysical analysis of the Sembar Formation, Central Indus Basin, as an unconventional resource. Journal of Natural Gas Science and Engineering, 101, p.104507.

Ali, A., Alves, T.M., Saad, F.A., Ullah, M., Toqeer, M. and Hussain, M., 2018. Resource potential of gas reservoirs in South Pakistan and adjacent Indian subcontinent revealed by post-stack inversion techniques. *Journal of Natural Gas Science and Engineering*, *49*, pp.41-55.

Ali, A., Kashif, M., Hussain, M., Siddique, J., Aslam, I. and Ahmed, Z., 2015. An integrated analysis of petrophysics, cross-plots and Gassmann fluid substitution for characterization of Fimkassar area, Pakistan: A case study. *Arabian Journal for Science and Engineering*, *40*, pp.181-193.

Ali, M., Jha, N.K., Pal, N., Keshavarz, A., Hoteit, H. and Sarmadivaleh, M., 2022. Recent advances in carbon dioxide geological storage, experimental procedures, influencing parameters, and future outlook. *Earth-Science Reviews*, *225*, p.103895.

Al-Menhali, A., Reynolds, C., Lai, P., Niu, B., Nicholls, N., Crawshaw, J.P. and Krevor, S., 2014, January. Advanced reservoir characterization for CO_2 storage. In *International Petroleum Technology Conference* (pp. IPTC-17253). IPTC.

Aminu, M.D., Nabavi, S.A., Rochelle, C.A. and Manovic, V., 2017. A review of developments in carbon dioxide storage. *Applied Energy*, *208*, pp.1389-1419.

Anwar, M.N., Fayyaz, A., Sohail, N.F., Khokhar, M.F., Baqar, M., Khan, W.D., Rasool, K., Rehan, M. and Nizami, A.S., 2018. CO_2 capture and storage: a way forward for sustainable environment. *Journal of environmental management*, *226*, pp.131-144.

Asim, S., Qureshi, S.N. and Khan, N., 2014. Study of an uplift of Sargodha High by stratigraphical and structural interpretation of an east-west seismic profile in Central Indus Basin, Pakistan. *International Journal of Geosciences*, *5*(9), p.1027.

Bacon, M., Simm, R. and Redshaw, T., 2007. *3-D seismic interpretation*. Cambridge University Press.

Banks, C.J. and Warburton, J., 1986. 'Passive-roof'duplex geometry in the frontal structures of the Kirthar and Sulaiman mountain belts, Pakistan. *Journal of structural Geology*, *8*(3-4), pp.229-237.

Barlass, D., Head, S. and Barnett, H., 2023. Improving Carbon Storage Play Assessment through Seismic Interpretation. *First Break*, *41*(7), pp.81-88.

Chadwick, A., Arts, R., Bernstone, C., May, F., Thibeau, S. and Zweigel, P., 2008. *Best practice for the storage of* CO_2 *in saline aquifers-observations and guidelines from the SACS and* CO_2*STORE projects* (Vol. 14). British Geological Survey.

Chang, H.C., Kopaska-Merkel, D.C. and Chen, H.C., 2002. Identification of lithofacies using Kohonen self-organizing maps. *Computers & Geosciences*, *28*(2), pp.223-229.

Coffeen, J.A., 1986. Seismic exploration fundamentals.

Cook, P.J., 2012. Clean energy, climate and carbon. *Carbon Management*, *3*(3), pp.259-263.

Czernichowski-Lauriol, I., Arts, R., Durand, D., Durucan, S., Johannessen, P., May, F., Olivier, M.L., Persoglia, S., Riley, N., Sohrabi, M. and Stokka, S., 2009. CO_2GeoNet, the unique role of the European scientific body on CO_2 geological storage. *Energy Procedia*, *1*(1), pp.2043-2050.

Fischetti, A.I. and Andrade, A., 2002. Porosity images from well logs. *Journal of Petroleum Science and Engineering*, *36*(3-4), pp.149-158.

Furre, A.K., Eiken, O., Alnes, H., Vevatne, J.N. and Kiær, A.F., 2017. 20 years of monitoring CO_2-injection at Sleipner. *Energy procedia*, *114*, pp.3916-3926.

Gibbins, J. and Chalmers, H., 2008. Carbon capture and storage. *Energy policy*, *36*(12), pp.4317-4322.

Gilmore, T., Bonneville, A., Sullivan, C., Kelley, M., Appriou, D., Vermeul, V., White, S., Zhang, F., Bjornstad, B., Cornet, F. and Gerst, J., 2016. Characterization and design of the FutureGen 2.0 carbon storage site. *International Journal of Greenhouse Gas Control*, *53*, pp.1-10.

Gnos, E., Immenhauser, A. and Peters, T.J., 1997. Late Cretaceous/early Tertiary convergence between the Indian and Arabian plates recorded in ophiolites and related sediments. *Tectonophysics*, *271*(1-2), pp.1-19.

Gupta, R. and Peter, S.C., 2020. CO_2 capture and sequestration-A solution for enhanced recoveries of unconventional gasses and liquids. *Energy and Climate Change*, *1*, p.100003.

Guthikonda, S.M., 2005. Kohonen self-organizing maps. *Wittenberg University*, *98*.

Hill, B., Hovorka, S. and Melzer, S., 2013. Geologic carbon storage through enhanced oil recovery. *Energy Procedia*, *37*, pp.6808-6830.

https://www.globaldata.com/industries-we-cover/oil-gas/

Hsu, C.W., Chen, L.T., Hu, A.H. and Chang, Y.M., 2012. Site selection for carbon dioxide geological storage using analytic network process. Separation and Purification Technology, 94, pp.146-153.

Hussain, M., Butt, A.R., Uzma, F., Ahmed, R., Islam, T. and Yousaf, B., 2019. A comprehensive review of sectorial contribution towards greenhouse gas emissions and progress in carbon capture and storage in Pakistan. *Greenhouse Gases: Science and Technology*, *9*(4), pp.617-636.

IEAGHG, A., 2008. regional assessment of the potential for CO_2 storage in the Indian subcontinent. *IEA Greenhouse Gas R&D Programme*.

Irlam, L., 2017. Global costs of carbon capture and storage. *Global CCS institute*, *16*.

Jaiswal, P., Grana, D., Stright, L., Daigle, H., Pashin, J. and Dupuy, B., 2022. Developments in reservoir characterization for carbon dioxide sequestration. *Frontiers in Earth Science*, *10*, p.1028220.

Karpatne, A., Ebert-Uphoff, I., Ravela, S., Babaie, H.A. and Kumar, V., 2018. Machine learning for the geosciences: Challenges and opportunities. *IEEE Transactions on Knowledge and Data Engineering*, *31*(8), pp.1544-1554.

Kazmi, A. H., & Jan, M. Q., 1997. Geology and tectonics of Pakistan (p. 554). Karachi: Graphic publishers.

Kou, Z., Wang, H. and Alvarado, V., 2022. Reservoir characterization and multiphase flow property in the upper Minnelusa sandstone: Implication for geological carbon storage. *Advances in Geo-Energy Research*, *6*(6), pp.535-536.

Krogh, A., 2008. What are artificial neural networks?. *Nature biotechnology*, *26*(2), pp.195-197.

Leiphart, D.J. and Hart, B.S., 2001. Case history: Comparison of linear regression and a probabilistic neural network to predict porosity from 3-D seismic attributes in Lower Brushy Canyon channeled sandstones, southeast New Mexico. Geophysics, 66(5), pp.1349-1358.

Macini, P., Mesini, E., Salomoni, V.A. and Schrefler, B.A., 2006. Casing influence while measuring in situ reservoir compaction. *Journal of Petroleum Science and Engineering*, *50*(1), pp.40-54.

Mahesh, B., 2020. Machine learning algorithms-a review. *International Journal of Science and Research (IJSR).[Internet]*, *9*(1), pp.381-386.

Maurya, S.P. and Singh, K.H., 2015. Reservoir characterization using model-based inversion and probabilistic neural network. Discovery, 49(228), pp.122-127.

Mavko, G., Mukerji, T. and Dvorkin, J., 2020. *The rock physics handbook*. Cambridge university press.

Meadowcroft, J. and Langhelle, O., 2009. The politics and policy of carbon capture and storage. *Caching the Carbon. The Politics and Policy of Carbon Capture and Storage*, pp.1-21.

Milan, G. and Rodgers, M., 1993. Stratigraphic evolution and play possibilities in the Middle Indus area, Pakistan. In *SPE Pakistan Seminar, Islamabad, January* (Vol. 19).

Mohamed, I.A., Shenkar, O. and Mahmoud, H., 2017. Understanding reservoir heterogeneity through water-saturation prediction via neural network—A case study from offshore Nile Delta. The Leading Edge, 36(4), pp.298-303.

Naseem, S., Carbon Storage by Geological Sites in Pakistan.

Niu, D., Sun, P., Ma, L. and Ding, C., 2023. Porosity evolution of Minhe oil shale under an open rapid heating system and the carbon storage potentials. Renewable Energy, 205, pp.783-799.

Pratama, E., Ismail, M.S. and Ridha, S., 2017. Screening criteria of optimum carbon dioxide injection for enhanced coalbed methane recovery and prediction of carbon dioxide storage capacity: A case study in south sumatera basin, Indonesia. Chemical Engineering Transactions, 56, pp.997-1002.

Rashid, M., Luo, M., Ashraf, U., Hussain, W., Ali, N., Rahman, N., Hussain, S., Aleksandrovich Martyushev, D., Vo Thanh, H. and Anees, A., 2022. Reservoir quality prediction of gas-bearing carbonate sediments in the Qadirpur field: Insights from advanced machine learning approaches of SOM and cluster analysis. *Minerals*, *13*(1), p.29.

Rashid, M.I., Benhelal, E. and Rafiq, S., 2020. Reduction of greenhouse gas emissions from gas, oil, and coal power plants in Pakistan by carbon capture and storage (CCS): A Review. *Chemical Engineering & Technology*, *43*(11), pp.2140-2148.

Raza, A., Gholami, R., Rezaee, R., Rasouli, V. and Rabiei, M., 2019. Significant aspects of carbon capture and storage–A review. *Petroleum*, *5*(4), pp.335-340.

Russell, B. and Hampson, D., 1991. Comparison of poststack seismic inversion methods. In SEG Technical Program Expanded Abstracts 1991 (pp. 876-878). Society of Exploration Geophysicists.

Sheriff, R.E. and Geldart, L.P., 1995. *Exploration seismology*. Cambridge university press.

Siddiqui, N.K., 2004. Sui Main Limestone: Regional geology and the analysis of original pressures of a closed-system reservoir in central Pakistan. *AAPG bulletin*, *88*(7), pp.1007-1035.

Terry, R.E., 2001. Enhanced oil recovery. *Encyclopedia of physical science and technology*, *18*(1), pp.503-518.

Tomić, L., Karović-Maričić, V., Danilović, D. and Crnogorac, M., 2018. Criteria for CO_2 storage in geological formations. *Podzemni radovi*, (32), pp.61-74.

Tufail, A. K., 2016. Hydrocarbon Occurrence and future potential in Pakistan.

Yao, Z., Lum, Y., Johnston, A., Mejia-Mendoza, L.M., Zhou, X., Wen, Y., Aspuru-Guzik, A., Sargent, E.H. and Seh, Z.W., 2023. Machine learning for a sustainable energy future. *Nature Reviews Materials*, *8*(3), pp.202-215.